Computational Molecular Modeling Studies of the Interactions of Estrogens with Their Receptors and Intracellular Binding Protein PDIp

BY

Pan Wang

B.S. Tsinghua University, Beijing, China 2005

Submitted to the graduate degree program in Pharmacology and the
Graduate Faculty of the University of Kansas
in partial fulfillment of the requirements for the degree of
Doctor of Philosophy

Dissertation Committee members:

Bao Ting Zhu, Ph.D. (Chair)

Bruno Hagenbuch, Ph.D.

Curtis D. Klaassen, Ph.D.

Brian K. Petroff, Ph.D.

Scott J. Weir, Pharm. D., Ph.D.

Dissertation Defended 09/27/2010

The Dissertation Committee for Pan Wang certifies

that this is the approved version of the following dissertation:

Computational Molecular Modeling Studies of the Interactions of Estrogens with Their Receptors and Intracellular Binding Protein PDIp

Pan Wang

B.S. Tsinghua University, Beijing, China 2005

Dissertation Committee:

Bao Ting Zhu, Ph.D. (Chair)

Bruno Hagenbuch, Ph.D.

Curtis D. Klaassen, Ph.D.

Brian K. Petroff, Ph.D.

Scott J. Weir, Pharm. D., Ph.D.

Dissertation Defended 09/27/2010

DEDICATION

I would like to dedicate the work herein to my beloved parents

Guanglian Wu and Xingwu Wang

ACKNOWLEDGEMENTS

I am heartily thankful to the many people who helped me complete this dissertation. First and foremost, I owe my deepest gratitude to my mentor, Dr. Bao Ting Zhu, for all of his guidance, support, encouragement, and advice throughout my graduate study. This dissertation would not have been possible without the great amount of effort and time he has put in to guide me through the last five years. It has been a great honor for me to work with Dr. Zhu to learn not only how to be a better researcher but also how to be a better person.

I am also grateful to the rest of my dissertation committee members, Dr. Bruno Hagenbuch, Dr. Curtis D. Klaassen, Dr. Brian Petroff, and Dr. Scott Weir, for all of their scientific advice, as well as for being so generous with their time in reviewing my dissertation proposal and draft. It would not have been possible for me to complete this project without the help of my committee.

I would also like to thank other faculty members in the department, Dr Grace Guo, Dr Xiao-bo Zhong, Dr Xiaochao Ma, Dr. Thomas L. Pazdernik, and a visiting professor Dr. Lirong Zhang, who provided me lots of support and encouragement along the way.

Thanks also go to the previous and current members of Dr. Zhu's laboratory, especially Dr. Masayuki Fukui, Dr. Hye-Joung Choi, Stephanie Bishop, Angelia Choi,

Jihoon Song, Dr. Hyoung-Woo Bai, Jina Yu, Dr. Jian Ding, Dr. Xiangchen Dai, Dr. Jun Liu, Elisabeth Yan Zhang, Aaron Yun Chen, and Dr. Xiang-Rong Jiang who have provided me with great guidance and help. They are all kind, generous, and wonderful people to work with.

I would like to acknowledge the suggestions given by Dr. Campbell McInnes from University of South Carolina on my computational modeling study. Dr. Gerry Lushington from University of Kansas, Lawrence helped with the installation of SYBYL software used for the molecular modeling study. Dr. Carolyn L. Smith from Baylor College of Medicine kindly helped us with the estrogen receptor reporter assay. Dr Benyi Li from Department of Urology generously provided us the androgen receptor reporter plasmid. Thanks also go to the people in the flow cytometry facility, electron microscope facility and laboratory animal resources for their technical help with some of my other projects.

I would also like to thank my colleagues in the Department of Pharmacology, Toxicology and Therapeutics for their friendship and academic support. Special thanks go to Connie Kai Wu, Youcai Zhang, Dr. Yi Miao Weaver, Dr. Pengli Bu, Dr. Dan Li, Dr. Chieko Saito, Huimin Yan, Dr. Min Yang, Dr. Bo Kong, Dr. Chunshan Gui, Dr. Jie Lu, Xiaohong Lei, Dr. Shary Shelton, Dr. Shuang Mei, and Ruipeng Wang who generously provided lots of mental and technical help whenever I needed them.

I also appreciate the help from the Pharmacology department administration staffs, particularly Ms. Rosa Meagher, Ms. Dorothy McGregor and Mr. Cody Tully. They not only keep the department running efficiently, but also have the best interest of the students in mind. I am also grateful to the people from the International program for their help, especially Ms. Julia Shaw.

I would like to express my deepest appreciation to my family who have always trusted and believed in me. I want to thank my mother Guanglian Wu, my father Xingwu Wang, and my husband Dr. Xinmiao Fu, who have always emotionally supported me with their everlasting love, which is what keeps me moving on through difficult times. For this reason, I share this degree with them.

Thanks also go to the National Institutes of Health for the funding support that my mentor Dr. Zhu has received in the past few years which were used to support my graduate study and research, as well as the Department of Defense Breast Cancer Research Program for awarding me the Predoctoral Fellowship.

ABSTRACT

The endogenous estrogens are vitally important female sex hormones with diverse biological functions. Disruptions of their actions contribute to the pathogenesis of a number of disease states in humans, such as endocrine malfunction, infertility, and development of cancers. Therefore, it is important to be able to predict whether a given chemical may have the potential to alter estrogen's actions through binding to the estrogen receptors (ERs) or other estrogen-binding proteins in the body. As opposed to some of the widely-used methods such as biochemical assays and crystallography, computational molecular modeling methods have the potential advantages of low cost, high speed, and high throughput. My dissertation research sought to explore the potential usefulness of computational molecular modeling tools in studying the interactions of various estrogen derivatives (e.g., endogenous estrogen metabolites, non-aromatic steroids, and synthetic antiestrogens) with human ERα and ERβ as well as with a recently-identified intracellular estrogen-binding protein.

As described in SECTION I of this dissertation, I estabolished and validated a molecular docking approach for studying the binding interactions of estrogens with human ERα and ERβ, and then I used this method to determine the binding characteristics of 27 structurally-similar estrogen derivatives with the ligand binding domains (LBDs) of human ERs. I found that while the binding modes of these estrogen derivatives are very similar to that of 17β-estradiol (E_2), there are distinct subtle

differences. In the case of *A*-ring E_2 derivatives, for instance, the small differences in the length of the hydrogen bonds formed between the phenolic 3-hydroxyl group of the estrogens and the ERs were found to be a major determinant of their overall binding affinity. This study reveals some of the structural features of the binding interactions of steroidal ligands with human ERs.

All previously characterized endogenous estrogens are steroids with their *A*-ring being an aromatic ring. Based on the computational analysis of the binding characteristics of various aromatic estrogens for human ERs as described above, I tested an intriguing hypothesis that some of the non-aromatic androgen metabolites or precursors may also be able to bind to human ERs. This work is described in SECTION II of my dissertation. With the aid of the computational molecular modeling tools together with a number of *in vitro* ER binding assays, I identified, for the first time, several non-aromatic metabolites or synthetic precursors of endogenous androgens that can bind to human ERα and ERβ with physiologically-relevant binding affinity, and these non-aromatic steroids can also activate the ERs to elicit estrogenic responses in human cancer cell lines. These results lead to the suggestion that some of the endogenously-formed androgen precursors or metabolites may serve as male-specific ER modulators.

It is known that compounds such as ICI-172,780, which possesses a long linear side chain attached to the C-7α position of E_2, could serve as effective ER pure antagonists. The studies described in SECTION III of my dissertation sought to test the

hypothesis that estrogen analogs with a shorter but bulky side chain may also be able to function as effective ER antagonists, and theoretically, these compounds may be structurally more stable. Our laboratory designed and synthesized nine of these novel estrogen analogs. Four of them were identified as having a strong antiestrogenic activity in ER-positive human breast cancer cells. Computational molecular modeling studies found that these compounds could tightly bind the ERα LBD similar to ICI-182,780, which helps to explain the mechanism of their antiestrogenic actions.

Recently, our laboratory identified, for the first time, the pancreas-specific protein disulfide isomerase (PDIp) as a novel intracellular E_2-binding protein with the binding site located in its *b-b'* domain. As described in SECTION IV of my dissertation, I used computational molecular modeling methods to determine the detailed E_2-binding site structures of the human PDIp protein. Molecular docking analysis predicted the binding site in the hydrophobic pocket between the *b* and *b'* domains. The hydrogen bond formed between the 3-hydroxyl group of E_2 and PDIp-His278 is indispensable for the binding interaction. Selective point mutations of relevant amino acid residues and selective modifications of the ligand structures both confirmed this predicted binding mode. Altogether, these results precisely define, for the time, the E_2-binding site structure of human PDIp.

As a whole, the results of my dissertation projects offer important insights into the three-dimensional structural characteristics of the binding interactions of various estrogen

analogs with the human ERα, ERβ, and PDIp. These studies provide a platform for the future development of an automated docking-based computational approach that can screen numerous environmental compounds for their potential ability to bind human ERs as well as other estrogen binding proteins in the body.

TABLE OF CONTENTS

LIST OF FIGURES

LIST OF TABLES

LIST OF ABBREVIATIONS

AR	androgen receptor
ARE	androgen response element
CoMFA	comparative molecular field analysis
DES	diethylstilbestrol
ER	estrogen receptor
ERE	estrogen response element
ERT	estrogen replacement therapy
E_1	estrone
E_2	17β-estradiol
E_3	estriol
GPR	G protein-coupled receptor
Helix 12	H12
LBD	ligand binding domain
PC	principle component
PDI	protein disulfide isomerase
PDIp	pancreas-specific PDI homolog
QSAR	quantitative structure-activity relationship
RAL	raloxifene
RMS	root mean square
RBA	relative binding affinity
SEC	size exclusion chromatography
SERM	selective estrogen receptor modulator
SHBG	sex hormone binding globulin

T_3	3,3’,5-triiodo-L-thyronine
TAM	tamoxifen
VDW	van der Waals

CHAPTER ONE

GENERAL INTRODUCTION

ESTROGENS AND ANTIESTROGENS

Biosynthesis and metabolism of estrogens. In women, estrogens are synthesized from cholesterol mainly in the theca and granulosa cells of the ovary. Theca cells secrete androgens that diffuse into the granulosa cells where the androgens are aromatized by aromatase to estrogens (Hillier et al., 1994). Some estrogens are also produced in smaller amounts by other tissues such as the liver, adrenal glands, and the breasts.

Estrogens are metabolized mainly in liver by oxidation (largely hydroxylations by cytochrome P450 enzymes) (Martucci and Fishman, 1993), glucuronidation (Lucier and McDaniel, 1977), sulfation (Brooks and Horn, 1971), and/or *O*-methylation (Ball and Knuppen, 1980). The hydrophilic metabolites are excreted into the bile or urine. Hydroxylation of estrogens yields 2-hydroxyestrogens, 4-hydroxyestrogens, and 16α-hydroxyestrogens. The unique functions of these estrogen metabolites have been reviewed (Zhu and Conney, 1998). Notably, 4-hydroxyestradiol and 16α-hydroxyestradiol are considered to be carcinogenic. 4-Hydroxyestradiol is capable of undergoing metabolic redox cycling, a process that yields semiquinone/quinone intermediates, formation of free radicals, and covalent binding to DNA (Liehr et al., 1986). In addition, catechol estrogens have relatively weaker estrogenic activity compared to E_2 and they may inhibit catechol-*O*-methyltransferase.

Physiological functions of estrogens. Estrogens have a wide array of

physiological functions. They promote the development of female secondary sexual characteristics, such as breasts. In young women, the lobular units of their breast terminal ducts are highly responsive to estrogens. Estrogens can stimulate the growth and differentiation of ductal epithelium, induce mitotic activity of ductal cylindric cells, and stimulate the growth of connective tissue (Porter, 1974). Estrogens are also involved in the thickening of the endometrium and other aspects of regulating the menstrual cycle. Estrogens can serve as feedback control to inhibit production of GnRH by hypothalamus. Besides these reproductive functions, estrogens have beneficial effects on the bone, cardiovascular system, and central nervous system.

Estrogen deficiency accelerates bone loss and increases risk of fractures. Estrogen therapy diminishes bone loss (Christiansen et al., 1981) and reduces the risk of fracture in women with osteoporosis and in those without this condition for the duration of therapy. Both osteoclasts and osteoblasts express ERs (Eriksen et al., 1988) and are the targets of estrogen actions. Estrogens directly inhibit the function of osteoclasts. In oophorectomized mice, estrogen deficiency increases the production of interleukin-6, interleukin-1, and tumor necrosis factor in osteoblasts and other bone-derived stromal cells (Manolagas et al., 1993).

Estrogens are natural vasoprotective agents. ERs have been detected in smooth muscle cells of coronary arteries and vascular endothelial cells at various locations (Karas et al., 1994). Estrogens cause short-term vasodilation by increasing the formation and

release of nitric oxide and prostacyclin in endothelial cells (Kim et al., 1999). They also reduce vascular smooth-muscle tone by opening specific calcium channels mediated by second messenger cGMP (White et al., 1995). On the cellular level, estrogens inhibit apoptosis of endothelial cells (Spyridopoulos et al., 1997) and promote their angiogenic activity *in vitro* (Morales et al., 1995).

Recently, estrogens were found to have neuroprotective effects. In brain tissue from adult rats, estrogens have been reported to induce synaptic and dendritic remodeling (Naftolin et al., 1990) and cause glial activation (Garcia-Segura et al., 1999). In neurons of the hippocampus, an area involved in memory, estrogens increase the density of N-methyl-D-aspartate receptors and increase neuronal sensitivity to input mediated by these receptors (Woolley et al., 1997). In cultured human neuroblastoma cells, estrogens have neuroprotective effects (Green et al., 1997) and reduce the generation of beta-amyloid peptides (Xu et al., 1998). Some epidemiologic data suggest that in postmenopausal women, estrogen deficiency is associated with a decline in cognitive function and an increased risk of Alzheimer's disease (Paganini-Hill and Henderson, 1996).

Carcinogenic effects of estrogens. Several of the most common cancers in western societies occur in hormonally responsive tissues, including breast, endometrium, and ovary in women, and prostate in men. These cancers have been causally linked to exposure to synthetic or endogenous steroidal hormones or their metabolites (Henderson et al., 1991). Breast cancer has also been linked to exposures to various environmental

xenobiotics or their metabolites with estrogenic or androgenic activities (Falck et al., 1992; Lewis, 1994). Exposure *in utero* to diethylstilbestrol (DES) resulted in an increased incidence of cervicovaginal clear-cell carcinomas in young women and of testicular cancer in men (Bern et al., 1992). The great interest in treating and preventing these cancers has generated research on the mechanisms involved and spawned development of the field of hormonal carcinogenesis.

The most widely appreciated and investigated effect of estrogens is increased cell proliferation (Nandi et al., 1995). Moreover, it has become clear that several hydroxylated estrogen metabolites can, directly or indirectly through redox cycling processes that generate reactive radical species, cause oxidative DNA damage (Li et al., 1994). Thus, the mechanism of estrogen carcinogenesis involves both nongenotoxic, i.e. cell proliferative, as well as direct and indirect genotoxic effects, with the importance of either or both being a function of the tissue and cell type (Yager and Liehr, 1996).

Environmental estrogens. There is mounting evidence that increased exposure to certain hormone-mimicking environmental chemicals increases the risk of breast cancer (Brody et al., 2007; Rudel et al., 2007). They can also disrupt reproductive system functions (Abaci et al., 2009; Ma, 2009; Rogan and Ragan, 2003) and development (Colborn et al., 1993). It is estimated tens of thousands of chemicals existing in our environment have varying degrees of estrogen-like activity. Polychlorinated biphenyls, dioxins, pesticides, polycyclic aromatic hydrocarbons from vehicle exhaust and air

pollution, and disinfection products from chlorinated drinking water are among the well-known examples (Bernstein, 2002).

Selective estrogen receptor modulators (SERMs) and antiestrogens. Estrogen replacement therapy (ERT) is used to treat the syndromes associated with menopause. For example, estrogens can inhibit bone resorption and be used for the treatment and prevention of osteoporosis (Turner et al., 1994). In addition, many studies have indicated that estrogens have beneficial activities in the cardiovascular system and decrease the incidence of coronary heart disease by as much as 50% (Zumoff, 1993). ERT may also have beneficial activities in the central nervous system, as several studies have shown improvements in cognitive function and delaying the onset of Alzheimer's disease by ERT (Grady et al., 1992). However, several large studies have shown that the incidence of breast cancer is increased in patients taking ERT (Dupont and Page, 1991). Most studies put the relative risk somewhere between 1.1 and 1.3. Thus pharmaceutical companies have developed Selective ER Modulators (SERMs) that retain the beneficial effect of estrogens but have no stimulatory effect in breast. One example of an approved SERM is Raloxifene for the prevention of osteoporosis (Delmas et al., 1997). Raloxifene is an ER agonist in the bone and ER antagonist in the breast.

Another example of SERMs is Tamoxifen, which is used as an adjuvant hormonal therapy for ER-positive human breast cancer (Jordan, 2003). In addition, it is also effective in preventing estrogen-inducible breast cancer in high risk populations (Fisher et al., 2005). Tamoxifen has predominant antiestrogenic activity (i.e., ER antagonist

activity) in the breast; it also has a weak estrogenic activity (i.e., ER agonist activity) in bone and cardiovascular systems.

The pure ER antagonists, such as ICI-182,780 (fulvestrant) and ICI-164,384, which are devoid of any ER agonistic activity, have been developed as effective alternatives to tamoxifen (Howell et al., 2000). Studies have shown that human breast cancer cells that became resistant to tamoxifen were still sensitive to the anticancer effect of fulvestrant.

ESTROGEN RECEPTORS AND ESTROGEN BINDING PROTEINS

Estrogen receptors (ERs). Many of the hormonal actions of estrogens are mediated by specific estrogen receptors (ERs), which are members of the nuclear receptor superfamily. ERs have several functional domains. The DNA-binding domain contains two zinc fingers that are involved in DNA binding and dimerization. The ligand-binding domain (LBD) contains different sets of amino acids that bind different ligands and this domain also interacts with coregulatory proteins. The N-terminal domain has a high degree of variability and normally contains a transactivation domain that can interact directly with factors of the transcriptional machinery. The C-terminal domain contributes to the transactivation capacity of the receptor (Rollerova and Urbancikova, 2000). ERs can form dimers upon binding with estrogens and then migrate into the nucleus, bind to estrogen response elements, recruit coactivators, and induce downstream gene expression.

There are two subtypes of ERs, and for each ER subtype, there are several known isoforms and splice variants. The first subtype, the classic ERα, was first cloned in 1986 (Green et al., 1986). The second subtype, ERβ, was discovered more recently (Kuiper and Gustafsson, 1997). The DNA-binding domains of ERα and ERβ are very similar, but the ligand-binding domains of these two ERs exhibit only 55 percent amino acid sequence homology (Witkowska et al., 1997). As a result, most ligands can bind to these two ERs with different binding affinities (Zhu et al., 2006). The SERM raloxifene binds with higher affinity for ERα, whereas several environmental pollutants, such as the

alkylphenols, have higher affinity for ERβ. The activated ERα and ERβ (i.e. receptor bound with an agonist such as E_2) can form homodimers or heterodimers (ERα + ERβ), and these dimerized ERs can bind to various estrogen response elements in highly similar fashions (Katzenellenbogen et al., 1993).

The tissue distributions of ERα and ERβ are different. Endometrium, breast-cancer cells, and ovarian stroma contain mostly ERα. In contrast, ERβ is present in several nonclassic estrogen target tissues, including the kidney, intestinal mucosa, lung parenchyma, bone marrow, bone, brain, endothelial cells, and prostate gland (Enmark et al., 1997).

In addition to their different tissue distributions, ERα and ERβ also have very different biological functions. A number of studies have shown that ERβ often counteracts the actions of ERα in many systems. For instance, while ERα mediates the proliferative effect of estrogens in breast cancer cells, ERβ appears to be antiproliferative and negatively regulates the transactivation of ERα in human breast cancer cells (Strom et al., 2004). In agreement with this suggestion, it was shown that induced expression of ERβ in T47D human breast cancer cells reduced E_2-stimulated proliferation of these cells when the levels of ERβ mRNA equaled the levels of ERα. Induction of ERβ suppressed the growth of rapidly-proliferating cells with a concomitant decrease in cell cycle-regulatory proteins, namely, cyclin E, Cdc25A, p45, and an increase in the Cdk inhibitor p27. Similarly, in the prostate, whereas ERα predominatly mediated the proliferative

effect of the estrogens, ERβ mediated the antiproliferative effect of the estrogens (Ellem and Risbridger, 2007). Mechanistically, studies in human breast cancer cells have led to the suggestion that ERβ may negatively regulate the transactivation of ERα (Zhao et al., 2007).

Crystal structures of ERs' ligand binding domain in complex with several agonist or antagonist revealed the structural mechanism of antagonism (Brzozowski et al., 1997; Tanenbaum et al., 1998). As shown in **Figure 1**, in the E_2-liganded complex, Helix12 (H12) sits snugly over the ligand binding cavity, forms the "lid" of the binding cavity, and projects its inner hydrophobic surface towards the bound hormone. This precise positioning of H12 is a prerequisite for transcriptional activation by generating a competent transactivation domain that is capable of interacting with coactivators. Upon binding with antagonist, the ligand binding domain undergoes drastic conformational change. The alignment of H12 over the cavity is prevented by the antagonist and H12 undergoes rotation of 130 degrees combined with a 10-Å rigid-body shift towards the amino terminus of the LBD compared with the agonist-induced conformation, which renders the transactivation domain incompetent.

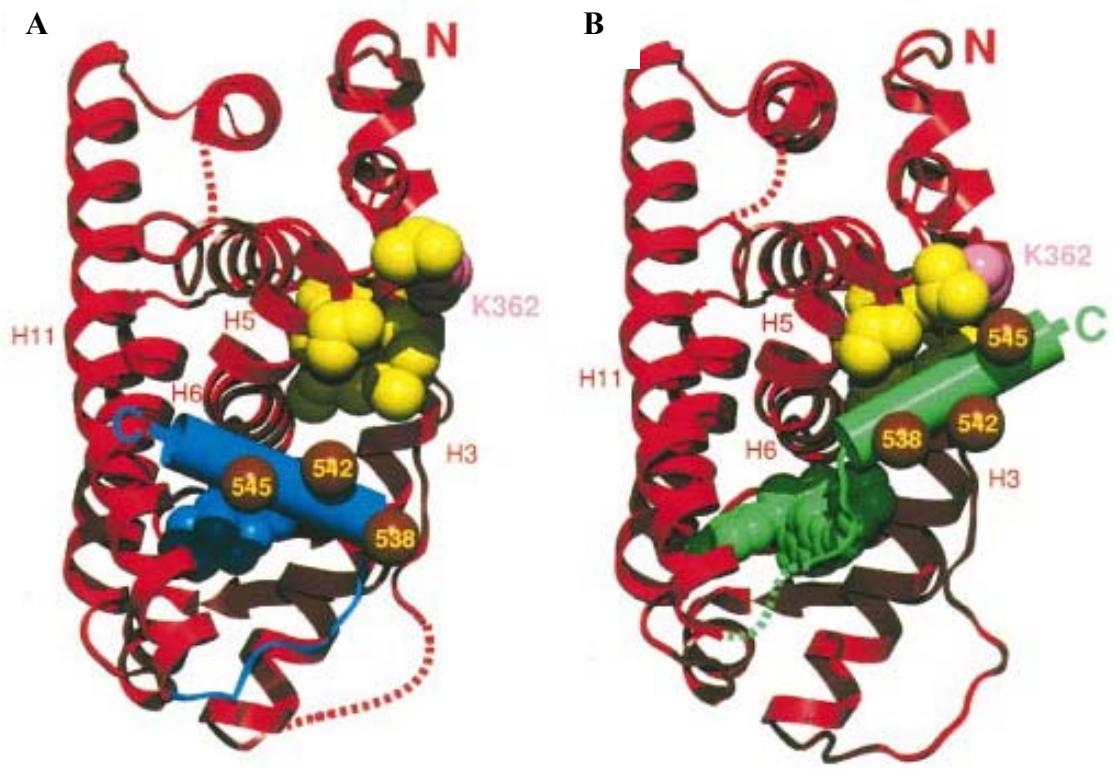

Figure 1 Comparison of positioning of Helix12 (H12) in ERα structures bound with an agonist and an antagonist. H12 position is shown in **A**, the ER LBD–E_2 complex; and **B**, the ERLBD–RAL complex. H12 is drawn as a cylinder and colored blue (E_2 complex) or green (RAL complex). The remainder of the ER LBD is shown in red. Dotted lines indicate unmodelled regions of the structures. Hydrophobic residues located in the groove between H3 and H5 (yellow) and Lys362 (K362, pink) are depicted in space-filling form. The locations of Asp538, Glu542, and Asp545 are highlighted (brown spheres) along with the helices that interact with H12 in the two complexes.

Estrogen binding proteins. Estrogens in humans are synthesized mainly in the ovary and transported through blood circulation to various target organs for hormonal actions and also to liver for metabolic disposition. During this coordinated biological process, many factors affect the half-life and concentration of estrogens in the blood and particularly in target tissues/cells, and also affect the levels of ERα and ERβ and their ratios (ERα/ERβ). Although most of the hormonal functions of estrogens are mediated by their intracellular ERs (ERα and ERβ), here I will discuss a few well-known examples of estrogen-binding proteins with a focus on their unique biological functions in modulating and/or diversifying endogenous estrogens' actions in the body.

(1) Sex hormone-binding globulin (SHBG). It has been known for decades that SHBG is a plasma glycoprotein that can tightly bind steroids, in particular estrogens. It is perhaps the most powerful regulator of the concentrations of free (unbound) estrogens and androgens in the blood as well as their availability to target tissues or cells (Zhang et al., 2005). In addition to this important function as a circulating estrogen-binding protein, studies in recent years have surprisingly revealed that SHBG may have its specific membrane-bound receptor (SHBG-R). This SHBG-R was found to be expressed in MCF-10A cells (non-neoplastic human mammary cells), MCF-7 cells (ER-positive human breast cancer cells), and breast tissue samples from breast cancer patients, but it was not present in estrogen-insensitive MDA-MB-231 cells (Fortunati et al., 1998). Although the precise mechanism of its action is still unclear, studies of cultured MCF-7 cells revealed that the estrogen-bound SHBG interacted with a specific binding site on the cell

membrane, which resulted in activation of protein kinase A and subsequent synthesis of cAMP (Fortunati et al., 1999; Fortunati et al., 1996). The changes in intracellular cAMP lead to inhibition of ERα-mediated activation of ERK (Fortunati and Catalano, 2006). Similarly, it was reported that estrogens and 5α-androstan-3α,17β-diol stimulated the production of intracellular cAMP by binding to SHBG which then formed complex with its membrane receptor (SHBG-R) present on prostate cells (Fortunati et al., 1999).

(2) G protein-coupled receptor 30 (GPR30). GPR30 is a seven-transmembrane intracellular receptor, and it was reported that GPR30 has the binding and signaling characteristics of a membrane ER. The membrane proteins prepared from SKBR3 breast cancer cells that expressed GPR30 but lacked nuclear ERs were found to have a binding site with high affinity (K_d = 2.7 nM), limited binding capacity, displaceable, and single binding site kinetics for estrogens (Thomas et al., 2005). The activation of GPR30 bby estrogen resulted in intracellular calcium mobilization and synthesis of phosphatidylinositol 3,4,5-trisphosphate in the nucleus. Based on this observation, it is likely that GPR30 represents an important intracellular transmembrane ER that may contribute to the diversification of normal estrogen physiology as well as pathophysiology in various target tissues (Filardo et al., 2007).

(3) Protein disulfide isomerases. Protein disulfide isomerase (PDI) is a member of the thioredoxin superfamily (Freedman et al., 2002). During the maturation of extracellular proteins, disulfide bonds that chemically cross-link specific cysteines are

often added to stabilize a protein or to join it covalently to other proteins (Ellgaard and Ruddock, 2005). PDI interacts with unfolded/misfolded protein substrates and facilitates the arrangement of disulfide bonds by either introducing disulfide bonds into proteins (oxidase activity) or by re-arranging incorrect disulfides (isomerase activity). In addition, PDI also acts as a chaperone by binding to certain cellular proteins to prevent them from aggregation and/or to slow down their degradation by the ubiquitin–proteasome pathway (Grune et al., 2002).

PDI is constitutively expressed in most tissues and organs and is retained at a concentration approaching the mM range in the endoplasmic reticulum by its retention sequence signal, KDEL (Gruber et al., 2006). At present, more than a dozen homologs of the human PDI have been characterized and the best studied examples include PDI, PDIp (pancreas-specific PDI), ERp57, ERp72, ERp28, PDIR, and P5 (Ellgaard and Ruddock, 2005; Gruber et al., 2006; Maattanen et al., 2006; Wilkinson and Gilbert, 2004). Among this family of proteins, PDI is perhaps the most abundant member.

Structurally, PDI and many of its homologs all comprise two thioredoxin-like catalytic domains, *a* and *a′*, which are separated by two non-catalytic domains, *b* and *b′*. The catalytic domains contain a characteristic CXXC active-site motif, and the two amino acids that lie between the cysteine residues have a major role in determining the redox potential of the enzyme, and hence it functions as a disulfide reductase, oxidase, or isomerase. The *b′* domain provides the principal peptide-binding site of protein disulfide

isomerase but all domains contribute to binding of misfolded proteins (Klappa et al., 1998).

In addition to the well-known functions of PDI and its homologs described above, certain members of this protein family have also been reported to have other unique biological functions. Studies using mammalian cell models have shown that PDI is a protein that is strongly up-regulated in response to hypoxia/brain ischemia for the protection against apoptotic neuronal cell death (Tanaka et al., 2000; Uehara et al., 2006). In the context of estrogen, recent studies by us (Fu et al., 2008; Fu and Zhu, 2009) and also by others (Primm and Gilbert, 2001) have shown that PDI has estrogen-binding activity. Our recent data showed that (i) PDI and PDIp each can bind estrogens *in vitro*; (ii) We further demonstrated that PDI can help concentrate estrogens inside the mammalian cells and augment ERα-mediated transcriptional activity and growth stimulation. (iii) It was reported earlier that PDI is associated with ERα (Landel et al., 1997; Schultz-Norton et al., 2006), and this observation was confirmed in our recent study. (iv) We found that PDI knockdown in MCF-7 cells resulted in a strong down-regulation of ERα protein but a marked up-regulation of ERβ protein, which resulted in a drastic change in the ratio of ERα to ERβ. This is the first observation that an intracellular protein can alter the levels of human ERα and ERβ in a bi-directional manner. As briefly discussed above, it has been recognized in recent years that the ERα and ERβ ratio is a crucial determinant for the estrogen-responsiveness of breast and prostate cancer cells (Hall and McDonnell, 1999).

COMPUTATIONAL MOLECULAR MODELING

Interest in computer aided methods for studying biological problems has increased significantly in recent years due to the development of computational tools as their cost droped and the speed of calculation increased. There are mainly two categories of computational methods to study receptor-ligand interactions. One is the more traditional Quantitative Structure Activity Relationship (QSAR) approach, and the other one is the molecular docking approach. The QSAR approach relies solely on the structures of ligands to predict the three-dimensional properties of the receptor binding site as well as the binding affinity of a test ligand. Molecular docking analysis is based on the three-dimensional structures of both the receptor binding pocket and the ligand to predict the preferred binding conformations of the ligand in the receptor's binding pocket. The binding affinity of a ligand can then be predicted by computing the binding energy values.

These two approaches have their own advantages and disadvantages. The QSAR model usually can achieve a good prediction when the unknown test compounds are structurally similar to the training set of compounds used. In comparison, the molecular docking analysis theoretically can predict the binding conformations of structurally diverse compounds. I chose to focus primarily on the molecular docking analysis with QSAR models as a complementary approach.

QSAR. The general workflow of the QSAR process is schematically illustrated in **Figure 2**. The assumption behind a QSAR model is that there is a quantitative relationship between the molecular features of a chemical and its biological activity. There are mainly three steps to develop a QSAR model:

(1) Calculation of structural descriptors of small molecules. For 3 dimensional (3D) QSAR, Molecular Interaction Field is used to calculate the structural descriptors. By placing the molecule within a lattice divided into small grids, we can calculate the interaction energy (steric and electrostatic energies) of that molecule with a probe such as a sp3 carbon atom at each grid point. Because Molecular Interaction Field descriptors are directionally dependent, a critical step in 3D-QSAR analysis is the alignment of all the molecular 3D optimized structures in the dataset by superposition. For each chemical in the dataset, each descriptor column contains the energy value of the interaction field at a certain point of the grid.

(2) Input target properties to be studied as Y-block variable. In principle these can be any physicochemical or biochemical property as well as more biological activities such as binding affinity to estrogen receptors.

(3) Statistical analysis. This is the central step of the modeling task. It includes variable selection of relevant descriptors and the application of specific algorithms to find the relationship between variables and the target property. Principal Component Analysis

using the Partial Least Square method is most widely used. A regression map can be created by mapping the regression coefficient of the model back onto the grid created around the molecules. Therefore, the map identifies the most important regions around the molecule responsible for modulating the target properties. And these regions can also reflect the property of the receptor binding site. The most popular method in 3D-QSAR studies is Comparative Molecular Field Analysis (CoMFA) (Cramer et al., 1989) but other methods have been developed based on different force fields adopted to calculate the energy.

(4) Validation of the model. This includes the assessment of goodness-of-fit and robustness. Goodness-of-fit describes the model's prediction ability in the training set whereas robustness provides an indication of the model's stability in terms of its sensitivity to perturbation in the training set. The main statistical parameter for assessing the goodness-of-fit is the coefficient of determination R^2, reported in equation (1):

$$R^2 = 1 - \frac{\sum_1^n (y_i - \hat{y}_i)}{\sum_1^n (y_i - \bar{y}_i)} \quad (1)$$

where y_i, $\hat{y}_i$, and $\bar{y}_i$ are, respectively, the observed, calculated, and mean values of the Y dependent variable. The closer R^2 is to 1 the better the model fits. Robustness is usually assessed by the cross-validation procedure: the training set is iteratively perturbed by excluding one compound and the other compounds are used to generate a model predicting the excluded chemicals with this sub-model. This procedure is repeated for all compounds. Statistical parameters similar to accuracy or r^2 (usually called q^2) are then

calculated based on the predicted values and should maintain a considerable value, usually larger than 0.5.

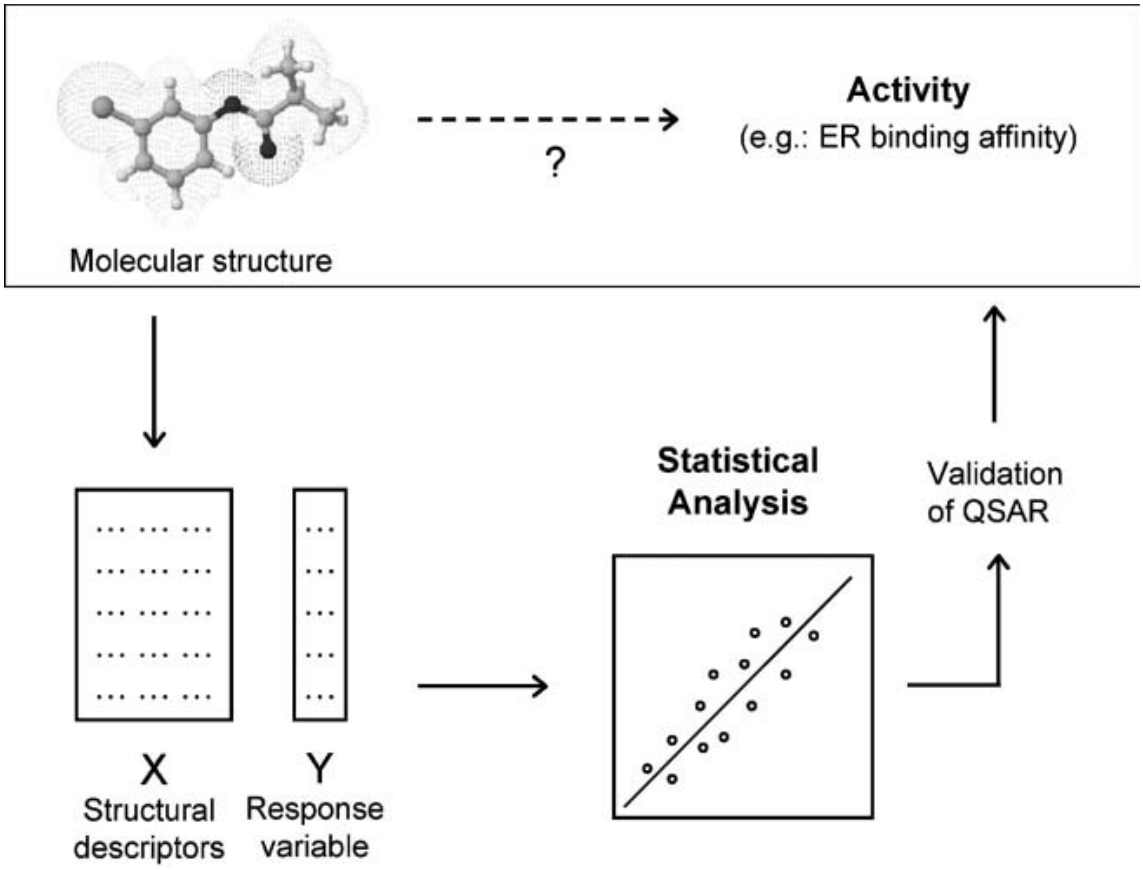

Figure 2 Scheme of the steps for developing QSAR models.

Molecular docking. Molecular docking computationally predicts the binding between a protein and a small molecule (ligand). For this kind of study, the 3D structure of the protein and the binding site must be known. Usually, the best source is the structure provided by X-ray crystallography. If this is not available, a structure determined with NMR spectroscopy or by homology modeling may be used. Homology modeling involves reconstructing the 3D structure of the protein of interest based on other proteins whose structure is known. There must be amino acid sequence similarities between the protein of interest and template proteins. The majority of current docking programs take into account ligand flexibility in contrast with rigid docking (where both the ligand and the protein are considered as rigid), but protein flexibility has not yet been fully integrated into docking protocols. The *Affinity* module of *InsightII* I used in this study was among the first to integrate protein flexibility in the docking protocols.

Among the searching strategies for the optimal binding of the ligand to the binding site, there are molecular dynamic simulations, Monte Carlo methods, genetic algorithms, and fragment-based methods (Taylor et al., 2002). Once a pool of ligand–protein complexes has been generated, scoring functions are used by docking programs to indicate the likelihood that the conformation offers a favorable binding interaction. The scoring functions may rely on force fields to calculate energies or on knowledge-based or empirical functions (including QSAR relationships).

Although the molecular docking method is a powerful tool in identifying the

favorable binding conformations, its drawback lies on the accuracy of energy calculation. Although fairly accurate ways exist for estimating these binding energies based on free energy perturbation or thermodynamic integration methods, the accuracy levels are usually not high enough for general purpose use, but may be useful in certain special cases. The most common application of the molecular docking approach is in virtual high throughput screening, where large virtual libraries of compounds are screened to find a subset of molecules with high binding affinities to a target receptor. This approach is often used in the drug discovery process to identify new lead compounds. The typical level of accuracy reached by docking programs in virtual high throughput screening usually does not allow direct correlation of their binding energies with the binding affinity.

CHAPTER TWO

STATEMENT OF PURPOSE

Estrogens have diverse physiological and pathophysiological functions in different organ systems, including reproductive organs, cardiovascular system, central nervous system, bone, and others. Disruption of their actions contributes to the pathogenesis of a number of disease states in humans, such as endocrine malfunctions, infertility, and cancers. There is evidence showing that increased exposure to certain hormone-mimicking environmental chemicals that can activate the human estrogen receptor α (ERα) also increases the risk of breast cancer and disrupt normal reproductive functions. In addition, some of the synthetic estrogen receptor antagonists (e.g., tamoxifen, reloxifene, and ICI-182,780) are found to be highly effective in the treatment and prevention of human breast cancer by antagonizing the actions of endogenous estrogens.

Whereas most of the existing studies on the actions of estrogens focus on the interactions of estrogens with the known ERα and ERβ, studies in recent years have also shown that their interactions with other estrogen-binding proteins such as the sex hormone-binding globulin (SHBG) may also play important roles not only in modulating the bioavailability of the free estrogen concentrations in blood and target tissues, but also in diversifying the biological actions of estrogens. At present, there are very few studies on other cellular estrogen-binding proteins besides ERα and ERβ.

Needless to say, it is important to have the ability to predict the estrogenic potency and efficacy of any given chemical and also to predict whether other cellular

proteins can bind estrogens. Compared to the widely-used methods such as the receptor binding assay, receptor activity assay and crystallography, computational molecular modeling methods have the potential advantages of low cost, high speed, and high throughput. Progress in this area of research will not only help develop the ability to predict and/or identify new environmental estrogens so that the general public can be informed and avoid excessive exposure to these chemicals, but it will also help upgrade our ability to rationally design more effective antiestrogens for treatment and prevention of human breast cancer as well as other estrogen-sensitive cancers. The identification of proteins with estrogen-interacting ability will facilitate the discovery of novel estrogen-binding proteins that may modulate cellular estrogen concentrations as well as biological activities.

Two main types of molecular computational modeling approaches are employed in my dissertation research: One is the more traditional Quantitative Structure Activity Relationship (QSAR) approach, and the other one is the molecular docking approach. The basic assumption behind the QSAR modeling approach is that there is a quantitative relationship between the structural features of the ligands and their biological activities. QSAR models rely solely on the structures of ligands to predict the three-dimensional properties of the receptor binding site as well as the potential binding affinity of a given test ligand. This method was the predominantly-used modeling method when the crystallographic structures of most receptors were not available. On the contrary, molecular docking analysis is based on the three-dimensional structures of both the

receptor binding pocket and the ligand to predict the preferred binding conformations of the ligand inside the receptor's ligand binding pocket. The binding affinity of a ligand theoretically can then be predicted by computing the binding energy values.

These two approaches have their own advantages and disadvantages. The QSAR model usually can achieve a very good prediction when the unknown test compounds are structurally similar to the training set of compounds used. However, this model will not reliably predict the binding interactions of a compound with completely different structural features. In comparison, the molecular docking analysis theoretically can predict the binding mode of structurally-diverse compounds, but usually this computational method is less accurate in predicting the binding affinity of a compound compared to the QSAR method. In my studies, I chose to focus more on the molecular docking analysis whereas the QSAR approach was basically used occasionally as a complementary approach for comparison.

Therefore, the **overall objective** of my dissertation research work was to apply computational molecular modeling tools to study the interactions of a number of representative estrogen analogs with human ERα and ERβ as well as with a recently-identified intracellular estrogen-binding protein, the human PDIp (pancreas-specific protein disulfide isomerase).

The chief significance of these studies is that they will provide insights into the

three-dimensional structural characteristics during the binding interactions of estrogen analogs with these estrogen-binding proteins. These studies also enhance our ability to develop computational tools for the prediction of structurally-diverse compounds for their binding affinities with these endogenous receptors and estrogen-interacting cellular proteins.

Specifically, my dissertation research project has two specific aims. The studies described under **SPECIFIC AIM 1** focused on determining the structural characteristics of the binding interactions of human ERα and ERβ with three representative classes of estrogen analogs (i.e., the endogenous metabolites of E_2, non-aromatic steroids, and synthetic E_2-based C-7α antagonists). The studies described under **SPECIFIC AIM 2** mainly sought to determine the E_2-binding pocket structure in a recently-identified estrogen-binding protein PDIp.

SPECIFIC AIM 1: To study the structural characteristics of the interactions of representative estrogen analogs with the human ERα and ERβ. This aim has three closely-related sub-aims.

AIM 1A: To determine the three dimensional structural characteristics of the binding interactions of endogenous estrogen metabolites with human ERα and ERβ.

We first used the well-characterized estrogen metabolites as model compounds to

study their interactions with human ERα and ERβ. The reason we chose estrogen metabolites is that they are structurally very similar to E_2 with only one more functional group added. However, their binding affinities for ERs vary drastically. By studying the interaction of these compounds with ERs, we can understand the detailed structural features of a ligand that are required in order to bind ERs. In this aim, I used molecular docking analysis to study the binding interactions of the E_2 derivatives with ERα and ERβ, and also the relationship between the calculated binding energy values and the experimentally-determined binding affinities.

AIM 1B: To determine the three dimensional structural characteristics of the binding interactions of non-aromatic steroids with human ERα and ERβ.

All currently-known endogenously-formed estrogens are steroids with their *A*-ring being aromatic. Based on the results from **AIM 1A**, *i.e.* the computational analysis of the binding characteristics of aromatic estrogens for human ERα and ERβ, we hypothesized that some of the non-aromatic androgen metabolites or precursors with hydroxyl groups at the C-3 and/or C-17 positions may also be able to bind ERα and ERβ with relatively high binding affinities, and thereby may serve as non-aromatic endogenous ER ligands. Based on this hypothesis, I employed computational molecular modeling tools coupled with *in vitro* ER-binding assays, ER-driven reporter assays, and cell proliferation assays, and characterized the interactions of several non-aromatic endogenous steroids with the human ERα and ERβ. The results of this part of the study led to the discovery that some

of the non-aromatic androgen derivatives that are preferentially formed in men can serve as male-specific estrogens.

AIM 1C: To determine the three dimensional structural characteristics of the interactions of E_2-based C-7α derivatives with human ERα and ERβ.

ER pure antagonists are useful in the treatment of ER-positive human breast cancer refractory to tamoxifen. ER pure antagonists, such as ICI-172,780 that have a long linear side chain attached to the C-7α position of their E_2 core, can displace helix 12 of the ER LBD and prevent dimerization and activation of the receptor. So we hypothesized that estrogen analogs with a shorter but bulky side chain attached to the C-7α position of E_2 may be ER antagonists with more stable steric structures. We designed and synthesized nine of them and studied their interactions with human ERα by using molecular docking analysis coupled with *in vitro* ER binding assays, ER-driven reporter assays, and cell proliferation assays.

SPECIFIC AIM 2: To study the binding interactions of E_2 with a novel estrogen binding protein, PDIp.

Recently, our laboratory identified an intracellular protein called pancreas-specific protein disulfide isomerase (PDIp) as a novel intracellular estrogen binding protein. The structure of its estrogen binding site is not known at present. Based on what

we learned from **SPECIFIC AIM 1** on the three-dimensional interactions of estrogens with ERs, I then used computational molecular modeling methods to predict the binding site structure of PDIp for the endogenous estrogen, E_2. Its predicted binding site structure was then confirmed using a series of biochemical experiments (performed by another researcher in Dr. Zhu's lab).

CHAPTER THREE

MATERIALS AND METHODS

CHEMICALS AND REAGENTS

Estrone (E_1), 17β-estradiol (E_2), and all non-aromatic steroids were obtained from Steraloids (Newport, RI). The non-aromatic steroids selected for testing in the present study all contained hydroxyl groups at their C-3 and/or C-17 position, which are critical for them to potentially form C-3 and C-17 hydrogen bonds with ERs. [^{3}H]E_2 (specific activity of 115 Ci/mmol), [^{3}H]methyltrienolone (specific activity of 85 Ci/mmol), and non-radiolabeled methyltrienolone were obtained from PerkinElmer (Waltham, MA). The recombinant human ERα, ERβ, and AR proteins were obtained from Invitrogen (Carlsbad, CA). According to the supplier, the purities of the human ERα, ERβ, and AR proteins were higher than 75%. Hydroxylapatite was obtained from Calbiochem (through EMD Biosciences, Inc. San Diego, CA).

Eagle's modified minimum essential medium (EMEM, phenol red-free) and RPMI-1640 medium were obtained from Sigma Chemical Co. (St. Louis, MO). Fetal bovine serum (FBS) used in cell culture was purchased from Hyclone Corporation (Logan, UT). The charcoal-stripping method was employed to remove the endogenous estrogens present in the serum by using dextran-coated charcoal (Sigma Chemical Co., St. Louis, MO) as described earlier (Liu and Zhu, 2004). The plasmid containing pGL-basic + ERE (estrogen response element) + E1b + luciferase was a gift from Dr. Carolyn L. Smith at Baylor College of Medicine (Houston, TX). The plasmid containing ARE (androgen response element) + luciferase was kindly provided by Dr. Benyi Li at the

University of Kansas Medical Center (Kansas City, KS). The renilla plasmid used in the ARE-based reporter assay was purchased from Promega (Madison, WI). Lipofectamine 2000 was purchased from Invitrogen (Carlsbad, CA) and the luciferase assay system was obtained from Promega (Madison WI).

Specific rabbit antibodies against a number of proteins were used in this study, and they were obtained from the following sources: PDI was from Sigma-Aldrich (catalog No. P7372, dilution of 1:2000 for western blotting), ERα from Santa Cruz (Santa Cruz, CA, sc-543, 1:200), and ERβ from Invitrogen (Carlsbad, CA, 51-7700, 1:100). The mouse anti-PDIp antiserum (dilution of 1:2500 for Western blotting) was raised in our laboratory. The human pancreatic tissue specimen was obtained from the National Disease Research Interchange (catalog No. 0060960-13).

ERα AND ERβ BINDING ASSAYS

ERα and ERβ competitive binding assays were performed according to the method described in our recent study (Zhu et al., 2006). The ER binding buffer used for dilution of the receptor preparations consisted of 10% glycerol, 2 mM dithiothreitol, 1 mg/mL Bovine Serum Albumin, and 10 mM Tris–HCl (pH 7.5). The ERα washing buffer contained 40 mM Tris-HCl and 100 mM KCl (pH 7.4), but the ERβ washing buffer contained only 40 mM Tris-HCl (pH 7.5). The 50% (*v/v*) hydroxylapatite (HAP) slurry was prepared by using the 50 mM Tris-HCl solution (pH 7.4). The reaction mixture contained 50 μL of varying concentrations of the test compound in the ER binding buffer, and 45 μL of [^{3}H]E_2 solution (at 22.22 nM) with a final [^{3}H]E_2 concentration of 10 nM. Then 5 μL of ERα or ERβ protein (at final concentration of 2.5 nM) was added and mixed gently. Nonspecific binding by [^{3}H]E_2 was determined by addition of a 400-fold excess non-radioactive E_2 (at 8 μM with final concentration 4 μM). The binding mixture was incubated at room temperature for 2 h. At the end of the incubation, 100 μL of the HAP slurry was added and the tubes were incubated on ice for 15 min with three times of brief vortexing. An aliquot (1 mL) of the washing buffer was added. The tubes were vortexed, centrifuged at 10,000 *g* for 1 min at 4^{o}C and the supernatants were discarded. This wash step was repeated twice. The HAP pellets were then resuspended in 200 μL ethanol and transferred to scintillation vials for measurement of the ^{3}H-radioactivity in a liquid scintillation counter (Packard Tri-CARB 2900 TR, Downers Grove, IL).

The IC_{50} value for each competing ligand was calculated according to the

sigmoidal inhibition curve, and the relative binding affinity (*RBA*) was calculated against E_1 or E_2 using the equation (2):

$$RBA = \frac{IC_{50} \text{ for } E_1 \text{ (or } E_2)}{IC_{50} \text{ for the test compound}} \qquad (2)$$

ANDROGEN RECEPTOR BINDING ASSAY

The same procedures as described above for the ER binding assay were used for assaying the relative AR binding affinity of various non-aromatic steroids. The nonspecific binding by [^{3}H]methyltrienolone was determined by addition of a 400-fold concentration (8 μM) of the non-radioactive methyltrienolone.

CULTURE OF HUMAN CANCER CELL LINES

The ER-positive human breast cancer cell line MCF-7, the ER-negative human breast cancer cell line MDA-MB-231 and the ER-positive human prostate cancer cell line LNCaP were obtained from ATCC (Manassas, VA) and cultured according to the instructions of the suppliers under 37^{o}C and 5% CO_2. For cell proliferation assay with non-aromatic steroids, cells were cultured with medium containing 10% dextran-coated charcoal (DCC)-stripped FBS for 3 days and then were seeded in 96-well plates with 10^4 cells/well. Cells were treated on the second and the fifth days. On the eighth day after seeding the cells, the cell density was determined by using the crystal violet staining method (Liu and Zhu, 2004). The absorbance values of each well were measured at 560 and 405 nm with a UVmax microplate reader (Molecular Device, Palo Alto, CA) and the difference in the absorbance values at these two wavelengths were used to represent the cell density. For cell proliferation assay with newly-synthesized E_2-based C-7α derivatives, MCF-7 and MDA-MB-231 were cultured and treated in medium containing normal FBS.

REPORTER ASSAYS

ERE-based reporter assay. MCF-7 cells were cultured in medium containing dextran-coated charcoal-stripped FBS for 3 days. Then the cells were seeded in 24-well plates with 2×10^5 cells/well. After 24 h, the cells were transfected with a plasmid containing pGL-basic + ERE + E1b + luciferase by using lipofectamine 2000. After another 24 h, various concentrations of compounds were added to each well. Cells were harvested 20 h later and used for luciferase assay by using the luciferase assay system. Protein concentration of each well was quantified with the protein assay reagent (Bio-Rad, Hercules, CA). The lucifierase activity in each well was normalized by the protein concentration. Notably, in this ERE-based luciferase reporter assay, little or no baseline luciferase expression level was detected when human ERα was not expressed in ER negative cells regardless of whether E_2 was present or not (Peterson et al., 2007).

ARE-based reporter assay. LNCaP cells were seeded in 24-well plates at a density of 6×10^4 cells/well. After 24 h, the cell culture medium was replaced with a medium containing 10% FBS that was pre-treated with dextran-coated charcoal to remove endogenous hormones. After an additional 24 h, the ARE-Luciferase and renilla plasmids were transfected into LNCaP cells with lipofectamine 2000 according to manufacturer's instructions. Twenty-four hours later, cells were treated with each of the testing compounds. The firefly luciferase and renilla luciferase activities were determined 24 h later using a dual-luciferase system obtained from Promega (Madison, WI).

CONSTRUCTION OF PLASMIDS

Human PDIp coding sequence was cloned from cDNA ordered (ATCC no 6706839) into pET-19b vector at the sites of 5'-NdeI/XhoI-3' without the signal peptide and also cloned into the pcDNA3.1 vector with the signal peptide at the sites of 5'-HindIII/XhoI-3'. The plasmids for the expression of histidine-tagged truncated PDIp proteins (*a-b, b-b', b'-x-a'-c* fragments) were constructed by cloning the corresponding cDNA sequences of the fragments into a modified pET-19b vector (as described earlier (Fu and Zhu, 2009)). Purification of the recombinant histidine-tagged proteins from *E. coli* was performed as described earlier (Fu and Zhu, 2009; Fu and Zhu, 2010). Fragment *b, b', x-a'-c* were cloned into a modified pGEX-4T-1 vector containing an introduced NdeI site at 5'-NdeI/SalI-3' and expressed as GST-tagged fusion proteins, which were purified by using Glutathione Sepharose 4 Fast Flow (GE Healthcare, Waukesha, WI). Site-directed mutagenesis was performed as described earlier (Fu and Zhu, 2010).

OVEREXPRESSION OF PDIP IN MAMMALIAN CELLS

Cos-7 cells were obtained from ATCC (Manassas, VA) and cultured according to the instructions of the suppliers. The plasmids pcDNA3.1 and pcDNA3.1-PDIp were used for overexpression of PDIp in cos-7 cells. Lipofectamine 2000 and Opti-MEM I reduced serum medium (both obtained from Invitrogen) were used for transfection according to manufacturer's instructions. Cells were harvested 36 h after transfection and used for [^{3}H]E_2-binding activity measurements, protein concentration determination, western blotting, or protein purification.

PROTEIN PURIFICATION OF PDIP FROM COS-7 CELLS

PDIp recombinant proteins over-expressed in cos-7 cells were partially purified using the following steps: Cos-7 cell pellets from 6-well plates overexpressing PDIp were re-suspended in 10 mM sodium phosphate buffer (pH 7.4) plus protease inhibitors. After sonication for 5 min on ice and centrifugation (12,000g for 16 min at 4°C), the supernatants were then loaded onto the Superdex 200 10/300 GL column (GE Healthcare, Waukesha, WI) for size exclusion chromatography (SEC), which was performed on an ÄKTA FPLC system and eluted with 10 mM sodium phosphate buffer (pH 7.4), at a flow rate of 0.6 ml/min at room temperature. The fractions were collected at 1 ml/tube in the ice bath and subjected to protein concentration assay, [^{3}H]E_2-binding assay and native gel electrophoresis followed by western blotting analysis.

[^{3}H]E_2-BINDING ASSAY FOR PURIFIED PDIP PROTEIN

We explored the desalting procedure to separate free [^{3}H]E_2 and protein-bound [^{3}H]E_2 as described earlier (Fu et al., 2008) with modifications. Each purified protein, or each fraction from sex exclusion chromatography (SEC) and ion exchange chromatography (IEC), was incubated with 4.5 nM [^{3}H]E_2 (final concentration) in 10 mM sodium phosphate buffer (pH 7.4) at 4°C overnight. The sample (100 μL) was desalted using a PD miniTrap G-25 column (obtained from GE healthcare) that was pre-equilibrated with 10 mM sodium phosphate buffer (pH 7.4, 0.15 M NaCl). Eluted fractions collected from 0.5 to 1.1 mL were collected and mixed with 5-volumes of scintillation cocktail (Fisher Scientific, Pittsburgh, PA) for radioactivity measurement on a liquid scintillation counter (Perkin Elmer, Waltham, MA). For saturation experiments, increasing concentrations of [^{3}H]E_2 were present during the incubation, and the same assay method as described above was used. The nonspecific binding was determined in the presence of 10 μM excess cold E_2.

QUANTITATIVE STRUCTURE-ACTIVITY RELATIONSHIP (QSAR) STUDY

All calculations described in the present study were carried out using the *SYBYL* molecular modeling program (V7.1, Tripos Inc., St. Louis, MO) installed on a Dell Precision 690 workstation running Red Hat Enterprise Linux WS4.0 (Red Hat Inc. Raleigh, NC) operating system.

Molecular models and structural alignment. A total of 58 non-aromatic endogenous steroids were used in this study. Note that 5α-androstan-3β-ol-16,17-dione-16-oxime was excluded for alignment because of its unique side chain, whereas 4-androsten-3β,17β-diol and 4,9(11)-androstadien-17β-ol-3-one were considered to be outliner compounds for ERα and ERβ, respectively. All molecules were constructed using the building tools of the *SYBYL7.1* molecular modeling software. The geometry of each molecule was optimized using the standard Tripos force field with the conjugate-gradient minimization to an energy change convergence criterion of 0.001 kcal/mol. All atomic partial charges were computed using the Gasteiger-Marsili method. All molecules were aligned by using 5-androsten-3β,17β-diol (compound ***1***) as template with the rigid-body least-squares fitting method. After alignment, the molecules were placed in a 3-D cubic lattice with 2 Å spacing. Any calculated steric and electrostatic energies that were >30 kcal/mol were truncated to this value.

3-D QSAR/CoMFA analysis. For 3-D QSAR/CoMFA analysis, the method of

partial least squares regression was used to analyze the compounds by correlating the percent inhibition of [^{3}H]E_2 binding for each compound and the CoMFA fields. 4-Androsten-3β,17β-diol and 4,9(11)-androstadien-17β-ol-3-one were the outline compounds for ERα and ERβ, respectively, and were excluded in the analysis. The optimum number of principal components (PCs) was determined by the leave-one-out cross-validation procedure. In this method, each compound was systematically excluded once from the data set, after which its activity was predicted by a model derived from the remaining compounds. Then the q^2 value (*i.e.*, the cross-validated r^2 value) was calculated based on these predictions. This q^2 value measures a model's predictive ability. By setting the number of PCs to this optimum number, the final partial least squares (PLS) analysis was carried out without cross-validation with correlation coefficient r^2. This r^2 tells the model's goodness of fit to the activity data of the compounds. A model for which $r^2 > 0.9$ and $q^2 > 0.4$ is normally considered to be predictive.

MOLECULAR DOCKING AND SIMULATION STUDY

Selection of the human ERα and ERβ 3-D structures as templates. The use of molecular docking approach to study the binding interaction of a ligand with its receptor protein is usually based on the known 3-D structure of the receptor protein. As listed in **Table 1**, at present, about a dozen crystal structures of the ligand binding domains (LBDs) of the human ERα and ERβ are available in the PDB database (discussed by (Pike et al., 2000). While some of the receptor proteins are in complex with agonists (such as E_2 or diethylstilbestrol), others are in complex with antagonists (such as raloxifene and tamoxifen). We compared the ERα structures in complex with three ER agonists, namely, E_2 (PDB codes 1ERE and 1A52), DES (PDB code 3ERD), and genistein (GEN) (PDB code 1X7R) by superimposing these structures on each other. The Root Mean Square (RMS), a parameter that is commonly used to reflect the average distance between the same atoms in different structures, was found to be only approximately 0.5 Å for these ERα structures when they were complexed with different agonists. This indicates that the receptor structures resolved by different research groups have very similar overall structures.

Table 1 Summary of current structures of ER with various ligands listed in chronological order of publication.

ER isoform	Ligands	PDB code	References	Comments
ERα-LBD	E_2	1ERE	(Brzozowski et al. 1997)	First steroid receptor structure with agonist bound
ERα-LBD	Raloxifene (RAL)	1ERR	(Brzozowski et al. 1997)	First ER structure with SERM bound, a model for receptor antagonism
ERα-LBD	E_2	1A52	(Tanenbaum et al. 1998)	Similar structure as 1ERE
ERα-LBD	DES/peptide	3ERD	(Shiau et al. 1998)	First ER structure with agonist and coactivator peptide bound
ERα-LBD	4-hydroxyl tamoxifene (OHT)	3ERT	(Shiau et al. 1998)	Ligand induces a similar orientation in H12 as 1ERR
ERβ-LBD	RAL	1QKN	(Pike et al. 1999)	First ERβ structure with antagonist bound
ERβ-LBD	ERB041	1X7B	(Manas et al. 2004)	ERβ structure with agonist bound
ERα-LBD	Genistein (GEN)	1X7R	(Manas et al. 2004)	ERα structure with agonist bound
ERβ-LBD	GEN	1X7J	(Manas et al. 2004)	ERβ structure with partial agonist bound. GEN has 40 fold higher binding affinity to ERβ than ERα

Energy minimization and molecular docking were performed with *InsightII* modeling program (Version 2005, Accelrys Inc. San Diego, CA) installed on a Dell Precision 690 workstation running Red Hat Enterprise Linux WS4.0 (Red Hat Inc. Raleigh, NC) operating system. Consistent valence force field was used for energy minimization.

ERα. The structures of six non-aromatic male-specific steroids were built with the *Builder* module in *InsightII* and minimized with the *Discover* module. The ligands were superimposed onto E_2 which was taken from the the *x*-ray crystal structure of ERα in association with E_2 (PDB code: 1ERE) (Brzozowski et al., 1997). The water molecule in the binding pocket forming a hydrogen bond with the 3-OH group of E_2 was also included. All other water molecules were deleted from the crystal structure. Energy minimization was carried out with the the Polak and Ribiere conjuate gradients method in the *Discover* module in *InsightII* until the final convergence criterion reached the 0.001 kcal/molÅ. The heavy atoms of the receptor were fixed during the minimization.

Because the crystal structure of human ERα in complex with a full antagonist is not available, the crystallographic structure of ERα in complex with RAL (PDB code: 1ERR) (Brzozowski et al., 1997), which is a partial agonist/antagonist, was thus used as a template for the docking study of ICI-182,780 and the newly synthesized ER antagonists. The structures of ICI-182,780 and ER antagonists were first built using the *Builder* module and then minimized with the *Discover* module of the *InsightII*. In brief, the

flexible docking procedures were carried out using the *Simulated Annealing Docking* method in *Affinity* module of *InsightII*. The binding pocket was defined to include all residues within the 7-Å reach of the original ligand RAL. A combination of *Monte Carlo* and *simulated annealing* methods was used to explore all possible conformations of the ligands. One hundred conformations were obtained and the one with the lowest potential energy was chosen for further minimization using the *Standard Dynamics Cascade* protocol in the *Discovery Studio.* The backbone of the protein and its key residues in the binding pocket (namely, E353, R394 and H524) were fixed during the docking procedures.

ERβ. The *x*-ray crystal structure of ERβ in complex with ERB-041 (PDB code: 1X7B) (Manas et al., 2004) was used as template for docking its binding interaction with E_2. The flexible docking procedures were carried out using the *Simulated Annealing Docking* method in the *Affinity* module of *InsightII*. The binding pocket was defined to include all residues within the 7-Å reach of the binding ligand ERB-041. The water molecule in the binding pocket was also included, which forms a hydrogen bond with one of the hydroxyl groups of ERB-041. All other water molecules were deleted from the crystal structure. A combination of *Monte Carlo* and *simulated annealing* methods was used to explore all the possible binding conformations of E_2. One hundred conformations were obtained and the one with the lowest potential energy was chosen for further minimization by *Discover*. The other ligands were superimposed onto E_2 in the minimized structure and energy minimization was carried out with the Polak and Ribiere

conjugate gradients method in the *Discover* module of *InsightII* until the final convergence criterion reached the 0.001 kcal/molÅ. The heavy atoms of the receptor were fixed during the minimization.

Calculation of binding energy value. With the *InsightII* program, $\Delta E_{\text{binding}}$ was calculated by using the *Evaluate_Intermolecular_Energy* function of the *Docking* module. The ΔE value includes two components, namely, the van der Waals (VDW) interaction energy (ΔE_{VDW}) and the Coulomb interaction energy (*i.e.*, electrostatic interaction energy $\Delta E_{\text{Coulomb}}$). Hydrogen bond energy was included as part of the Coulomb interaction energy. Equation (3) is commonly used to calculate the total interaction energy $\Delta E_{\text{binding}}$:

$$\Delta E_{\text{binding}} = \Delta E_{\text{VDW}} + \Delta E_{\text{Coulomb}} \quad (3)$$

Theoretically, $\Delta E_{\text{binding}}$ can be used to reflect the experimentally-determined log*RBA*, as expressed in equation (4) below:

$$\Delta E_{\text{binding}} = RT \ln (K_{\text{d}}) \approx RT \ln (IC_{50}) = \text{a log}RBA \quad (4)$$

Here, a higher value of ΔE would correlate with a lower binding affinity. A higher degree of correlation between $\Delta E_{\text{binding}}$ and log*RBA* would mean that the computational docking model has a higher degree of accuracy to predict a compound's relative binding affinity for the ERs.

HOMOLOGY MODELING OF HUMAN PDIP *B-B'* FRAGMENT

Since the x-ray structures of human PDIp *b-b*' fragment are not available at present, the PDI *b-b*' domain structure (PDB code: 2k18) (Denisov et al., 2009) was used as a template to build the structure of human PDIp *b-b*' fragment. Protein sequence alignment showed that the sequence identity between the PDIp *b-b*' fragment and PDI *b-b*' fragment is approximately 40%. The *Homology Modeling* module of *Insight II* was used to generate the 3-D structure model for PDIp *b-b*' domain. The side chain was manually optimized to minimize the intramolecular bump and then the protein structure was further optimized by the *Discover* module of *Insight II*.

BINDING SITE DETERMINATION AND MOLECULAR DOCKING FOR HUMAN PDIP *B-B*' FRAGMENT

The binding sites on the PDIp *b-b*' domain model for E_2 were determined by using the *Active-Site-Search* function in the *Binding-Site* module of *Insight II*. The site-open-size parameter was set at 5 Å and the site-cut-off-size parameter was set at 150 $Å^3$. The binding pocket included amino acid residues within 5 Å around the candidate binding site. The *Simulated Annealing* docking method in the *Affinity* module was used to dock E_2 into the candidate binding pockets. One hundred docking modes were calculated and the ones with the lowest binding energy were selected for further minimization.

CHAPTER FOUR

STRUCTURAL CHARACTERIZATION OF THE BINDING INTERACTIONS OF VARIOUS ESTROGEN METABOLITES WITH HUMAN ESTROGEN RECEPTOR ALPHA AND BETA SUBTYPES

INTRODUCTION

The endogenous estrogens are a group of vitally important female sex hormones with diverse biological functions. Disruption of their actions contributes to the pathogenesis of a number of disease states in humans, including the malfunctions of reproductive functions (Abaci et al., 2009; Ma, 2009; Rogan and Ragan, 2003), development of breast cancer (Brody et al., 2007; Falck et al., 1992; Henderson et al., 1991; Lewis, 1994; Rudel et al., 2007), and many other conditions (Colborn et al., 1993; Diamanti-Kandarakis et al., 2009). Undoubtedly, it is of considerable scientific interest to develop the ability to predict, beforehand, the estrogenic potency and efficacy of a chemical. Compared to the widely-used methods such as receptor binding assay, receptor activity assay, and crystallography, computational molecular modeling methods have the potential advantages of low cost and high speed. Progress in this area of research will help develop the ability to predict and/or identify new environmental estrogens so that the general public can be informed and avoid potential dangerous exposure to these chemicals.

In an earlier study (Zhu et al., 2006), we compared the relative binding affinity (*RBA*) of some 50 estrogen derivatives (mostly the endogenous metabolites of 17β-estradiol, E_2) for the human estrogen receptor α (ERα) and ERβ. These estrogen derivatives, while sharing the same core structure as E_2 with only one or two small functional group(s) added (their structures are shown in **Figure 3**), have vastly different *RBA*s for human ERα and ERβ, ranging from having a similar binding affinity as E_2 to

having little or no binding affinity at all (**Table 2**). In the present study, these well-characterized E_2 derivatives were used as model compounds to study their binding interactions with human ERα and ERβ using the molecular docking approach. There are two reasons why we chose these structurally-similar estrogen derivatives as model compounds. First, although the crystallographic structure of ERα in complex with E_2 is known, the interactions of the receptor with various E_2 metabolites are actually not known. Studying the interactions of these compounds with human ERα and ERβ may shed light on how a small modification in the E_2 structure can drastically disrupt its binding interactions with these two ERs. These results, in turn, may help us to better understand the detailed structural characteristics of the binding interaction of an estrogen with various amino acid residues in the LBDs of ERs. Second, we have successfully used the QSAR approach in an earlier study (Zhu et al., 2006) to predict the binding affinities of these estrogen derivatives for human ERs. However, as mentioned above, the drawback of the QSAR models is their lack of ability to predict the binding affinity of structurally-diverse chemicals. Therefore, in the present study, we sought to use the molecular docking approach to determine whether it could predict the binding interactions with the human ERα and ERβ as well as the relative binding affinities of these estrogen derivatives. Success of this approach may provide a useful platform for the future development of an automated docking-based computational approach that can screen many environmental compounds for their potential human ER-binding affinities.

The experimental strategies used in this study were as follows: We first evaluated whether the molecular docking method could be used to correctly predict the binding interaction of a ligand with the ligand binding domain (LBD) of the human ERα. Next, using the validated molecular docking method, we determined the binding interactions of a total of 27 representative E_2 metabolites/derivatives (structures shown in **Figure 3**) with the LBDs of human ERα and ERβ. Lastly, we explored ways to achieve a better prediction of the binding affinity of estrogen derivatives to ERs by modifying the calculation method for the binding energy (ΔE) values.

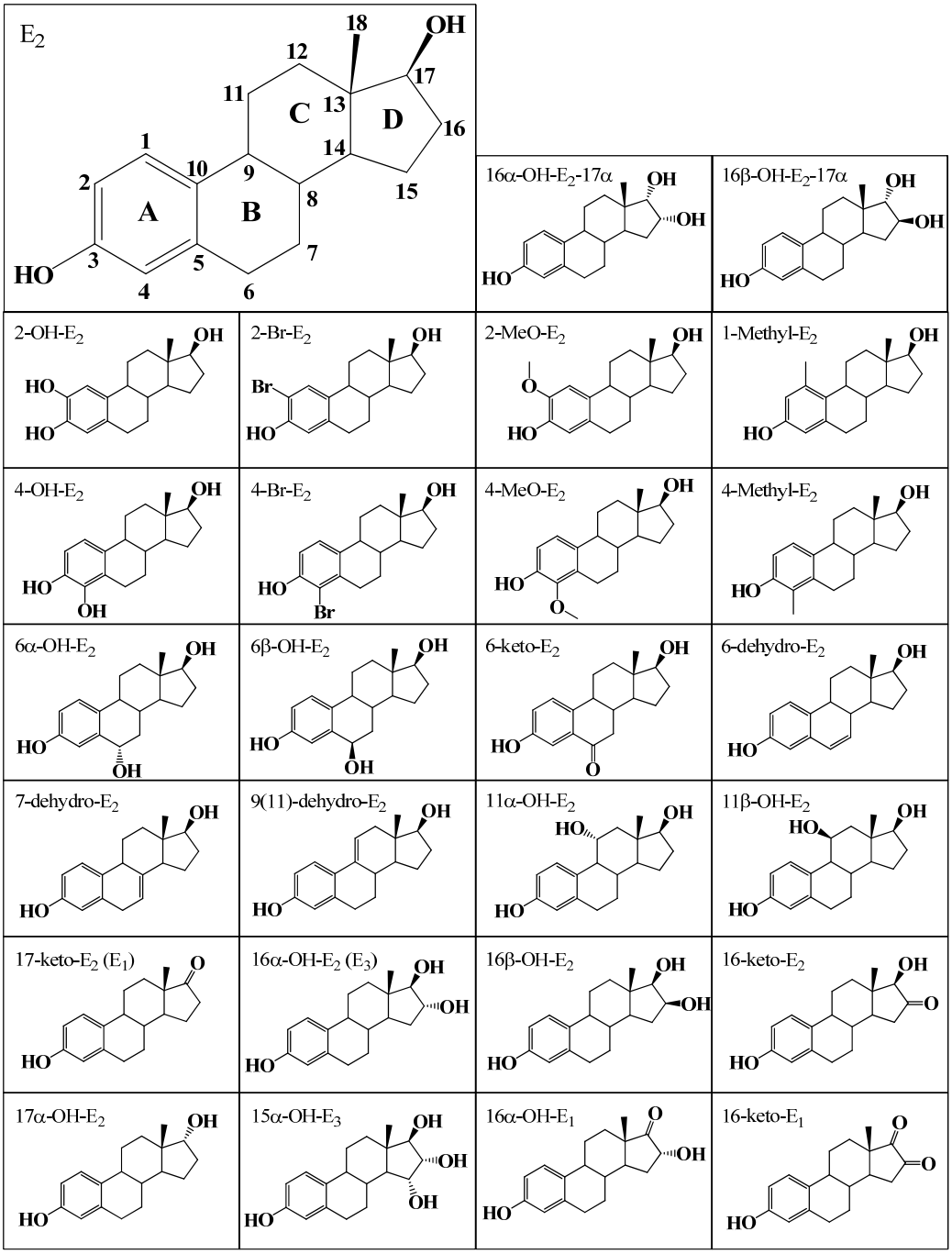

Figure 3 The chemical structures of E_2 and the 26 E_2 derivatives. The number of each carbon is labeled next to the atom in the E_2 structure. The names of the E_2 derivatives are shown in the upper left corner of each frame.

Table 2 Hydrogen bond lengths (Å) and calculated van der Waals interaction energy (ΔE_{VDW}, kcal/mol) and Coulomb interaction energy ($\Delta E_{Coulomb}$, kcal/mol) between estrogen derivatives and ERα or ERβ. Hydrogen bond lengths were quantified by measuring distances between the hydrogen atoms of the 3-hydroxyl group of estrogen derivatives and the O_ε of ERα-E353 or ERβ-E305, between oxygen atoms of the 3-hydroxyl group of estrogen derivatives and the H_η of ERα-R394 or ERβ-R346 and between the hydrogen atoms of 17-hydroxyl group of estrogen derivatives and N_δ of ERα-H524 or ERβ-H475. For the *D*-ring derivatives, two hydrogen bond lengths were listed. The first is formed by hydrogen atoms of 17-hydroxyl groups and the second is formed by hydrogen atoms of 16-hydroxyl groups. Relative binding affinity (*RBA*) was also listed for comparison.

Estrogen derivatives names		ERα						ERβ					
		RBA	E353	R394	H524	ΔE_{VDW}	$\Delta E_{Coulomb}$	*RBA*	E305	R346	H475	ΔE_{VDW}	$\Delta E_{Coulomb}$
A-ring	E_2	100	1.42	2.02	1.96	-53.37	-23.58	100	1.62	3.14	1.99	-52.06	-19.34
	2-OH-E_2	22	1.46	2.06	1.94	-51.40	-35.32	35	1.64	3.14	2.04	-52.86	-25
	2-Br-E_2	4	1.69	2.34	1.77	-39.88	-10.09	0.35	2.00	3.43	1.91	-40.03	-12.82
	2-MeO-E_2	2.2	2.59	2.52	1.83	-37.31	-12.57	1.4	2.26	3.54	1.87	-36.46	-14.6
	1-Methyl-E_2	14	1.60	2.03	2.0	-52.83	-16.04	8	2.05	3.30	2.05	-40.57	-14.05
	4-OH-E_2	70.4	1.44	2.14	1.94	-51.32	-25.73	56	1.62	3.19	1.97	-52.86	-22
	4-Methyl-E_2	8.9	1.42	2.24	1.87	-39.32	-22.95	35	1.79	3.42	1.83	-43.43	-18
	4-Br-E_2	7.1	1.45	2.35	1.87	-38.74	-22.56	35	1.71	3.40	1.82	-38	-18.5
	4-MeO-E_2	1.6	1.37	3.03	1.74	-24.34	-26.01	1	1.74	3.30	1.78	-30.57	-18.71
B/*C*-ring	6α-OH-E_2	5.6	1.44	2.0	2.02	-50.8	-27.88	3.5	1.65	3.2	1.93	-50.55	-19.3
	6β-OH-E_2	1.4	1.4	1.98	2.01	-47.37	-30.77	1.6	1.56	3.1	1.99	-50.96	-20.76
	6-Keto-E_2	70.4	1.45	2.06	2.0	-52.26	-31.27	56	1.61	3.2	1.95	-50.88	-20.32
	6-Dehydro-E_2	50	1.46	2.03	2.0	-51.17	-28.45	87	1.59	3.1	2.02	-52.8	-19.74
	7-Dehydro-E_2	141.8	1.44	2.02	1.93	-51.08	-28.92	113	1.58	3.12	2.12	-54.79	-19.11
	9(11)-Dehydro-E_2	87	1.44	1.98	2.03	-49.36	-27.85	119	1.61	3.09	1.98	-52.85	-19.82
	11α-OH-E_2	0.01	1.44	2.01	1.87	-49.83	-29.41	0.01	1.63	3.14	1.94	-51.13	-22.09
	11β-OH-E_2	0.01	1.44	2.01	1.97	-51.02	-27.44	0.01	1.62	3.14	1.98	-52.48	-20.26
D-ring	17-Keto-E_2 (E_1)	10	1.43	2.02	2.09	-50.48	-26.79	2	1.59	2.59	-	-51.17	-13.77
	16α-OH-E_2 (E_3)	11.2	1.43	1.99	2.01/2.0	-50.68	-32.45	35.4	1.59	3.11	2.05/3.81	-51.06	-16.69
	16β-OH-E_2	63	1.43	1.98	2.01/2.0	-50.49	-30.35	50	1.56	3.05	3.09/1.98	-51.37	-21.67
	16-Keto-E_2	10	1.41	1.94	2.09	-49.51	-28.06	17.8	1.70	2.6	2.01	-54.55	-14.89
	17α-OH-E_2	22.4	1.44	2.02	2.86	-50.45	-25.21	3.2	1.58	3.07	3.43	-51.81	-16.36
	15α-OH-E_3	4	1.43	1.98	1.98	-50.92	-34.71	2.5	1.58	3.11	2.05	-52.64	-18.09
	16α-OH-E_1	20	1.43	2.01	2.08	-51.56	-31.27	35.4	1.6	3.07	-	-50.71	-18.34
	16-Keto-E_1	1.8	1.41	1.95	2.11	-50.38	-27.18	10	1.54	2.52	-	-52.02	-11.63
	16α-OH-E_2-17α	70.9	1.43	2.01	3.02/1.99	-51.44	-29.66	79.5	1.58	2.57	3.87/2.0	-51.67	-20.89
	16β-OH-E_2-17α	0.9	1.43	2.01	3.45/1.96	-50.69	-28.67	12.6	1.55	3.01	3.74/2.02	-51.74	-21.52

RESULTS AND DISCUSSION

Validation of the molecular docking method

The 3-D structure of the ligand binding domain (LBD) of human ERα in complex with diethylstilboestrol (DES), a non-steroidal estrogen, has been previously determined (PDB code: 3ERD). To determine whether the computational docking approach can produce the same binding mode for DES as observed in the earlier crystallographic study, we used another crystal structure of the human ERα LBD in complex with E_2 (PDB code: 1ERE) as a template and then docked DES into this ERα structure. The docking model of ERα-DES complex was then compared with the known crystal structure of the ERα-DES complex (PDB code: 3ERD) by superimposing these two structures.

As shown in **Figure 4A**, the docked structure of ERα-DES complex has nearly the same overall structure as the known 3-D structure of this complex. The overall binding conformation of the DES ligand matched exactly the same as the known crystal structure. Also, both structures showed that the two aromatic rings of DES have the same steric orientation, forming four hydrogen bonds with the amino acid residues E353, R394 and H524 in the binding pocket. These three amino acids have less than 0.4Å RMS between the docked structure and the crystal structure. In addition, several other important amino acid residues in the binding pocket, namely, A350, L346, M343, L525, I424, L402, L391, F404 and L346 also form the same hydrophobic interactions with DES,

and their steric configurations (positions and orientations) are exactly the same in both modeled and crystal structures.

Similarly, by using the same method, we also took the crystal structure of ERα LBD in complex with DES (PDB code: 3ERD) as a template and then docked E_2 into its LBD. The docking results were compared with the known crystal structure of the ERα-E_2 complex (PDB code: 1ERE). As shown in **Figure 4B**, the docking method produced a nearly identical structure of the ERα-E_2 complex compared to the known 3-D structure of this complex. Three identical hydrogen bonds were identified in both docked and known crystal structures, which were formed between the two hydroxyl groups of E_2 and the amino acid residues E353, R394, and H524 in the binding pocket. Also, all hydrophobic amino acids in the binding pocket had nearly the same steric orientation and positioning in these two structures. Altogether, these two examples showed that the docking method that we used predicted the binding mode of a ligand in the LBDs of human ERs with a high degree of reliability and accuracy.

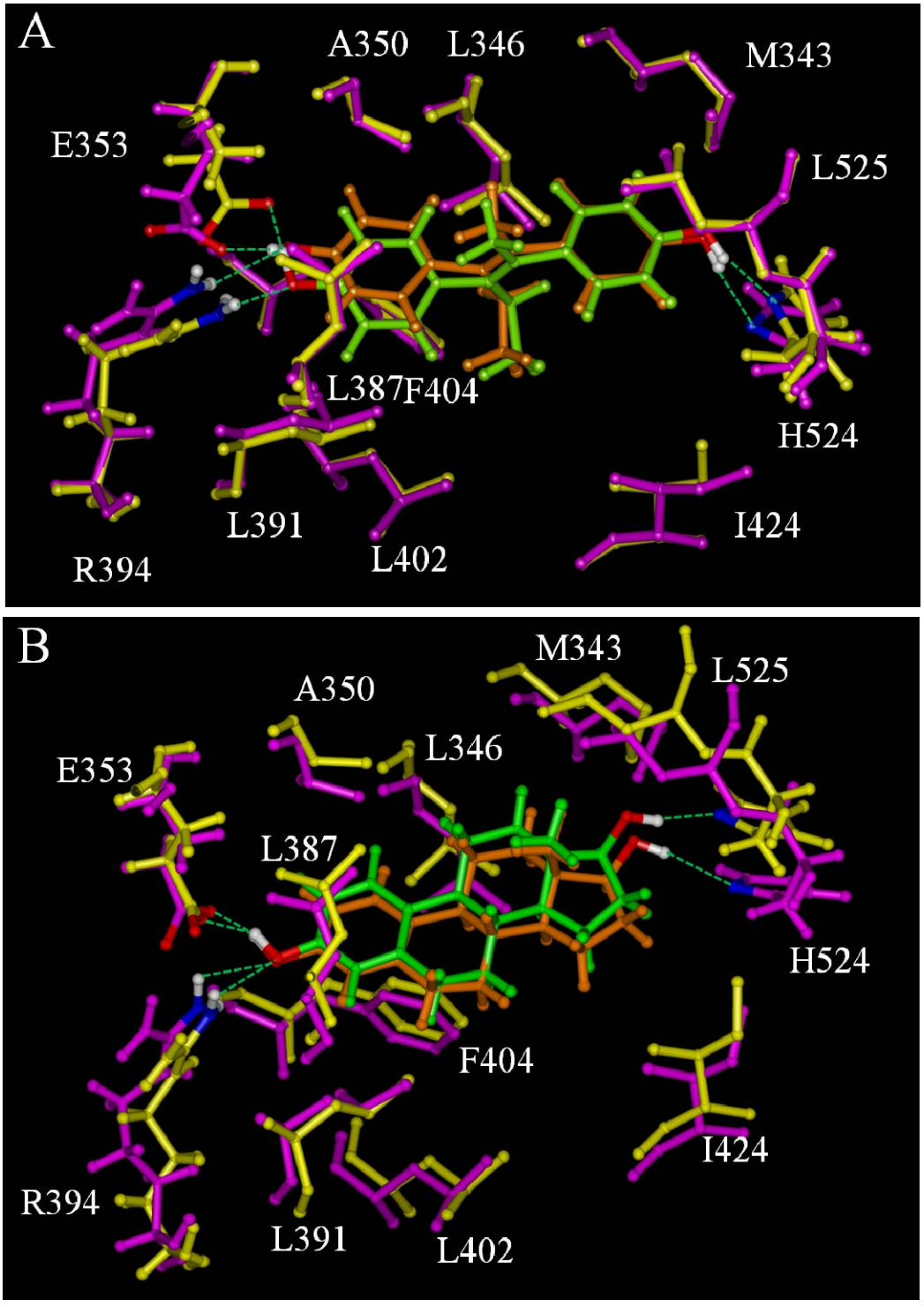
A
A350
L346
M343
E353
L525
L387F404
H524
L391
I424
R394
L402
B
M343
L525
A350
L346
E353
L387
H524
F404
I424
R394
L391
L402

Figure 4 Overlay of docked structure and the crystal structure of ERα LBD in complex with DES or E_2. **A**. Superimposed structures of docking result and the crystal structure of ERα LBD in complex with DES. The known crystal structure of ERα LBD in complex with DES (PDB code: 3ERD) was colored in yellow with DES colored in green. The docked DES was colored in orange and ERα LBD was colored in magenta. **B**. Superimposed structures of docking result and the crystal structure of ERα LBD in complex with E_2. The known crystal structure of ERα LBD in complex with E_2 (PDB code: 3ERE) was colored in yellow with E_2 colored in green. The docked E_2 was colored in orange and ERα LBD was colored in magenta. The green dashes indicated the hydrogen bonds formed. All structures were rendered in ball and stick format. The atoms involved with hydrogen bond formation were colored according to the atom type, i.e. white for hydrogen, red for oxygen, and blue for nitrogen. Hydrogen atoms in other amino acids were not shown.

Prediction of the binding mode of E_2 derivatives in the LBDs of human ERα and ERβ

By using the same docking approach as described above, we docked a total of 27 E_2 derivatives (including E_2 itself) into the LBDs of human ERα and ERβ. These 27 chemicals were selected from a pool of some 50 estrogen derivatives tested in our earlier study (Zhu et al., 2006). They were divided into three groups according to their structural relationship with E_2 (see **Figure 3**): *A*-ring derivatives (9 compounds including E_2 itself), *B*/*C*-ring derivatives (8 compounds), and *D*-ring derivatives (10 compounds). These 27 chemicals all share the same core structure as E_2 with only one or two small functional group(s) added to the steroid core. The purpose of the docking study was to determine how these subtle modifications in the ligand structures can drastically alter the binding conformation and binding energy values (which reflect the binding affinity) of these ligands.

While the crystal structure of ERα LBD in complex with E_2 is available (PDB code: 1ERE), the crystal structure of ERβ LBD in complex with E_2 has not been resolved. Therefore, we chose to use the known crystal structure of the human ERβ LBD in complex with a synthetic ERβ agonist ERB041 (PDB code: 1X7B) as a template to dock E_2 into its binding pocket. We found that E_2 shares a very similar binding mode when it is inside the LBDs of human ERα and ERβ. Hydrogen bonds are formed between the 3- and 17-hydroxyl groups of E_2 with amino acid residues E353, R394, and H524 in ERα and

with E305, R346 and H475 in ERβ (data not shown).

***A*-ring derivatives.** The docking results of various *A*-ring derivatives of E_2 with ERα LBD are shown in **Figure 5**. Overall, the binding modes of these *A*-ring derivatives were very similar to that of E_2. Two hydrogen bonds were formed between their 3-hydroxyl groups and the amino acid residues E353 and R394 in ERα or E305 and R346 in ERβ. A third hydrogen bond was formed between the 17-hydroxyl group of E_2 and ERα-H524 or ERβ-H475. All other hydrophobic amino acids in the binding pocket had nearly the same configuration and thus were not shown in **Figure 5.**

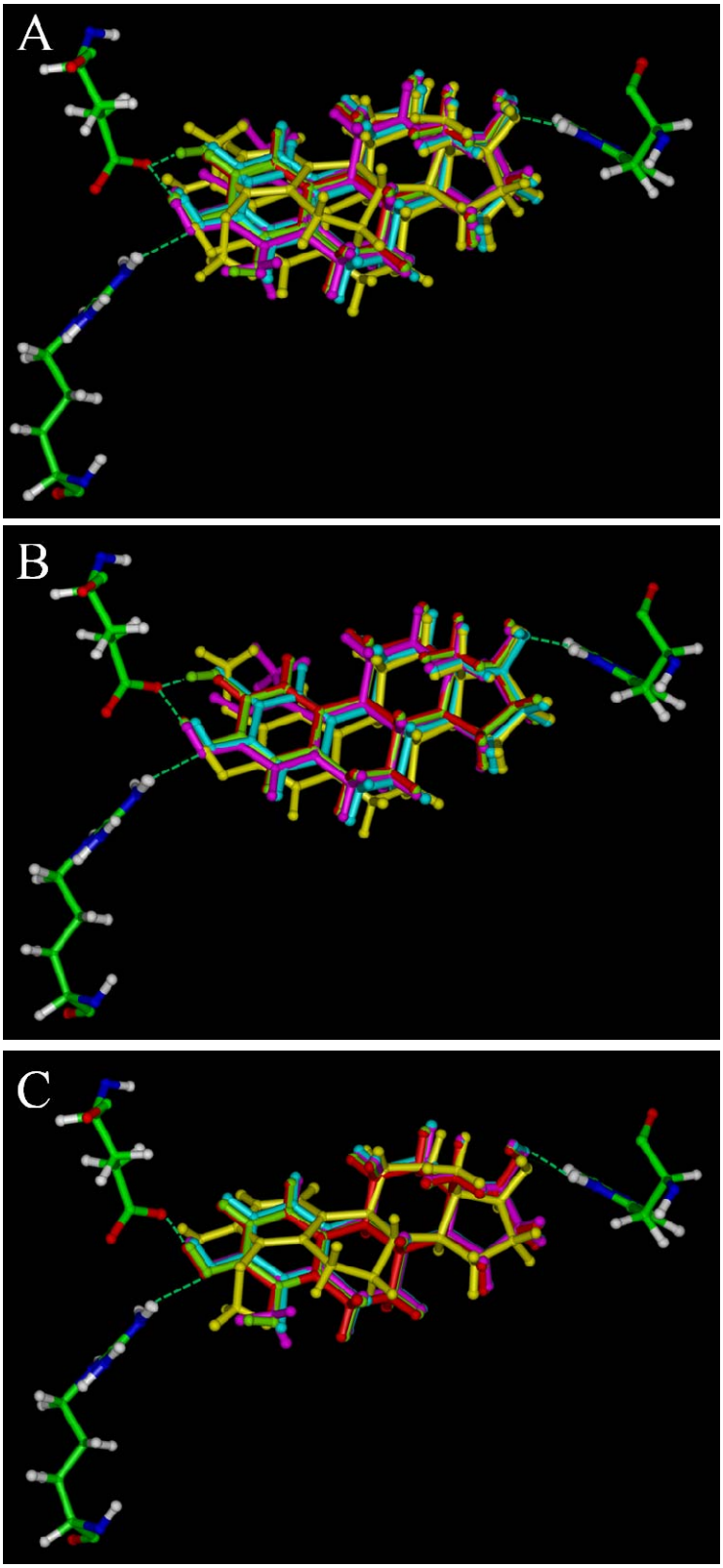
A
B
C

Figure 5 Interactions of *A*-ring derivatives with ERα LBD determined by the molecular docking method. The green dashes indicate the hydrogen bonds formed. All the structures were rendered in ball and stick format. The amino acids were colored according to the atom type, i.e. green for carbon, red for oxygen, blue for nitrogen and white for hydrogen. Among the amino acids in the binding site, only E353, R394 and H524 were shown in this figure. E_2 was colored in red; 1-methyl-E_2 and 4-methyl-E_2 were colored in magenta; 2-OH-E_2 and 4-OH-E_2 were colored in green; 2-Br-E_2 and 4-Br-E_2 were colored in blue; 2-MeO-E_2 and 4-MeO-E_2 were colored in yellow. **A**. Overlay of all the *A*-ring derivatives. **B**. Overlay of E_2, 1-methyl-E_2, 2-MeO-E_2, 2-OH-E_2 and 2-Br-E_2. **C**. Overlay of E_2, 4-methyl-E_2, 4-MeO-E_2, 4-OH-E_2 and 4-Br-E_2.

For most *A*-ring derivatives, there are only subtle differences between their binding modes with that of E_2. The small differences as observed in the docking models are believed to contribute importantly to their differential binding affinity for the ERs. One of the most notable differences in the binding of these *A*-ring estrogen derivatives is that the hydrogen bonds formed by their 3-hydroxyl group are of different lengths. It is hypothesized that the difference in the hydrogen bond distance, which would affect the hydrogen bond strength, is an important determinant of the binding affinity of a given ligand. To test this hypothesis, I computed for comparison the distances between the hydrogen atoms of the 3-hydroxyl group of various estrogen derivatives and the O_ε of ERα-E353 or ERβ-E305, the distances between the oxygen atoms of the 3-hydroxyl group of the estrogen derivatives and the H_η of ERα-R394 or ERβ-R346, and also the distances between the hydrogen atoms of the 17-hydroxyl group of estrogen derivatives and N_δ of ERα-H524 or ERβ-H475. The values are summarized in **Table 2**. To study the role of hydrogen bonds in determining the binding affinity of estrogen derivatives, we tried to correlate the hydrogen bond length with the experimentally log*RBA* values. Because the hydrogen bond interaction is generally thought to be an electrostatic interaction by nature and electrostatic potential is in an inverse first order relationship with the distance between the two atoms, I correlated log*RBA* values with hydrogen bond length with the inverse first order curve regression.

For the *A*-ring derivatives, two hydrogen bonds are formed between the 3-hydroxyl groups of these estrogen derivatives and the amino acid residues E353 and

R394 in ERα or E305 and R346 in ERβ. As shown in **Figure 6**, for ERα, the inverse correlation for the distance of the hydrogen bond with R394 is stronger than that for E353, suggesting that the hydrogen bond between the 3-hydroxyl group of E_2 and R394 is more important for the binding interaction than the bond with E353. For ERβ, the correlation for the length of the hydrogen bond formed with E305 is stronger than that for R346, again suggesting that these two hydrogen bonds contribute differentially to the binding affinity. The substantial correlation between the experimentally-determined log*RBA* values and the hydrogen bond lengths indicates the vital importance of the hydrogen bonds with the 3-hydroxyl group of E_2 in determining the overall binding affinity of a ligand. This correlation also suggests that computing the lengths of the hydrogen bonds formed between the 3-hydroxyl group of a steroidal estrogen and ERs can be used as an important predictor of the binding affinity of a given *A*-ring derivative of E_2. The hydrogen bonds formed between the 17-hydroxyl groups of *A*-ring derivatives of E_2 with H524 in ERα or H475 in ERβ were of similar lengths and less important to determine their binding affinities.

Earlier studies suggested that 4-OH-E_2 had a very low dissociation constant for the ERα compared to E_2, which means that 4-OH-E_2 could bind very tightly in the ERα LBD. Our computational docking model showed that 4-OH-E_2 can form a perfect hydrogen bond between its 3-hydroxyl group and E353 and R394 in the same way as seen with E_2. In addition, 4-OH-E_2 can also form an additional hydrogen bond between its 4-hydroxyl group and ERα-L387. In the case of ERβ, a similar additional hydroxyl

group is also formed with L339. This additional hydrogen bond is believed to account for its tight binding interactions with the ERs. In this context, it is also of note that our docking results show that 2-OH-E_2 can also form an additional hydrogen bond between its 2-hydroxyl group and ERα-E353 or ERβ-E305. Interestingly, despite the presence of additional hydrogen bond, 2-OH-E_2 actually has a much lower binding affinity for both ERα and ERβ compared to E_2. Our docking model of 2-OH-E_2 provides unique insights. Presence of an additional 2-hydroxyl group causes a slight interference with the hydrogen bond formation between its 3-hydroxyl group and ERα-E353 or ERβ-E305, which may reduce its binding affinity for the ERs.

Among the *A*-ring derivatives tested, 2-MeO-E_2 and 4-MeO-E_2 caused the most drastic shift of the ligand position relative to E_2 due to their bulkier methoxyl substituents, which interfered with the formation of hydrogen bonds between their 3-hydroxyl groups and ERα-E353 & R394 or ERβ-E305 & R346, ultimately resulting in low binding affinity.

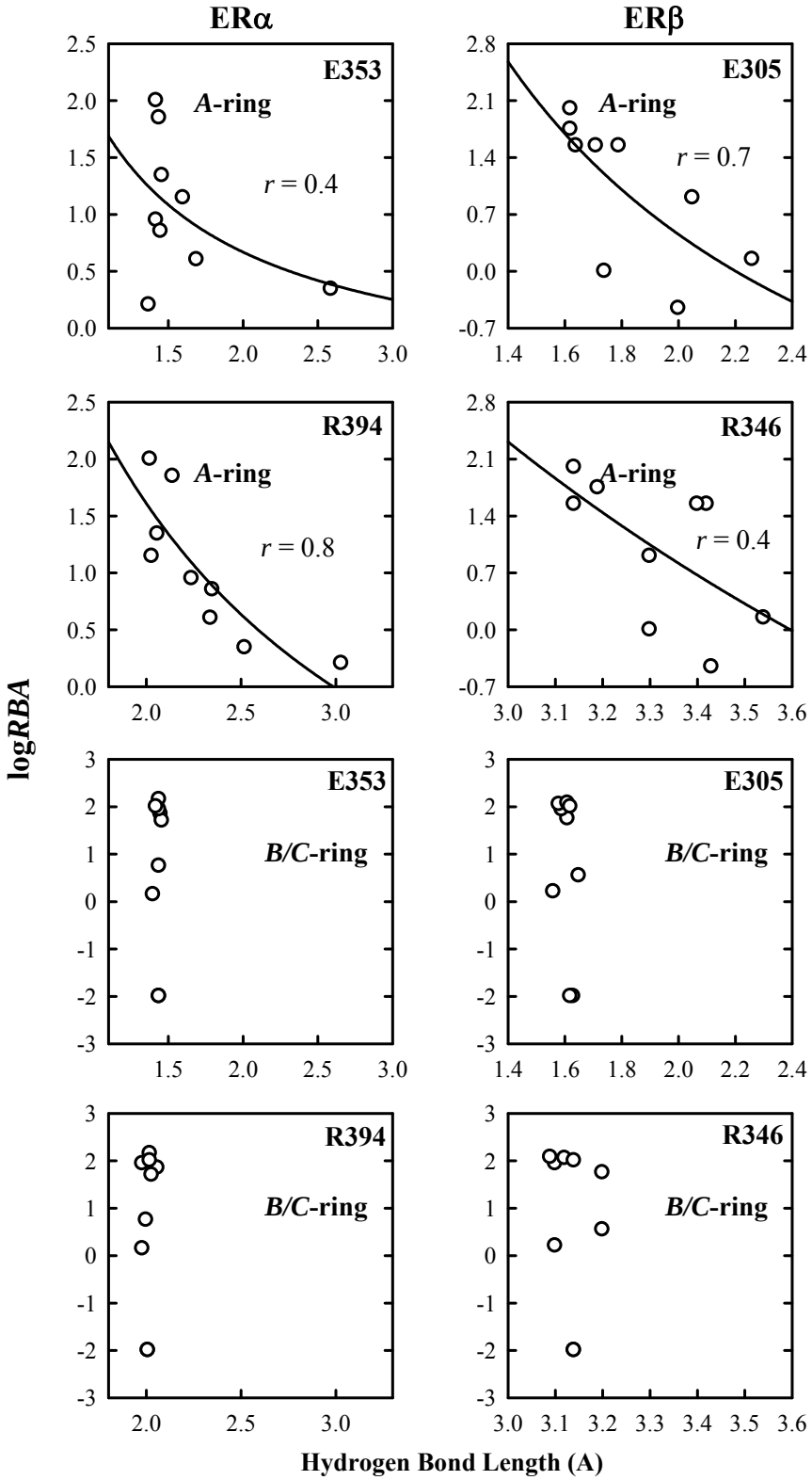
ERα
ERβ
E353
A-ring
r = 0.4
E305
A-ring
r = 0.7
R394
A-ring
r = 0.8
R346
A-ring
r = 0.4
E353
B/C-ring
E305
B/C-ring
R394
B/C-ring
R346
B/C-ring
log RBA
Hydrogen Bond Length (A)

Figure 6 Correlation of hydrogen bond length and log*RBA* of *A*-ring and *B*/*C* ring derivatives with ERs' LBDs. The hydrogen bond length data are shown in **Table 2**. The amino acids shown in the upper right corner of each figure indicated that the hydrogen bonds were formed between 3-hydroxyl groups of the *A*-ring derivatives and this specific amino acid in the binding pocket. The curve regression was performed according to the Inverse First Order equation $y = y_0 + a/x$.

***B/C*-ring and *D*-ring derivatives.** Docking results of *B/C*-ring and *D*-ring derivatives with ERα LBD are shown in **Figure 7.** Similar to *A*-ring derivatives, we can see that their binding modes are very close to those of E_2. Two hydrogen bonds are formed between their 3-hydroxyl groups with amino acid residues E353 and R394 in ERα or E305 and R346 in ERβ. No hydrogen bond was formed with either 6- or 11- hydroxyl groups of the *B*/*C*-ring derivatives.

For *B*/*C*-ring derivatives, the correlation coefficient *r* values between their hydrogen bond lengths and log*RBA* values are 0.1, 0.2, and 0.4 for the hydrogen bonds with E353, R394, and H524 of ERα, respectively. For ERβ, the *r* values are 0.3, 0.1, and 0.4 for the hydrogen bonds with E305, R346, and H475, respectively. C-6 and C-11 are surrounded by hydrophobic amino acid residues, and the addition of a hydroxyl group reduces the binding affinity because of the repulsive force at play. In such cases, the hydrogen bond formation with the 3- and 17- hydroxyl groups may not change much. This is probably the main reason why the correlation of their binding affinities to log*RBA* is poor.

For some *D*-ring derivatives with a hydroxyl group at the C-16 position, one more hydrogen bond can be formed with H524, which may contribute to their relatively higher binding affinities for the ERs as compared to other estrogen metabolites. The correlation coefficient r^2 values for the *D*-ring derivatives are 0.13, 0.06, and 0.04 for the hydrogen bonds with E353, R394, and H524 of ERα, respectively. For ERβ, the r^2 values are

0.00,(which indicated that no correlation was observed between the hydrogen bond lengths and log*RBA*s), 0.00, and 0.08 for the hydrogen bonds with E305, R346, and H475, respectively. For the *D*-ring derivatives, which form two hydrogen bonds with histidine, only the shorter hydrogen bond was used for the correlation. Similarly to the *B*/*C* ring derivatives, the poor correlation for the *D*-ring derivatives suggested that the repulsive force around *D*-ring area may be more important than hydrogen bond formation in determining the binding affinities of the ligands.

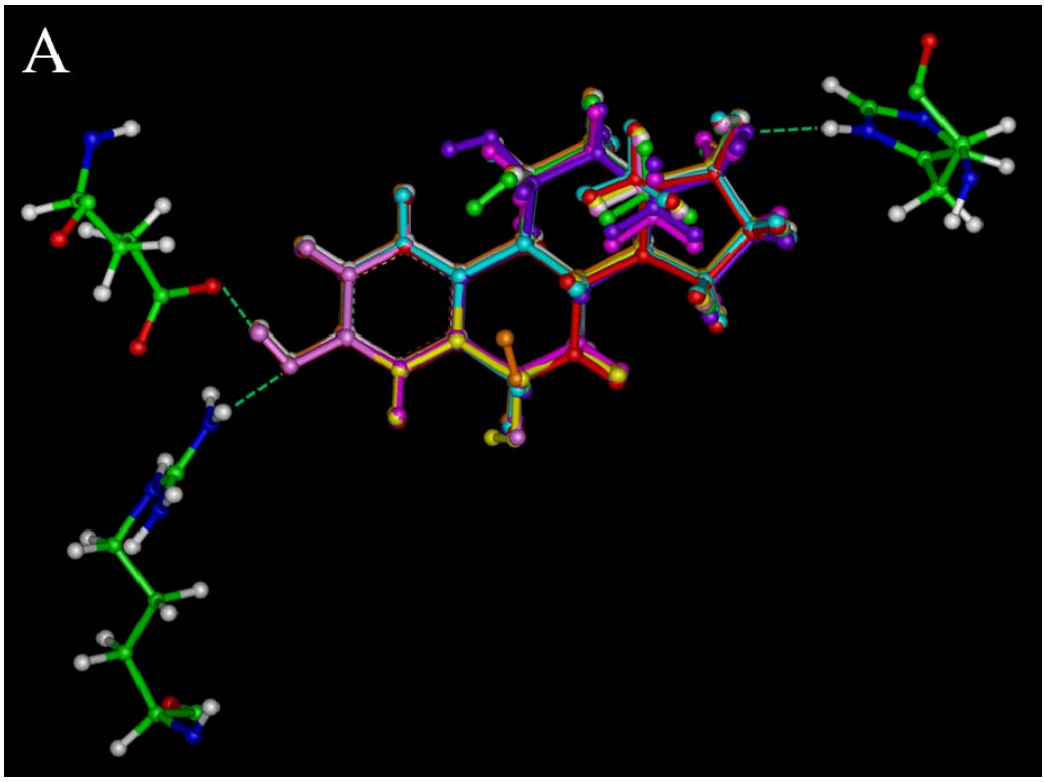
A

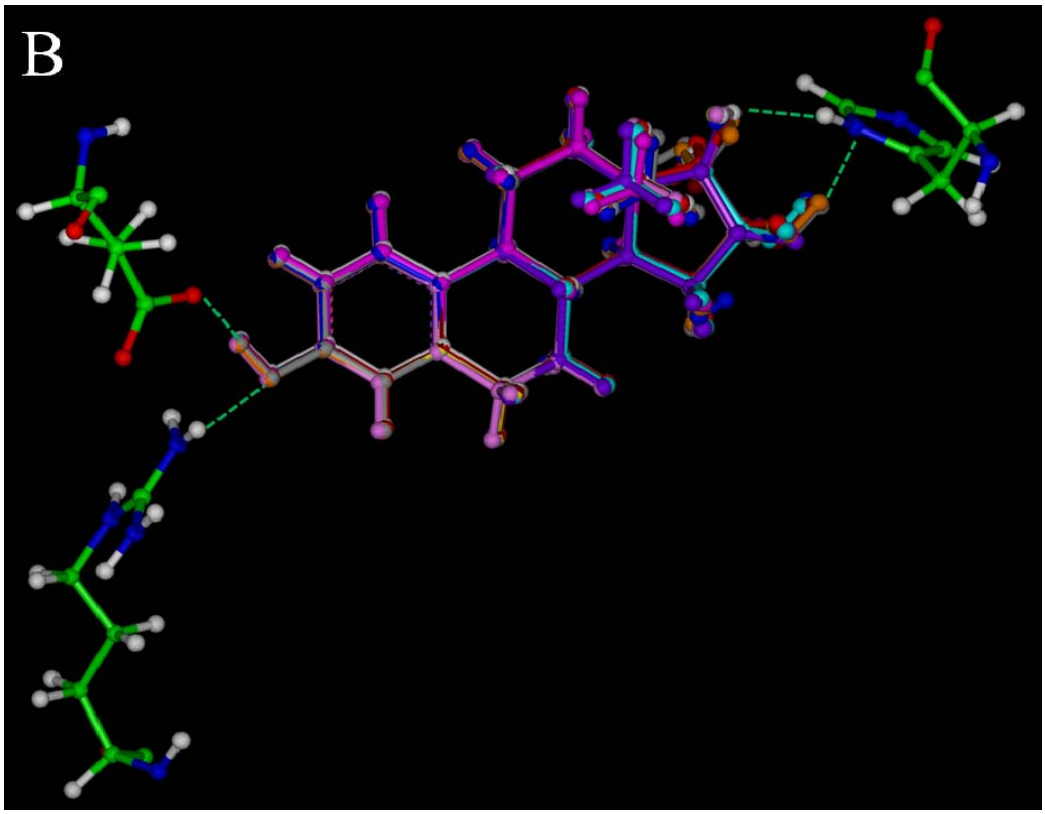
B

Figure 7 Interactions of *B/C*-ring derivatives (**A**) and *D*-ring derivatives (**B**) with ERα LBD determined by the molecular docking method. The green dashes indicate the hydrogen bonds formed. All the structures were rendered in ball and stick format. The amino acids were colored according to the atom type, i.e. green for carbon, red for oxygen, blue for nitrogen, and white for hydrogen. Among the amino acids in the binding site, only E353, R394, and H524 are shown in this figure. E_2 was colored in white. The ligands are shown in the following colors: in **panel A**, 6α-OH-E_2 (yellow), 6β-OH-E_2 (orange), 6-keto-E_2 (pink), 6-dehydro-E_2 (red), 7-dehydro-E_2 (magenta), 9(11)-dehydro-E_2 (light blue), 11α-OH-E_2 (purple), and 11β-OH-E_2 (green); in **panel B**, E_1 (magenta), estriol (16α-OH-E_2) (yellow), 16β-OH-E_2 (orange), 16-keto-E_2 (pink), 17α-OH-E_2 (red), 15α-OH-E_3 (dark blue), 16α-OH-E_1 (light blue), 16-keto-E_1 (purple), 16α-OH-E_2-17α (brown), and 16β-OH-E_2-17α (grey).

Prediction of binding affinities of estrogen derivatives with ERα and ERβ LBDs based on binding energy calculation

According to the docking models developed in this study for each of the 27 E_2 derivatives, I computed their binding energy (ΔE) values in complex with ERα or ERβ (listed in **Table 2**). The correlation between the computed $\Delta E_{binding}$ values and the experimentally-determined log*RBA* values for various E_2 derivatives is shown in **Figure 8**. For both ERα and ERβ, the correlation is highest for *A*-ring derivatives, with *r* values of 0.87 and 0.78, respectively. In contrast, there was no meaningful correlation observed between the computed values and experimental values for the *B*/*C*-ring derivatives or *D*-ring derivatives.

The poor correlation between the calculated binding energy values and the experimentally-determined *RBA*s for *B*/*C*-ring derivatives or *D*-ring derivatives may be, in part, due to the inherent problems associated with many of the currently-used molecular docking methods (Roncaglioni and Benfenati, 2008), which is the relative inaccuracy of the molecular mechanics approach in computing the energy levels. Here, we sought to modify the binding energy calculation by varying the weight of VDW interaction energy and Coulomb interaction energy through simply converting the commonly-used equation (3) to the following equation (5):

$$\Delta E_{\text{binding}} = x\,\Delta E_{\text{VDW}} + y\,\Delta E_{\text{Coulomb}} \qquad (5)$$

where x and y are assigned parameters to adjust the weights of ΔE_{VDW} and $\Delta E_{\mathrm{Coulomb}}$ in the total binding energy. Based on the above equation, by altering the x/y value, we can calculate the corresponding r value for the relationship between the computed $\Delta E_{\mathrm{binding}}$ and experimentally-determined log*RBA*. The relationship between x/y value and r value for the *A*-ring, *B*/*C*-ring, and *D*-ring derivatives is shown in **Figure** 9 with x/y value shown in log scale.

The optimal r value was achieved with different x/y values for *A*-ring and *B*/*C* ring derivatives with ERα or ERβ. For *A*-ring derivatives, in the case of ERα, when x/y is 2, the optimal r value is 0.9. For ERβ, the curve is basically flat, which means that VDW and Coulomb interaction energy are equally important in determining the *RBA* of a ligand. For *B*/*C*-ring derivatives with ERβ, the optimal r is 0.8 when x is 0, which indicates that Coulomb energy is more important to determine *RBA*. Interestingly, when x/y is 1, the correlation is the worst. However, for *B*/*C*- and *D*-ring derivatives, the prediction is still very low for both ERs. Thus the method used to calculate binding energy for *B*/*C* ring and *D*-ring derivatives merits further investigation.

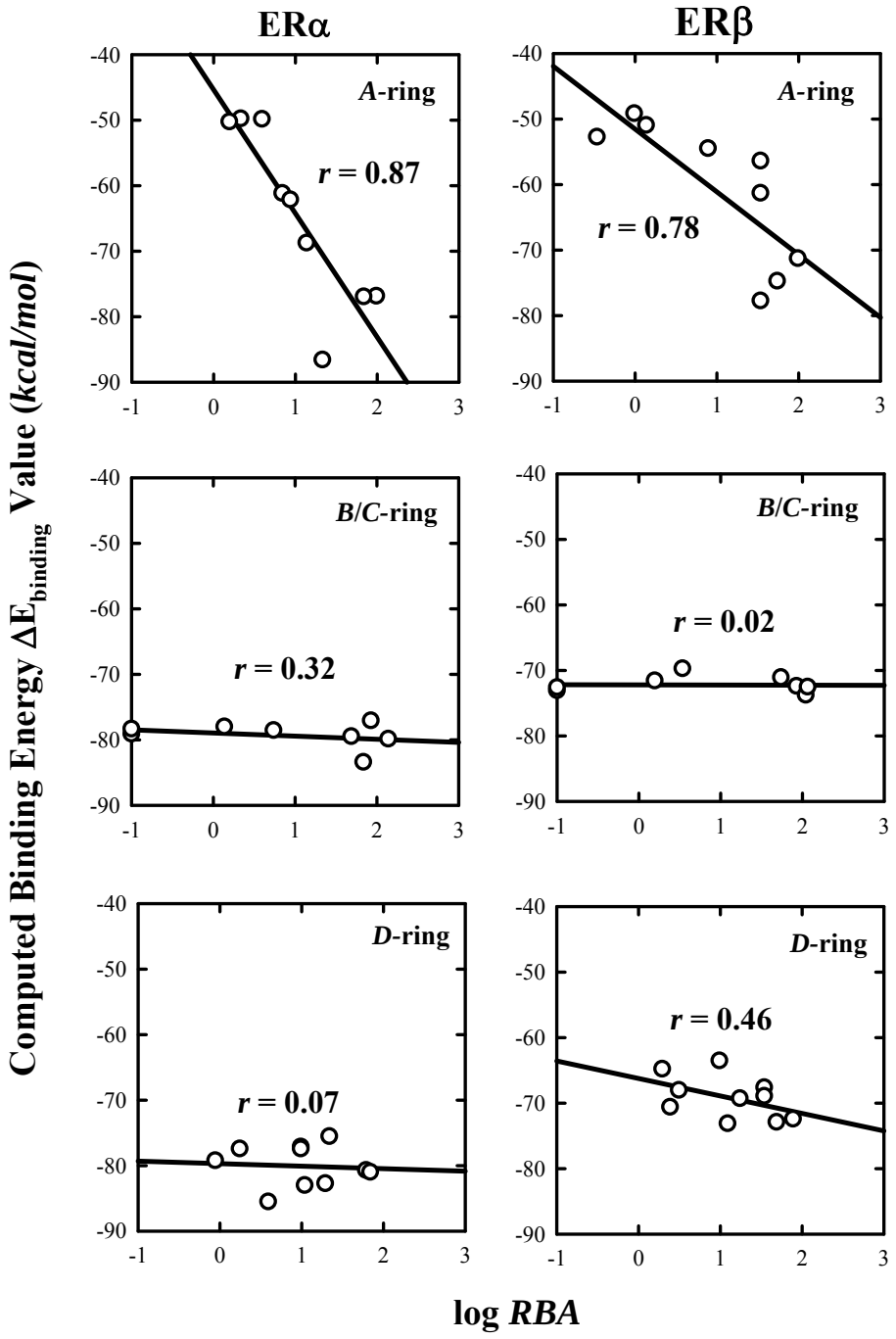

Figure 8 Correlation between log*RBA* and binding energy calculated according to equation (3) and data in **Table 2**. The correlation coefficient *r* value is shown inside the figure.

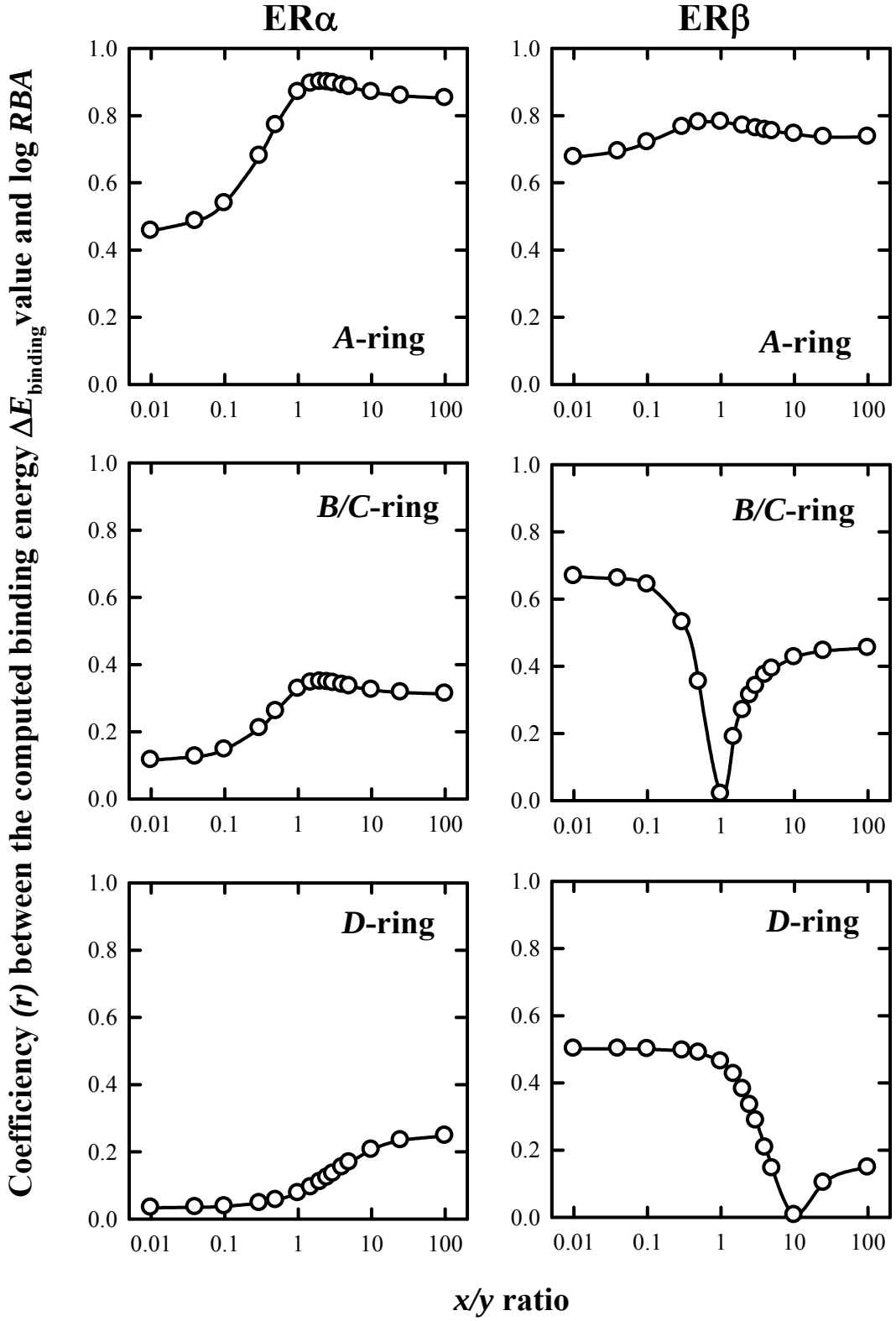
ERα
ERβ
A-ring
A-ring
B/C-ring
B/C-ring
D-ring
D-ring
Coefficiency (r) between the computed binding energy ΔE binding value and log RBA
x/y ratio
0.0
0.2
0.4
0.6
0.8
1.0
0.01
0.1
1
10
100

Figure 9 Relationship between the correlation coefficient *r* value and *x*/*y* value for the estrogen derivatives listed in **Table 2**. For each *x*/*y* value, the total binding energy was calculated according to equation (5) and the correlation coefficient *r* value was calculated by correlating the total binding energy for each chemical with its log*RBA*. The *x*/*y* value was shown in log scale.

CONCLUSIONS

This study sought to use the molecular docking method to characterize the interactions of E_2 derivatives with human ERα and ERβ. First, we tested the suitability of the molecular docking method for predicting the correct binding mode of a ligand in the binding pockets of the human ERα and ERβ. Using DES and E_2 as examples, we demonstrated that the docked structures are almost exactly the same as the known crystal structures of ERα LBD in complex with these two ligands. Using the same docking approach, we also docked 27 structurally-similar E_2 derivatives into the LBDs of human ERα and ERβ. Whereas their binding modes are very similar to that of E_2, there are notable subtle differences. These small differences contribute importantly to their different ER binding affinity. In the case of the *A*-ring estrogen derivatives analyzed, there is a strong inverse relationship between the length of the hydrogen bonds formed with ERs and the binding affinity. In the study, we optimized our approach's ability to predict the relative binding affinity of a given *A*-ring derivative of E_2 through re-adjusting the relative contribution of the van der Waals (VDW) interaction energy and Coulomb interaction energy in computing the overall binding energy (ΔE) value.

CHAPTER FIVE

CHARACTERIZATION OF THE ESTROGENIC ACTIVITY OF NON-AROMATIC STEROIDS: IMPLICATIONS FOR THE PRESENCE OF ESTROGEN RECEPTOR MODULATORS IN MEN

INTRODUCTION

The endogenous estrogens in women are biosynthesized from androgens through enzymatic aromatization of their *A*-rings, which occurs mostly in ovaries and, to a smaller extent, also in extragonadal tissues (Simpson and Davis, 2001). In comparison, aromatization of androgens to estrogens is quantitatively less important in men, and the blood levels of aromatic estrogens in men are usually very low (de Ronde et al., 2003). Nevertheless, studies in animals and humans have shown that the ERα and ERβ are present in many tissues or cell types in males, such as prostate, bladder, certain regions of the brain, lymphatic tissues, and heart (Adams et al., 2002; Prins et al., 2001). In addition, ERs present in various male tissues (*e.g.*, pituitary, breast, and prostate) are functionally active and can be readily activated by administration of an estrogen to elicit strong biological effects.

Among all classes of endogenous steroids, only estrogens (such as E_1 and E_2) contain an aromatic *A*-ring. For decades, it was generally thought that the aromatic *A*-ring in a steroid is a critical structural feature for its specific ER-binding activity. However, based on the results from **AIM 1A**, *i.e.* the computational analysis of the binding characteristics of aromatic estrogens for human ERα and ERβ, we hypothesized that some of the non-aromatic androgen metabolites or precursors with hydroxyl groups at the C-3 and/or C-17 positions may also be able to bind ERα and ERβ with relatively high binding affinities and thereby may serve as non-aromatic endogenous ER ligands.

To confirm this hypothesis, we set out to test a total of sixty non-aromatic steroids

for their ability to bind and activate the human ERα and ERβ in several *in vitro* bioassays. These non-aromatic steroids are selected from the steroid families of androstens, androstans, androstadiens, estrens, and estrans (some of the representative structures of non-aromatic steroids are listed in **Figure 10**), and they have a hydroxyl group at their C-3 and/or C-17 position, which are known to be important in forming hydrogen bonds with the ERs. Notably, all these non-aromatic steroids are potential precursors, intermediates, or metabolites that may be produced during the process of steroid biosynthesis and metabolism. A number of enzymes are known to catalyze the formation of some of these steroids (see **Figure 10**). For instance, the 3- and 17β-hydroxylsteroid dehydrogenases (HSD) can catalyze the interconversion of the ketone and hydroxyl groups at the C-3 and C-17 positions, respectively (Peltoketo et al., 1999; Simard et al., 2005). Whereas it is well-documented that an androsten can be readily converted to its 5α-androstan product in some of the male target tissues by 5α-reductase (Makridakis et al., 2000), testosterone (an androsten) and epiandrosterone (an androstan) can also be converted to 19-norandrosterone (an estren) and norepiandrosterone (an estran), respectively, by the 19-demethylation metabolic pathway (Grosse et al., 2005). In addition, many cytochrome P450 enzymes can readily catalyze the addition of a hydroxyl or keto group to various carbon positions in the steroid core structure (Lee et al., 2003). We demonstrated in this study that some of the metabolic derivatives of endogenous androgens can bind and activate human ERα and ERβ to elicit hormonal responses. These observations suggest that some of the endogenous androgen precursors or metabolites may serve as ER modulators in men.

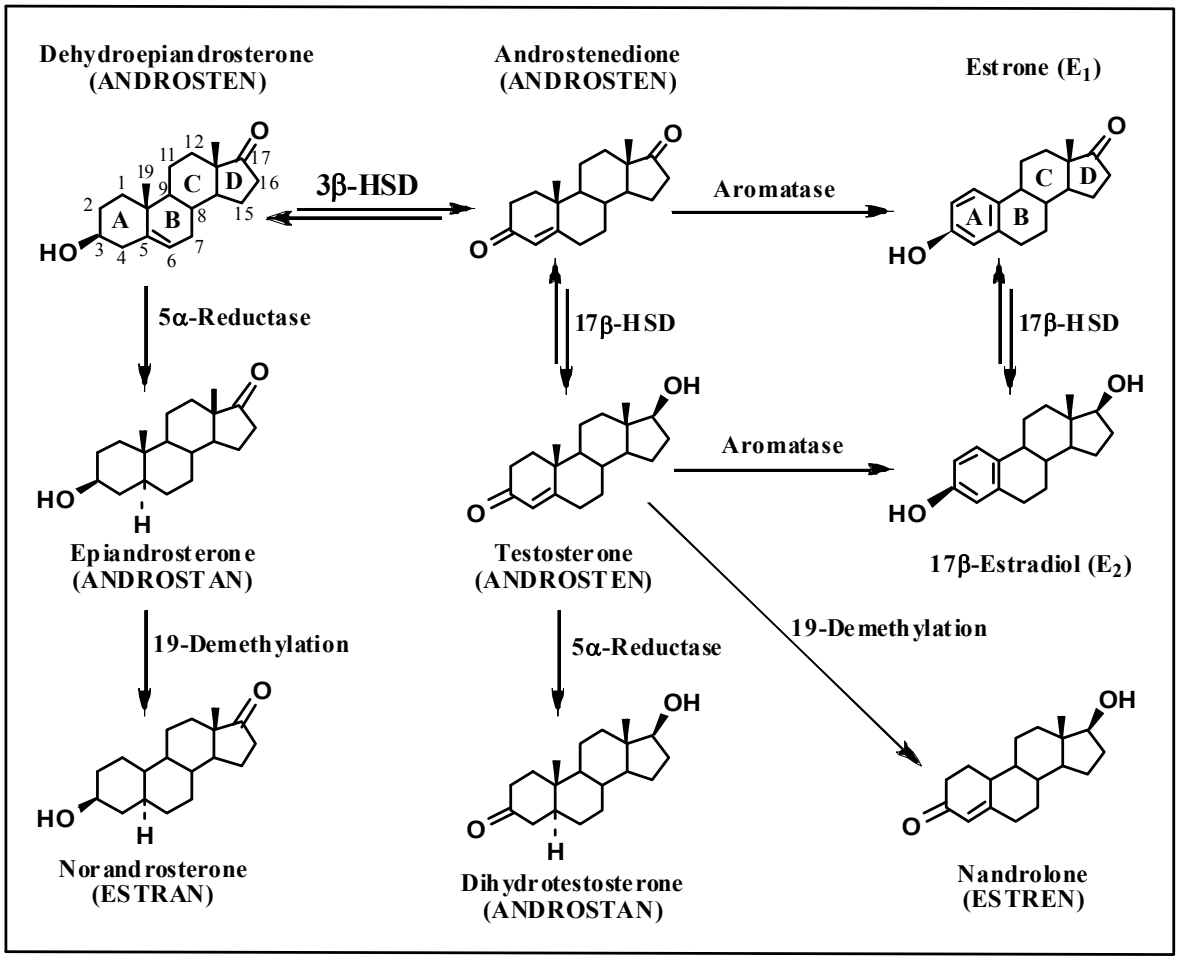
Dehydroepiandrosterone
(ANDROSTEN)
Androstenedione
(ANDROSTEN)
Estrone (E1)
3β-HSD
Aromatase
5α-Reductase
17β-HSD
17β-HSD
Aromatase
Epiandrosterone
(ANDROSTAN)
Testosterone
(ANDROSTEN)
17β-Estradiol (E2)
19-Demethylation
5α-Reductase
19-Demethylation
Norandrosterone
(ESTRAN)
Dihydrotestosterone
(ANDROSTAN)
Nandrolone
(ESTREN)

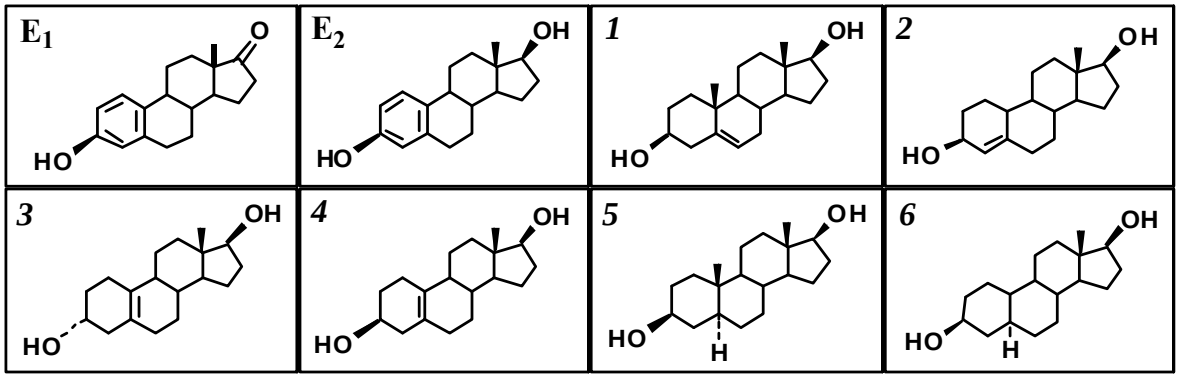
E1
E2
1
2
3
4
5
6

Figure 10 **Upper panel.** Potential precursors and metabolic intermediates produced during the biosynthesis and metabolism of endogenous androgens with dehydroepiandrosterone (DHEA) as the starting compound. Note that the name of the corresponding sub-class for each non-aromatic steroid was provided under each name (upper case). The representative structures for the androstadien class were omitted for clarity. This sub-class of non-steroids can be produced from the androstens by forming an additional double bond at various positions. **Lower panels.** Chemical structures of E_2, E_1, and compounds ***1–6***. The names of compounds ***1–6*** are listed below. ***1***: 5-androsten-3β,17β-diol; ***2***: 4-estren-3β,17β-diol; ***3***: 5(10)-estren-3α,17β-diol; ***4***: 5(10)-estren-3β,17β-diol; ***5***: 5α-androstan-3β,17β-diol; ***6***: 5α-estran-3β,17β-diol.

RESULTS

Non-aromatic steroids have physiologically-relevant high binding affinities for human ERα and ERβ

We tested a total of sixty non-aromatic steroids for their binding affinity for human ERα and ERβ. For each of these compounds, we first assessed its binding affinity for human ERα and ERβ at 1 μM (data are summarized in **Table 3**). We found that six of the non-aromatic steroids (highlighted in **Table 3,** with their structures shown in **Figure 10 lower panels,** referred to as compounds ***1–6***) had high binding activity for both human ERα and ERβ when present at 1 μM. Notably, some of the steroids, such as 5-androstan-3β,4α,17β-triol and 4-androsten-3β,17β-diol, had a weak but selective binding activity for ERβ, with no appreciable binding activity detected for ERα.

Next we determined the entire competition curves (at concentrations of 0.24, 0.98, 3.9, 15.6, 62.5, 250, and 1000 nM) for each of these six active compounds (**Figure 11**). The data obtained from duplicate measurements were expressed in **Figure 11** as the % specific binding of [^{3}H]E_2 compared to the control (in the absence of competing compound). Calculated according to the IC_{50} values determined in this study, the relative binding affinities (*RBA*s) to E_1 for compounds ***1–6*** are 16.7, 39.5, 24.6, 98.2, 12.3, and 115.8%, respectively, for human ERα, and 253.6, 251.1, 100.0, 567.8, 128.8, and 164.3%, respectively, for human ERβ. Similarly, the *RBA*s to E_2 for these compounds ranged

between 1.4 – 13.2%, for ERα, and 2.8 – 15.9%, for ERβ. Notably, their binding affinities are physiologically relevant because they are comparable to those of E_1, the quantitatively most important endogenous estrogen found in the circulation of a non-pregnant woman (Zhu and Conney, 1998).

In addition, we assessed the relative binding affinities of these six compounds for the human androgen receptor (AR) (data summarized in **Table 3**). Compounds ***1***, ***3***, and ***4*** had a selective binding affinity for the ERs with little binding activity for the AR. In comparison, compounds ***2***, ***5***, and ***6*** showed substantial binding activity for human AR (based on their ability to compete off the binding of [^{3}H]methyltrienolone from AR) when they were present at 1 μM, although their relative binding affinity was significantly weaker than that of testosterone.

Table 3 Inhibition of [^{3}H]E_2 binding to human ERα and ERβ *in vitro* by a total of sixty non-aromatic steroids from several steroid classes. Steroids with a high activity for ER binding (labeled ***1***–***6***) were also tested for their relative binding activity for human AR by measuring the inhibition of [^{3}H]methyltrienelone binding to the human AR protein *in vitro*. The binding by a radioligand to the respective receptor protein in the absence of any inhibitor was considered to be 100%, and each value was the mean of duplicate measurements of each test compound (at 1 μM) as the percentage inhibition of the radiolabeled ligand binding. A higher percentage inhibition value means a higher binding activity of the test compound for the respective receptor. For details of the assays, refer to the Methods section. The highlighted and numbered compounds are the focus of further analyses described in additional experiments. N.I. stands for no inhibition detected.

	ERα	ERβ	AR
Estrone (E_1)	**88.79**	**70.84**	**10.62**
Estradiol (E_2)	**98.71**	**99.91**	**-**
Testosterone	**-**	**-**	**77.19**
Androsten			
4-Androsten-3β,17β-diol	**11.76**	**50.49**	**-**
4-Androsten-16β,17α-diol-3-one	**11.96**	**42.95**	**-**
4-Androsten-16α-ol-3,17-dione	**8.55**	**10.28**	**-**
4-Androsten-16α,17β-diol-3-one	**8.72**	**11.70**	**-**
5-Androsten-3β,17β-diol (*1*)	**60.61**	**63.85**	**9.49**
5-Androsten-3β,17α-diol	**14.94**	**2.92**	**-**
5-Androsten-3β,4α,17β-triol	**12.18**	**54.42**	**-**
1,5α-Androsten-3,17-dione	**N. I.**	**N. I.**	**-**
1,5α-Androsten-1β-methyl-17β-ol-3-one	**12.58**	**2.14**	**-**
1,5α-Androsten-17β-ol-3-one	**N. I.**	**10.11**	**-**
9(11), (5β)-Androsten-3α-ol-17-one	**10.64**	**-0.34**	**-**

9(11), (5α)-Androstan-3β-ol-17-one	**6.53**	**13.55**	**-**
Androstan			
5α-Androstan-3β,17β-diol (*5*)	**61.09**	**70.54**	**54.75**
5α-Androstan-3β,16α-diol	**12.31**	**13.18**	**-**
5α-Androstan-3β,16β-diol	**11.67**	**15.09**	**-**
5α-Androstan-3α,17β-diol	**13.15**	**20.98**	**-**
5α-Androstan-3β,17α-diol	**12.57**	**11.17**	**-**
5α-Androstan-3β,17β-diol-16-one	**15.55**	**8.10**	**-**
5α-Androstan-3β-ol-16-one	**12.53**	**13.30**	**-**
5α-Androstan-3α,16α-diol-17-one	**5.21**	**5.47**	**-**
5α-Androstan-3β,16α-diol-17-one	**16.28**	**13.94**	**-**
5α-Androstan-17α-methyl-3α,17β-diol	**13.84**	**36.36**	**-**
5α-Androstan-17α-methyl-3β,17β-diol	**33.09**	**41.35**	**-**
5α-Androstan-3β-ol-16,17-dione-16-oxime	**13.84**	**15.71**	**-**
5β-Androstan-3β,17β-diol	**N. I.**	**14.65**	**-**
5β-Androstan-3β,16α-diol-17-one	**10.76**	**7.74**	**-**
5β-Androstan-3β,17α-diol	**12.85**	**7.09**	**-**
Androstadien			
1, 4-Androstadien-3, 17-dione	**N. I.**	**N. I.**	**-**
1,4-Androstadien-17β-ol-3-one	**N. I.**	**N. I.**	**-**
4, 6-Androstadien-3, 17-dione	**N. I.**	**N. I.**	**-**
4, 6-Androstadien-17β-ol-3-one	**N. I.**	**1.50**	**-**
4, 9(11)-Androstadien-3, 17-dione	**1.43**	**N. I.**	**-**
4, 9(11)-Androstadien-17β-ol-3-one	**1.40**	**35.47**	**-**
5, 9, (11)-Androstadien-3β-ol-17-one	**N. I.**	**0.11**	**-**
Estren	**ERα**	**ERβ**	**AR**
4-Estren-3β,17β-diol (*2*)	**78.16**	**81.68**	**41.28**
4-Estren-3α, 17α-diol	**N. I.**	**13.61**	**-**
4-Estren-3β, 17α-diol	**16.85**	**30.35**	**-**
4-Estren-3α,17β-diol	**27.03**	**28.25**	**-**
4-Estren-17α-ol-3-one	**N. I.**	**9.58**	**-**
4-Estren-17β-ol-3-one	**N. I.**	**12.91**	**-**
4-Estren-6β-ol-3, 17-dione	**N. I.**	**N. I.**	**-**
5(10)-Estren-3α,17β-diol (*3*)	**66.61**	**64.04**	**11.83**
5(10)-Estren-3β,17β-diol (*4*)	**89.24**	**87.95**	**1.41**

5(10)-Estren-3, 17-dione	**2.08**	**N. I.**	**-**
Estran			
5α-Estran-3β, 17β-diol (*6*)	**76.14**	**69.14**	**31.89**
5α-Estran-3α, 17α-diol	**11.16**	**5.63**	**-**
5α-Estran-3β, 17α-diol	**35.33**	**42.36**	**-**
5α-Estran-3α, 17β-diol	**34.55**	**23.90**	**-**
5α-Estran-3, 17-dione	**27.30**	**18.91**	**-**
5α-Estran-17α-ol-3-one	**1.29**	**3.07**	**-**
5α-Estran-17β-ol-3-one	**20.59**	**18.95**	**-**
5α-Estran-3β-ol-17-one	**21.90**	**18.29**	**-**
5α-Estran-3α-ol-17-one	**10.52**	**7.02**	**-**
5β-Estran-3α, 17β-diol	**N. I.**	**3.06**	**-**
5β-Estran-3α, 17α-diol	**8.05**	**10.54**	**-**
5β-Estran-3β, 17β-diol	**N. I.**	**7.47**	**-**
5β-Estran-3, 17-dione	**N. I.**	**20.18**	**-**
Other			
1,4,6-Androstatrien-17β-ol-3-one	**20.64**	**9.61**	**-**
4, 6-Estradien-3, 17-dione	**N. I.**	**8.28**	**-**
4, 6-Estradien-17β-ol-3-one	**2.18**	**5.73**	**-**

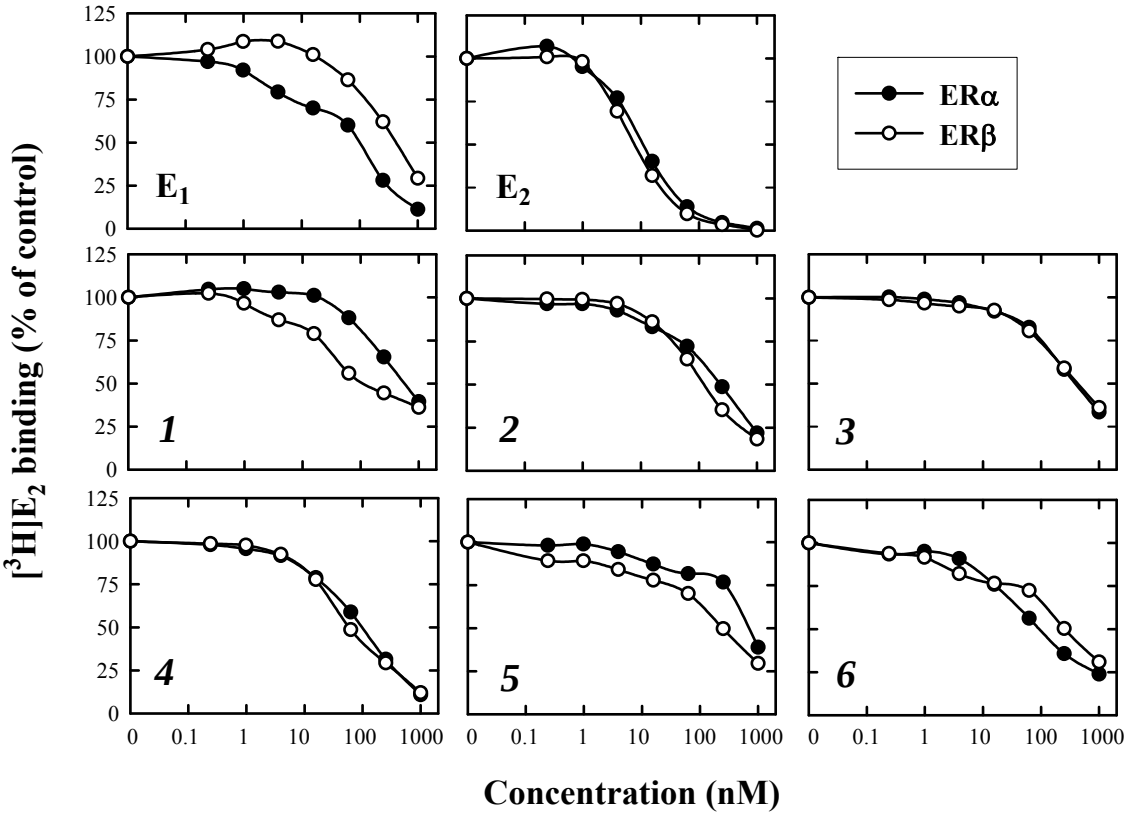

Figure 11 Competition of [^{3}H]E_2 binding to human ERα and ERβ by various non-aromatic steroids (compounds ***1***–***6***) and also by aromatic steroids E_2 and E_1. Each point was the mean of duplicate measurements. For the chemical names of compounds ***1***–***6***, please refer to the legend of **Figure 10.**

Active non-aromatic steroids can activate ERα in cultured cells

Next we determined whether the non-aromatic steroids that were found to have binding affinity for human ERα and ERβ were receptor agonists or antagonists. It is known that the estrogen-activated ERs are translocated into the nucleus and then bind the specific DNA sequences called estrogen response elements (ERE) to activate the expression of downstream target genes. First, we used a reporter plasmid consisting of an ERE and a luciferase reporter gene to determine the estrogenic activity of the non-aromatic steroids (**Figure 12A**). In this assay system, we found that E_1 at 1.6 nM could strongly induce luciferase gene expression. Compounds ***1–6*** could also induce luciferase gene expression dose-dependently, with EC_{50} values around 5 nM, which were comparable to the EC_{50} value of E_1 (approximately at 3 nM).

Similarly, to assess the androgenic activity of the three compounds (*i.e.*, ***2***, ***5***, and ***6***) that also retained significant AR-binding affinity, an androgen response element (ARE)-based reporter assay was employed. The AR-positive LNCaP cells were transfected with an ARE-luciferase reporter plasmid and a renilla plasmid (as the transfection control). In this assay system, the relative ability of compounds ***2***, ***5***, and ***6*** at 1 nM to induce the transcription of the luciferase reporter gene was 45.3 ± 11.5%, 7.1 ± 3.7%, and 56.5 ± 3.1%, respectively, of the activity of 1 nM methyltrienolone (**Figure 12B**).

A. Estrogen receptor α transcriptional activity

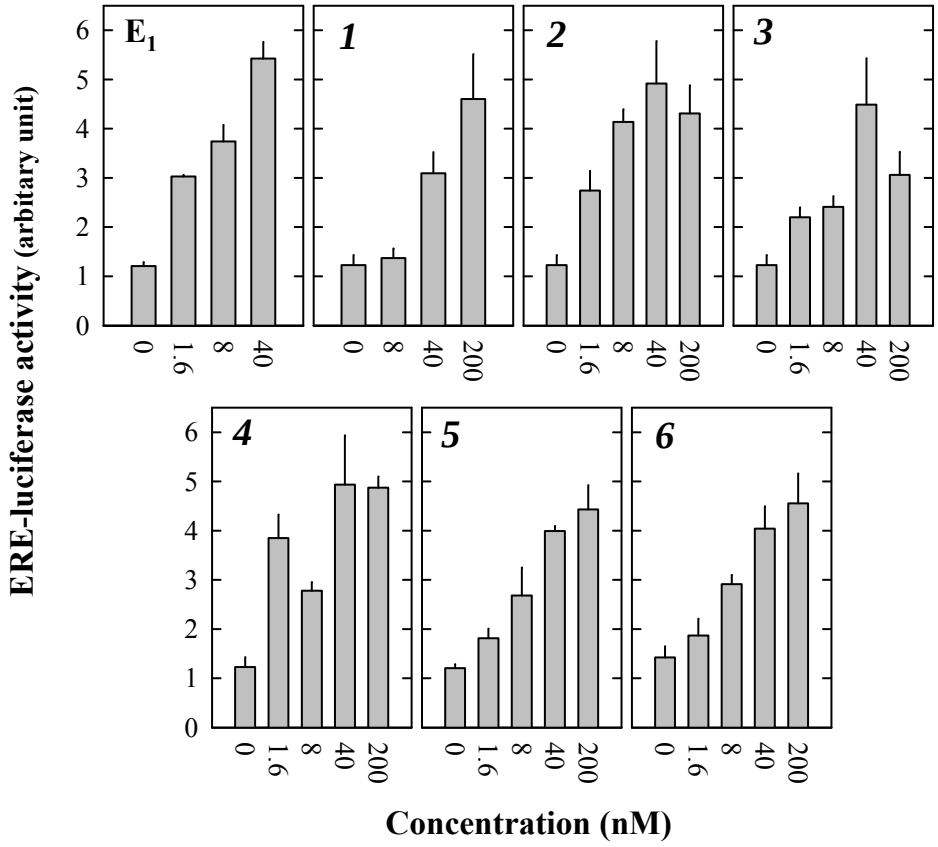

B. Androgen receptor transcriptional activity

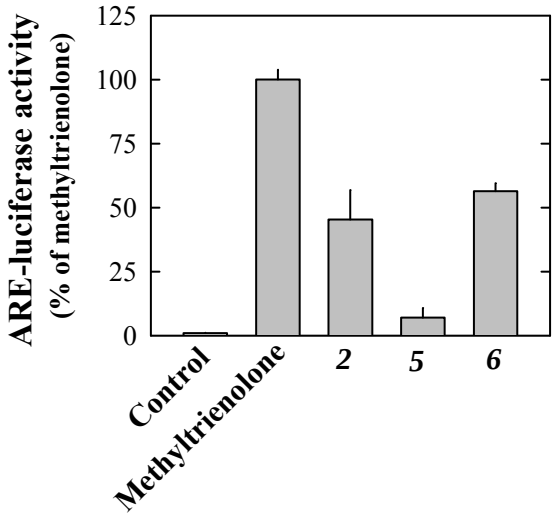

Figure 12 ERα and AR transcriptional activity of various non-aromatic steroids. **A.** Reporter assay in MCF-7 cells transfected with an ERE-luciferase reporter plasmid and treated with various concentrations of compounds ***1–6*** and E_1. The y-axis is the luciferase activity normalized with the total protein concentration. **B.** Reporter assay in LNCaP cells transfected with an ARE-luciferase reporter plasmid and a renilla plasmid and then treated with 1 nM methyltrienolone or compound ***2***, ***5***, or ***6***. The y-axis is the firefly luciferase activity normalized with renilla luciferase activity and expressed as % of the activity of methyltrienolone-treated group. Each value is the mean ± S.D. of triplicate measurements.

We also utilized two representative ER-positive human cancer cell lines (*i.e.*, MCF-7 breast cancer cells and LNCaP prostate cancer cells) to determine whether the presence of these non-aromatic steroids could stimulate cell growth (**Figure 13**). Whereas the rate of cell growth in the absence of exogenous estrogen was relatively low, treatment of the estrogen-starved MCF-7 cells (which express predominantly ERα) with E_1 at the lowest concentration tested (0.1 nM) strongly stimulated cell growth (**Figure 13A**). When these cells were treated with varying concentrations of compounds ***1–6***, the rate of their cell growth was also increased in a concentration-dependent manner, with EC_{50} values of approximately 2 nM.

LNCaP cell line is a human prostate cancer cell line that expresses both AR and ER and is sensitive to estrogen-induced growth stimulation. Compounds ***1–6*** exerted a similar maximal stimulation of their growth as did E_1 (**Figure 13B**). Consistent with the proliferative effect seen in MCF-7 cells, the EC_{50} values of compounds ***1–6*** ranged from 0.5 to 5 nM in LNCaP cells, indicating that these compounds are less potent than that of E_1. Since all six compounds (some of them have little androgenic activity) exerted a similar maximal proliferative effect in LNCaP cells, this suggests that this effect is largely mediated by the ER signaling pathways. The EC_{50} values of the non-aromatic steroids are well within the physiologically-achievable concentrations for androgens and/or their derivatives in men (circulating concentrations of androgens in men are at least 10 times higher than those of circulating estrogens in women).

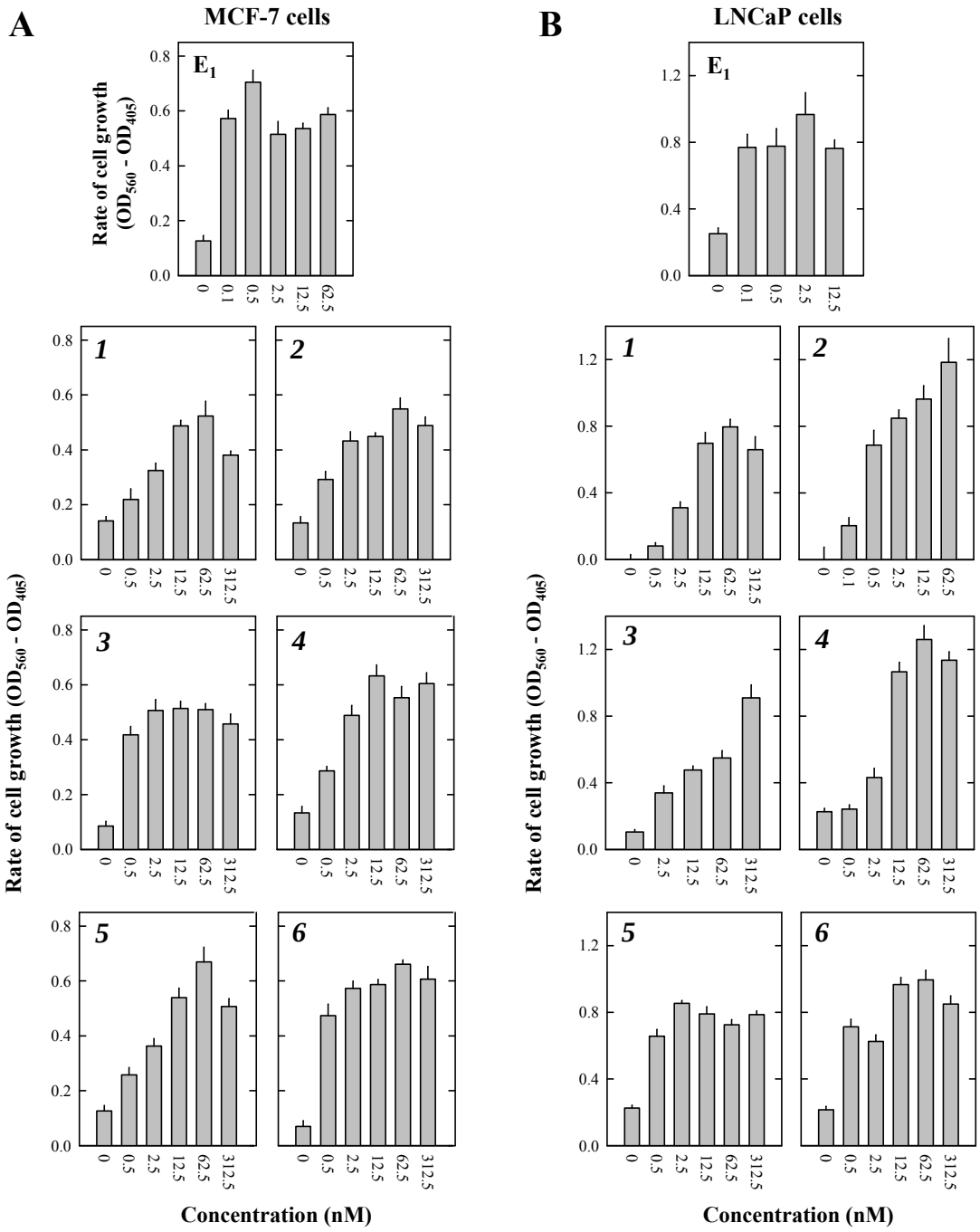
A
MCF-7 cells
B
LNCaP cells
E1
1
2
3
4
5
6
Rate of cell growth (OD560 - OD405)
Concentration (nM)

Figure 13 Comparison of the estrogenic activity of compounds ***1–6*** with E_1. **A.** The mitogenic activity of compounds ***1–6*** in the ER-positive MCF-7 human breast cancer cells in culture. **B.** The mitogenic activity of compounds ***1–6*** in the ER-positive LNCaP human prostate cancer cells in culture. The cells were seeded in 96-well plates and treated with the compounds for 6 days with a medium change at the 3rd day. The *y*-axis is the cell density measured using the crystal violet staining method (Liu and Zhu, 2004). Each value is the mean ± S.D. (N = 6).

Molecular modeling study of the binding interactions of non-aromatic steroids with human ERα and ERβ

To probe the structural determinants of various non-aromatic steroids for binding human ERα and ERβ, we performed the 3-D QSAR/CoMFA analysis of the non-aromatic steroids used in the present study (**Figure 14**). The 3-D QSAR/CoMFA models for human ERα and ERβ were developed using 58 compounds (excluding two of the compounds as outliers). Of several variations in the structural alignment schemes that were considered and tested in this study, the best results were obtained by superimposing the backbone carbons in the middle *C*-ring. It is likely that this ring of different non-aromatic steroids experienced less change upon binding to the receptors. The statistical results of CoMFA models for both human ERα and ERβ are summarized below. For ERα: r^2 = 0.907, q^2 = 0.402, Principle Components (PCs) = 8, SEE = 9.050, F = 38.870; for ERβ: r^2 = 0.932, q^2 = 0.400, PCs = 10, SEE = 7.280, F = 49.095. The correlations of the predicted specific binding values for ERα and ERβ are shown in **Figure 14A** with the filled squares representing compounds ***1–6***. The values of r^2 were higher than 0.9, which is considered to be indicative of good overall correlation for both ER subtypes between the predicted binding affinity values and the experimentally-determined values. The values of q^2 were higher than 0.4, which reflected good overall predictive ability of the 3-D QSAR/CoMFA models developed in this study. Individual contributions from the steric and electrostatic fields were 52% and 48%, respectively, for the ERα CoMFA model, and 47% and 53%, respectively, for the ERβ CoMFA model.

The color contour maps derived from the ERα and ERβ CoMFA models are shown in **Figure 14B**. Note that 5(10)-estren-3β,17β-diol (compound ***4***) is shown inside the field only for demonstration purposes. The contours of the steric map are shown in yellow and green, and those of the electrostatic map are shown in red and blue. Green contours indicate regions where a steric bulky substituent would decrease the inhibition of [^{3}H]E_2 binding with the receptor (decrease the binding affinity of test compound), whereas the yellow contours would indicate areas where a steric bulky substituent would increase the inhibition of [^{3}H]E_2 binding (increase binding affinity of the test compound). The red contours indicate regions where a substituent with stronger negative charge would decrease the inhibition of [^{3}H]E_2 binding (decrease the binding affinity of test compound), whereas the blue contours show areas where a substituent with strong negative charge would increase the inhibition of [^{3}H]E_2 binding (increase binding affinity of the test compound).

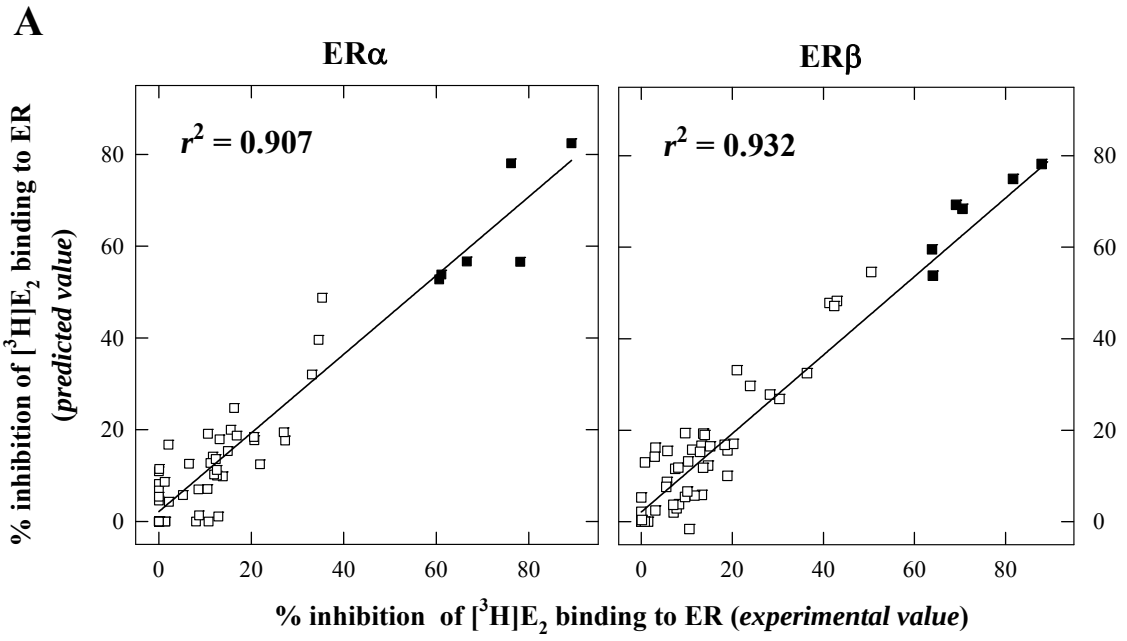
A
ERα
ERβ
r^2 = 0.907
r^2 = 0.932
% inhibition of [^{3}H]E$_2$ binding to ER (*predicted value*)
% inhibition of [^{3}H]E$_2$ binding to ER (*experimental value*)
0
20
40
60
80

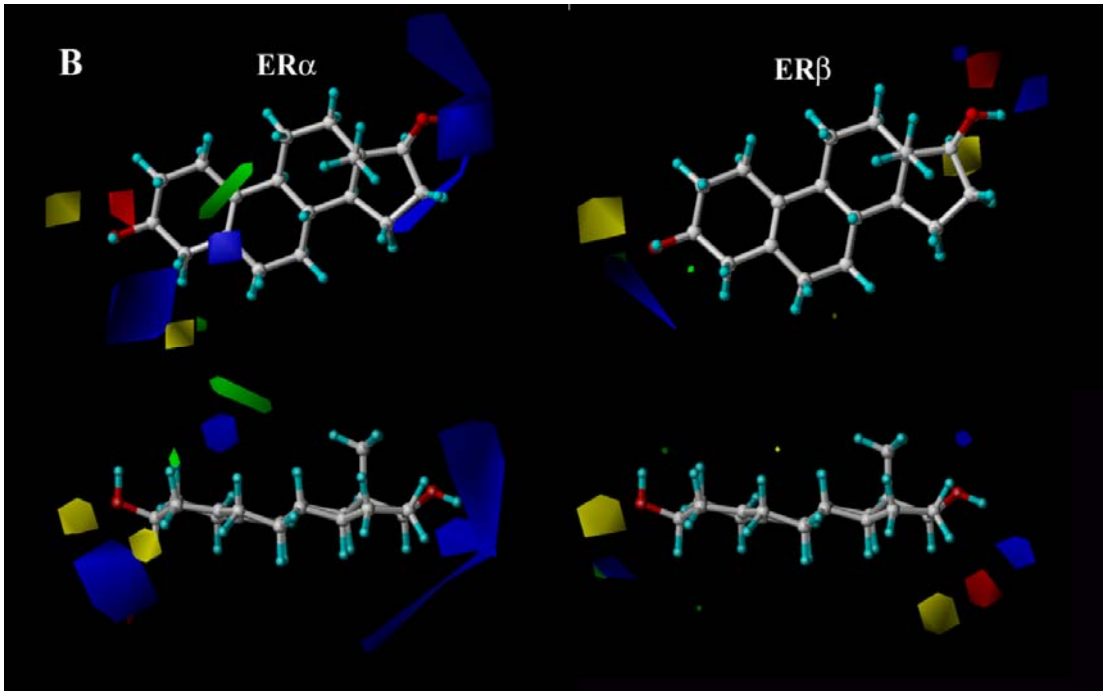
B
ERα
ERβ

Figure 14 3-D QSAR/CoMFA analysis of 58 non-aromatic steroids for their binding with ERα and ERβ. 5α-Androstan-3β-ol-16,17-dione-16-oxime was excluded because of its unique side chain. 4-Androsten-3β,17β-diol and 4,9(11)-androstadien-17β-ol-3-one were considered to be out-liner compounds for ERα and ERβ, respectively. **A.** The correlations of the predicted % inhibition of [^{3}H]E_2 binding for ERα and ERβ with the corresponding experimental values that were determined in the present study (data listed in **Table 3**). The filled squares represent data points for compounds ***1–6***. **B.** The color contour maps of the CoMFA models for human ERα and ERβ. Note that 5(10)-estren-3β,17β-diol was shown inside the field only for demonstration purposes. The contours of the steric map were shown in yellow and green, and those of the electrostatic map were shown in red and blue. Green contours indicated regions where a relatively bulky substitution would decrease the inhibition of [^{3}H]E_2 binding of some ligands with the receptor, whereas the yellow contours indicated areas where a bulkier substituent would increase the inhibition of [^{3}H]E_2 binding. The red contours were regions where a negative-charged substitution likely would decrease the inhibition of [^{3}H]E_2 binding, whereas the blue contours showed areas where a negative-charged substitution would increase the inhibition of [^{3}H]E_2 binding. Ligands with greater values of the inhibition of [^{3}H]E_2 binding (higher binding affinity) were correlated with: (***i***) less bulk near green; (***ii***) more bulk near yellow; (***iii***) less positive charge near blue; and/or (***iv***) less negative charge near red.

In addition, we conducted molecular simulation and docking studies to further characterize the binding interactions of these six non-aromatic steroids with the ligand binding domains (LBDs) of human ERα and ERβ. The known *x*-ray crystallographic structure of human ERα's LBD in complex with E_2 (PDB code: 1ERE) was directly used for energy minimization with various ligands, including non-aromatic steroids. Because no *x*-ray crystallographic structure of ERβ's LBD in complex with E_2 is available in the protein data bank, we used the ERβ LBD in complex with the agonist analog ERB-041 (PDB code: 1X7B) as a template for docking the binding of E_2 and also other non-aromatic steroids (**Figure 15A**).

Our molecular models showed that the binding of non-aromatic steroids with human ERα and ERβ closely resembled the binding of E_2 in these receptors (**Figure 15B**, **D**), especially the interaction of their C-3 and C-17 hydroxyl groups with the receptors by forming four hydrogen bonds between each of the ligands and the receptors (***i.e.***, Glu353, Arg394, His524, and a water molecule for ERα; Glu305, Leu339, His475, and a water molecule for ERβ). **Figure 15C and 15E** illustrated that the non-aromatic *A*-rings, which are not as planar as the aromatic *A*-ring of E_2, affected the formation of a strong hydrogen bond between the receptor and the C-3 hydroxyl group of the non-aromatic steroids. Also, the *van der Waals* interactions between the non-aromatic *A*-rings and the key hydrophobic amino acids of the binding pockets (such as Phe404 and Leu387 of ERα and Leu339 of ERβ) were much lower compared to their interactions with the aromatic *A*-rings because of the non-planar structure of the non-aromatic *A*-rings. These are the main

reasons why the non-aromatic steroids generally have very weak or little binding affinities for the ERα and ERβ, although they can fit inside the binding pocket in a similar manner.

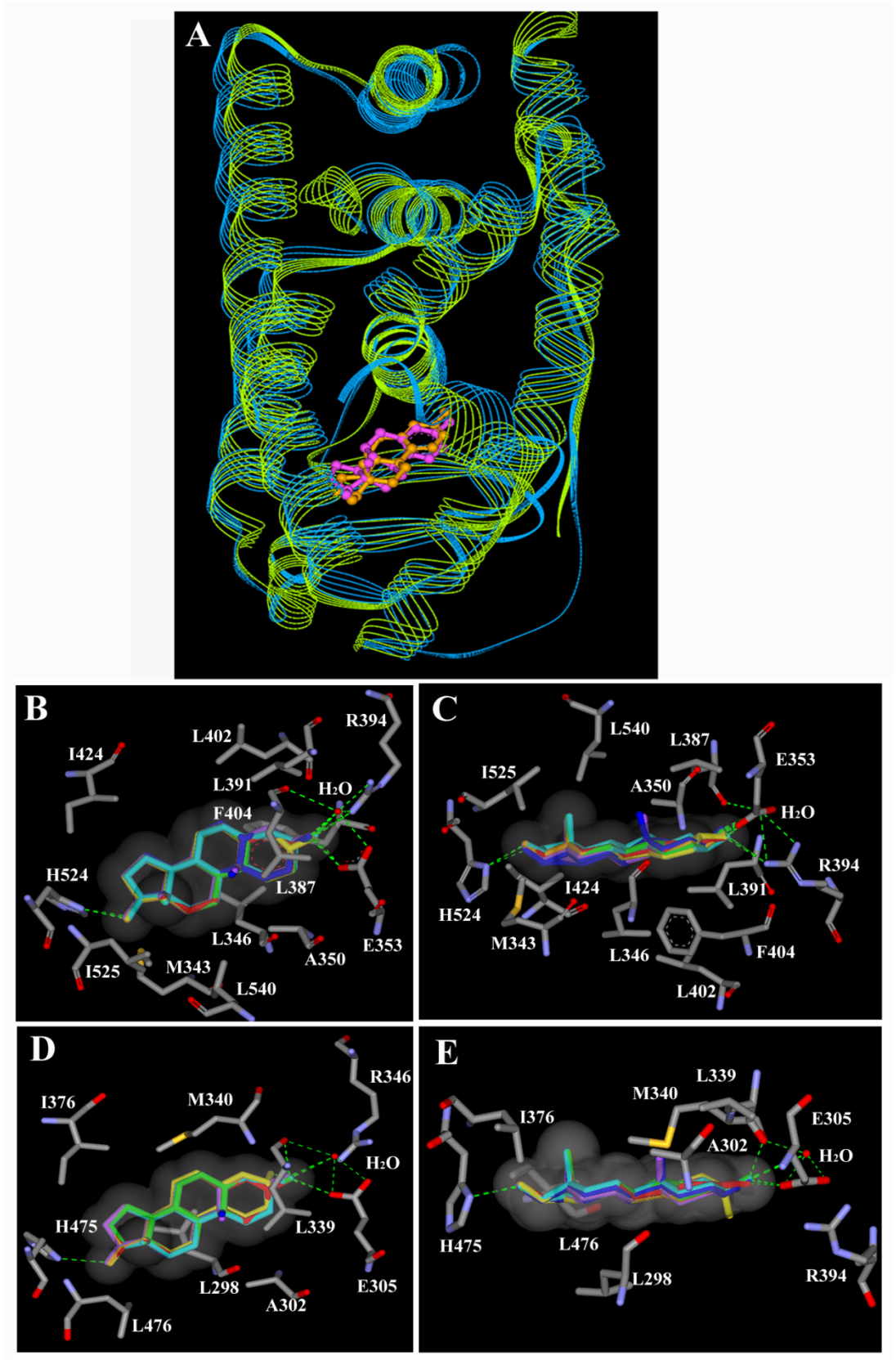
A
B
I424
L402
R394
L391
H2O
F404
H524
L387
L346
E353
A350
I525
M343
L540
C
L540
L387
E353
I525
A350
H2O
R394
I424
L391
H524
M343
L346
F404
L402
D
I376
M340
R346
H2O
H475
L339
L298
E305
A302
L476
E
L339
M340
I376
E305
A302
H2O
H475
L476
L298
R394

Figure 15 Comparison of ERα and ERβ binding sites in complex with E_2 or compounds ***1–6*** in the docking models developed in this study. The figure was drawn using the *Discovery Studio* software (Version 1.7, Accelrys, Inc. San Diego, CA). **A.** Overlay of the ligand binding domains (LBDs) of human ERα and ERβ in complex with E_2. Blue wires represent ERα and green wires represent ERβ. E_2 in complex with ERα is colored red, and E_2 in complex with ERβ is colored orange. **B.** E_2 and compounds ***1–6*** in the ERα binding pocket interacting with key amino acid residues Met343, Leu346, Ala350, Glu353, Leu387, Leu391, Arg394, Leu402, Phe404, Ile424, His524, Ile525, and Leu540. **C.** Horizontal view of ligands interacting with the ERα binding pocket. **D.** E_2 and compounds ***1–6*** in the ERβ binding pocket interacting with key amino acid residues Leu298, Ala302, Glu305, Leu339, M340, Arg346, Ile376, His475, and Leu476. **E.** Horizontal view of ligands interacting with the ERβ binding pocket. E_2 and compounds ***1–6*** were colored in red, orange, yellow, green, magneta, dark blue, and light blue, respectively. Hydrogens were omitted from all molecules. Green dash lines represented hydrogen bonds between ligands and receptors. The gray shadows represented the *van der Waals* surfaces of the ligands. For simplicity, the amino acids are labeled with their single letter abbreviations in the figure.

DISCUSSION

In this study, we identified six non-aromatic steroids, from a total of sixty compounds tested, that have physiologically-relevant high binding affinities for human ERα and ERβ, comparable to those of E_1. *In vitro* cell culture-based assays showed that these non-aromatic steroids could effectively activate the ER-mediated genomic actions with EC_{50} at low nM concentrations, and they can also elicit hormonal responses (such as strong growth stimulation) in the ER-positive human breast and prostate cancer cell lines (MCF-7 and LNCaP) in culture with comparable efficacy as E_1.

It is known that estrogens exert a wide range of important biological functions in many organ systems in male animals or men. In ERα-knockout male mice that lacked estrogen actions, their serum luteinizing hormone (LH) levels were markedly elevated although high levels of circulating testosterone were present in these animals (Lindzey et al., 1998). These phenotypic changes in male ERα-knockout mice are consistent with the well-known physiological functions of estrogens in females as crucial feedback regulators of the pituitary secretion of LH and follicle-stimulating hormone (FSH). Similarly, studies in men with an aromatase gene mutation also showed higher serum levels of LH and FSH, in addition to infertility in these subjects (Rochira et al., 2001). These findings suggest that the endogenous estrogens present in men have important physiological functions in regulating the release of gonadotropins. In recent years, estrogens have also been suggested to play an important role in modulating the

development of prostate diseases (including cancer) in elderly men (Bosland, 2006; Ellem and Risbridger, 2007). A recent study showed that 5α-androstan-3β,17β-diol (compound ***5***) activated ERβ and inhibited prostate development in animals (Weihua et al., 2002). Notably, whereas some of the non-aromatic steroids (compounds ***1***, ***3*** and ***4***) have a selective binding affinity for ERs, some of the others (compounds ***2, 5*** and ***6***) have binding activity for both human ERs and AR. Because AR and ER have both been recognized to play important roles in the normal development as well as pathogenesis of the prostate, it will be of interest to further explore their potential unique biological functions in various other target organs in man.

Our 3-D QSAR/CoMFA analysis of 58 selected steroidal estrogens (**Figure 14**) showed high r^2 and q^2 values for human ERα and ERβ, suggesting high degrees of overall correlation and predictability for both ER subtypes between predicted values and experimental values determined in this study for these estrogens (**Figure 14A**). It is of note that there are a number of similarities between the contour maps for human ERα and ERβ (**Figure 14B**). Firstly, contour maps for both receptors indicate the importance of negatively-charged moieties around the regions of the C-3 and C-17 for enhanced ER binding (**Figure 14B**; blue area). This suggestion agrees with the higher ER binding affinities of some of the compounds with C-3 and C-17 hydroxyl groups compared with the compounds containing a ketone group. In addition, the contour maps for both receptors also suggest that the slightly bulkier moieties in the vicinity of the *A*-ring may favor ER binding (**Figure 14B**, yellow area).

The molecular models developed in this study were based on the known *x*-ray structures of the LBDs of human ERα and ERβ, which provided valuable information concerning the interactions of these non-aromatic steroids with the ERs. The hydroxyl groups in C-3 and C-17β are key functional groups that form hydrogen bonds with the amino acid residues inside the binding pocket (note that three hydrogen bonds are formed with the C-3 hydroxyl group and one formed with the C-17 hydroxyl group). Based on our recent study (Zhu et al., 2006), the C-3 hydroxyl group appears to be a relatively more important determinant of binding strength compared to the C-17β hydroxyl group because 17-deoxyestrone (an analog of E_2 with the 17-hydroxyl group removed) still retained considerable binding affinity for ERα and ERβ, whereas the lack of a free C-3 hydroxyl group completely removed a steroid's ER binding activity. One major difference between the aromatic steroids (such as E_2 and E_1) and the non-aromatic steroids is the aromaticity of their *A*-rings. This difference can be clearly visualized in **Figure 15C** and **15E** that the non-aromatic *A*-rings are not flat as the aromatic *A*-rings of E_2 and E_1. This difference reduces the strength of the hydrogen bonds and even jeopardizes the formation of the hydrogen bonds between the C-3 hydroxyl group of the non-aromatic steroids and the binding pocket residues, resulting in a drastically reduced binding affinity. This is believed to be one of the major determinants for the low binding affinity of the non-aromatic steroids with a C-3α hydroxyl group. Another important determinant of the binding affinity of the non-aromatic steroids is the lower *van der Waals* interactions between the non-aromatic *A*-ring and the hydrophobic amino acid residues in the binding pockets of human ERα and ERβ. In addition, the *A*- and *B*-rings of

5β-androstans and 5β-estrans are not on the same plane due to the configuration of their C-5 hydrogen atoms, which also interferes with the formation and strength of the C-3 hydrogen bond, and ultimately contributes to the reduced binding affinity of the 5β-compounds for the ERs compared to the 5α-compounds (see **Table 3**).

CONCLUSIONS

We have identified a group of non-aromatic steroids (potential precursors and/or metabolites of endogenous androgens) that can bind human ERα and ERβ with physiologically-relevant high binding affinity, and they can also activate the ERs and elicit hormonal responses in an ERα-positive cell line in culture. The results of this study suggest an intriguing possibility that some of the endogenous androgen precursors or metabolites may serve as ER modulators in men. These findings also call for further studies to determine which of these non-aromatic ER modulators can be produced in men in physiologically-relevant quantities and what their physiological/pathophysiological functions are.

CHAPTER SIX

CHARACTERIZATION OF THE INTERACTIONS OF THE NEWLY-SYNTHESIZED E_2-BASED C-7ALPHA DERIVATIVES WITH HUMAN ESTROGEN RECEPTORS

INTRODUCTION

Since the 1970s, the incidence of breast cancer remains highest among all cancers for women living in the United States, and at present, it is one of the leading causes of cancer-related mortality in women in this country. The use of estrogen receptor (ER) antagonists such as tamoxifen has become an valuable strategy as an adjuvant hormonal therapy for ER-positive human breast cancer (Jordan, 2003). In addition, these antiestrogens are also effective for the prevention of estrogen-inducible breast cancer in high risk populations (Fisher et al., 2005). Tamoxifen is a well-known partial ER agonist at the ERs. Whereas it has a predominant antiestrogenic activity (*i.e.*, ER antagonist activity) under most conditions, it also has a weak estrogenic activity (*i.e.*, ER agonist activity) under certain conditions. The pure ER antagonists, such as ICI-182,780 (fulvestrant) and ICI-164,384 that are devoid of any ER agonistic activity, have already been developed as effective alternatives to tamoxifen. Human breast cancer cells that became resistant to tamoxifen are still sensitive to the anticancer effect of fulvestrant, which has been approved for clinical use in the United States.

Structurally, most of the pure ER antagonists contain the core structure of 17β-estradiol (E_2) with a long side-chain attached to the C-7α position. The long side chain can interfere with the interaction between the two liganded ERs to form active homodimers necessary for ER's transcriptional activity. We hypothesized that estrogen analogs with a shorter but bulkier side chain attached to the C-7α position of E_2 may also function as effective ER antagonists with a more stable side-chain structure. A number of

in vitro bioassays have been used to test the biological functions of these E_2 derivatives to see whether they could function as ER antagonists. Out of a total of nine compounds synthesized, four were shown to have ER antagonist activity with a rather high binding affinity for ERα and ERβ. Computational docking studies were conducted to model the interactions of these antagonists with the ligand binding domain (LBD) of human ERα. These newly-synthesized ER antagonists can tightly bind the ERα binding pocket in a similar way as other known ERα antagonists such as ICI-182,780, which helps explain the mechanism of their antiestrogenic actions. The results of this study provide an example that attachment of a short but bulky structure to the C-7α position of E_2 can yield ER antagonists with comparable receptor binding affinity as ICI-182,780, a prototypical pure ER antagonist. They are promising candidates for further testing as anti-breast cancer agents. Studies are ongoing to further test these ER antagonists for their potential usefulness and efficacy in the prevention and treatment of ER-positive breast cancer *in vivo*.

RESULTS AND DISCUSSION

In recent years, our laboratory has successfully synthesized and purified adequate amounts of nine novel E_2-based C-7α derivatives. This part of the study (the synthesis and purification of these nine compounds) was carried out by Dr. Xiang-Rong Jiang, a former postdoc in Dr. Zhu's laboratory. Structures of these compounds are shown in **Figure 16**. As described below, we performed a series of *in vitro* experiments to test their biological functions, which included the ER binding assays, reporter assays for the ERα transactivation, and cell proliferation assay with both ER-positive and ER-negative breast cancer cell lines.

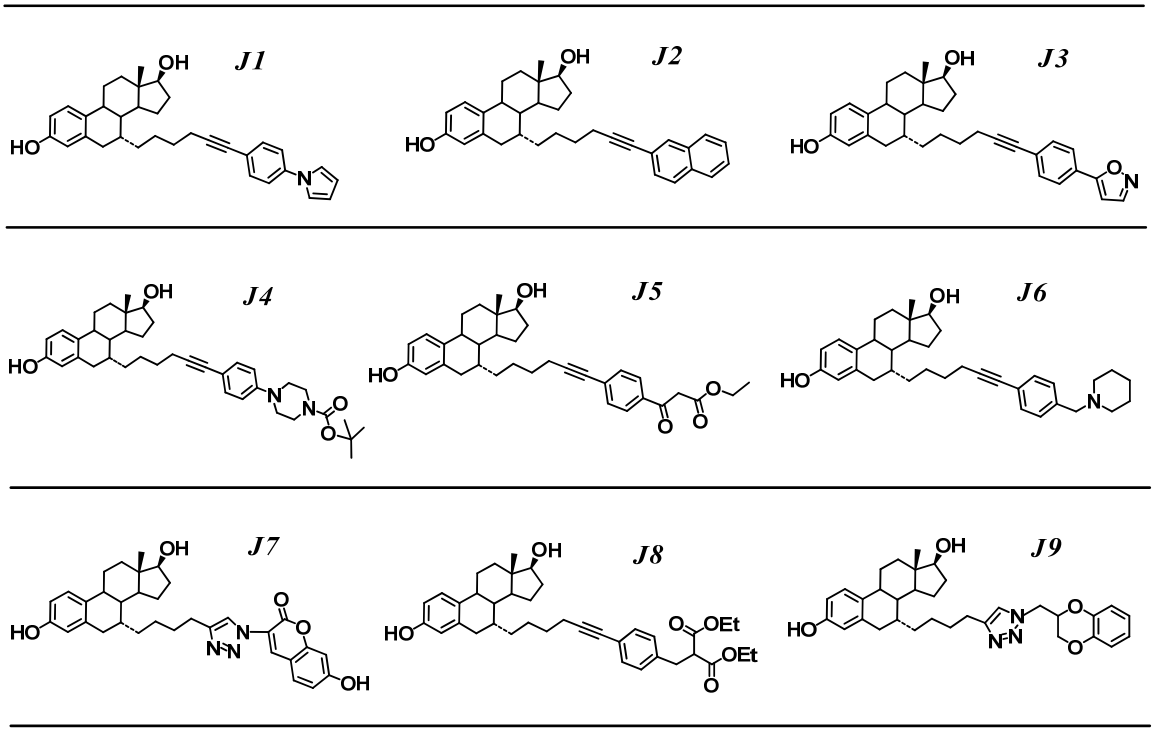

Figure 16 Structures of newly-synthesized E_2-based C-7α derivatives ***J1-J9***.

Newly-synthesized E_2 derivatives retain high binding affinity for ERα and ERβ

First, we determined the relative binding affinities of these newly-synthesized E_2 derivatives for human ERα and ERβ *in vitro*. Although each of them has a rather bulky moiety attached to the C-7α position, the binding affinities of these E_2 derivatives are quite high (data are summarized in **Figure 17** and **Table 4**). It was predicted, beforehand, that these compounds most likely would still retain the ability to interact with the binding domains of human ERα and ERβ in a similar way as E_2, by forming crucial hydrogen bonds between the C-3 and C-17β hydroxyl groups between the ligand molecule and the receptor binding domain. Of the nine chemicals synthesized and tested, ***J1*** and ***J7*** showed the highest binding affinities (their *RBA* values were higher than 20% of E_2). In comparison, the *RBAs* of ***J5***, ***J6***, ***J8***, and ***J9*** were 3 to 5% of E_2, and the *RBAs* of ***J2***, ***J3***, and ***J4*** were approximately 1% of E_2. There were no substantial differences between the binding affinities of these new E_2 analogs for human ERα and ERβ. Notably, the binding affinities of ***J1*** and ***J7*** are comparable to those of ICI-182,780 (*RBA* 40% of E_2), whereas some of the compounds with lower ER binding affinity were comparable to tamoxifen (*RBA* 3% of E_2).

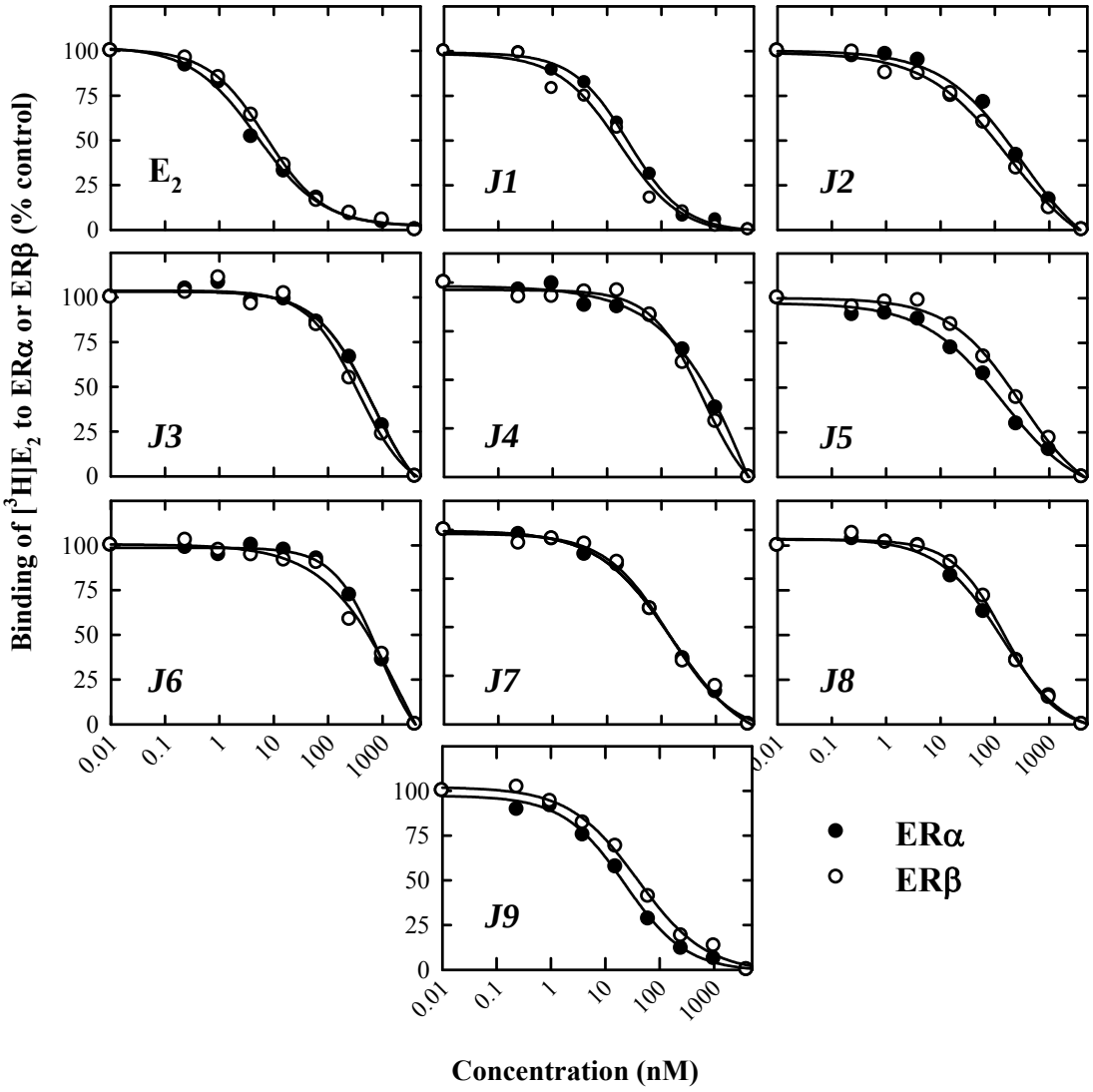
Binding of [3H]E2 to ERα or ERβ (% control)
E2
J1
J2
J3
J4
J5
J6
J7
J8
J9
100
75
50
25
0
0.01
0.1
1
10
100
1000
ERα
ERβ
Concentration (nM)

Figure 17 Comparison of the relative ER binding affinities of ***J1***-***J9*** with that of E_2. The relative binding affinity of each chemical was determined by measuring its inhibition of the binding of 10 nM [^{3}H]E_2 to the recombinant human ERα and ERβ. Eight concentrations (0.06, 0.24, 0.98, 3.9, 15.6, 62.5, 250, and 1000 nM) of each competing ligand were tested. Each point was the mean of duplicate measurements (average variations were <5%). The incubation mixture in the absence of a competing chemical was set as control.

Table 4 The IC_{50} and *RBA* values of ***J1-J9*** for ERα and ERβ. The IC_{50} values for each competing compound were calculated according to the sigmoidal inhibition curves as shown in **Figure 17**, and the relative binding affinity (*RBA*) values for each test compound were calculated against E_2 by using the following equation: *RBA* = (IC_{50} for E_2) / (IC_{50} for the test compounds).

Compounds	**ERα**		**ERβ**	
	***IC_{50}* (nM)**	***RBA (%)***	***IC_{50}* (nM)**	***RBA (%)***
E_2	**6.0**	**100.0**	**8.7**	**100.0**
J1	**28.3**	**21.2**	**19.1**	**45.7**
J2	**481.8**	**1.2**	**331.0**	**2.6**
J3	**567.4**	**1.1**	**436.4**	**2.0**
J4	**637.8**	**1.0**	**565.9**	**1.5**
J5	**116.0**	**5.2**	**111.9**	**7.8**
J6	**126.4**	**4.7**	**150.6**	**5.8**
J7	**24.4**	**24.6**	**41.2**	**21.1**
J8	**96.5**	**6.2**	**185.0**	**4.7**
J9	**175.7**	**3.4**	**120.4**	**7.2**

Several newly-synthesized E_2 derivatives can antagonize E_2's action in the ERα reporter assay.

To determine whether ***J1***-***J9*** were agonists or antagonists for ER, we carried out the ERE reporter assay using HeLa cells (Performed in collaboration with Dr. Carolyn L. Smith at Baylor College of Medicine). As shown in **Figure 18A**, ***J1***, ***J2***, ***J5***, ***J6***, and ***J8*** activated ERα's transcriptional activity to a similar extent as E_2, which indicated that they are full agonists. In contrast, ***J7*** and ***J9*** could not activate ERα, which indicated that they are antagonists. ***J3*** and ***J4*** could stimulate ERα to a very low extent compared with E_2. When we used 1 nM E_2 in combination with ***J3***, ***J4***, ***J7***, and ***J9***, we observed that the ERα's activity stimulated by E_2 was inhibited (**Figure 18B**), which confirmed that these four compounds have ER antagonist activity. ***J7*** and ***J9*** are full antagonists because they cannot activate ERα by themselves. ***J3*** and ***J4*** are partial agonists because they can activate ERα although with very low efficacies.

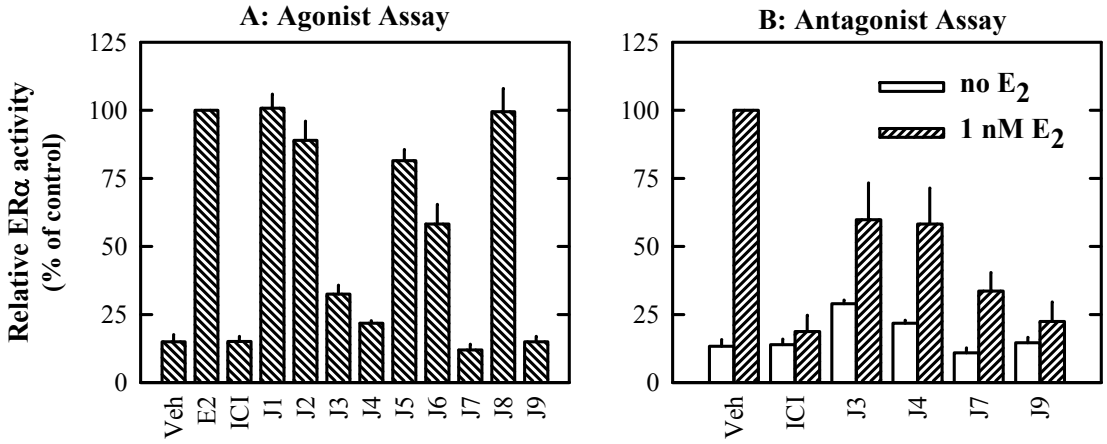

Figure 18 ERα reporter assay with ***J1-J9*** in HeLa cells. **A**. HeLa cells were transfected with an ERE-luciferase reporter plasmid and ERα expression vector. 100 nM ***J1-J9*** and ICI-172,780 (ICI) were used to treat the transfected cells for 24 h. 1 nM E_2 was used as positive control. The y-axis was the luciferase activity normalized with the internal control renilla activity. **B.** The same experiments were carried out as in panel **A**. 100 nM ***J3***, ***J4***, ***J7***, ***J9***, and ICI were used in combination with 1 nM E_2 to treat the transfected Hela cells. Each value is the mean ± S.D. of triplicate measurements.

Several new E_2 derivatives can inhibit estrogen-induced growth of ER-positive human breast cancer cells

Growth of ER-positive MCF-7 cells can be stimulated by ER agonists and inhibited by ER antagonists (Lippman and Bolan, 1975). Of the nine chemicals synthesized in the present study, four of them, *i.e.*, ***J3***, ***J4***, ***J7***, and ***J9***, showed a concentration-dependent inhibitory effect on the growth of MCF-7 cells (**Figure 19A**). However, the other five compounds showed either no effect or a stimulatory effect on MCF-7 cell growth (**Figure 19B**). We could see that the inhibition of cell growth was effective at as low as 1 or 10 nM concentrations. When higher concentrations (10 nM to 1 μM) of these antiestrogens were present, the growth of these cells was inhibited in a concentration-dependent manner. The IC_{50} values of ***J3***, ***J4***, and ***J9*** for growth-inhibition were approximately 50 nM, and the IC_{50} value for ***J7*** was approximately 100 nM. Although these compounds are not as potent as ICI-182,780 (IC_{50} of ~2 nM), their inhibitory potency is higher than that of tamoxifen (IC_{50} of 200 nM). Using ***J3*** and ***J4*** as representative compounds, we also tested their activity in ER-negative MDA-MB-231 cells. As predicted, no appreciable effect (inhibition or stimulation) on the growth of these ER-negative cells was observed when either ***J3*** or ***J4*** was present (**Figure 19C**).

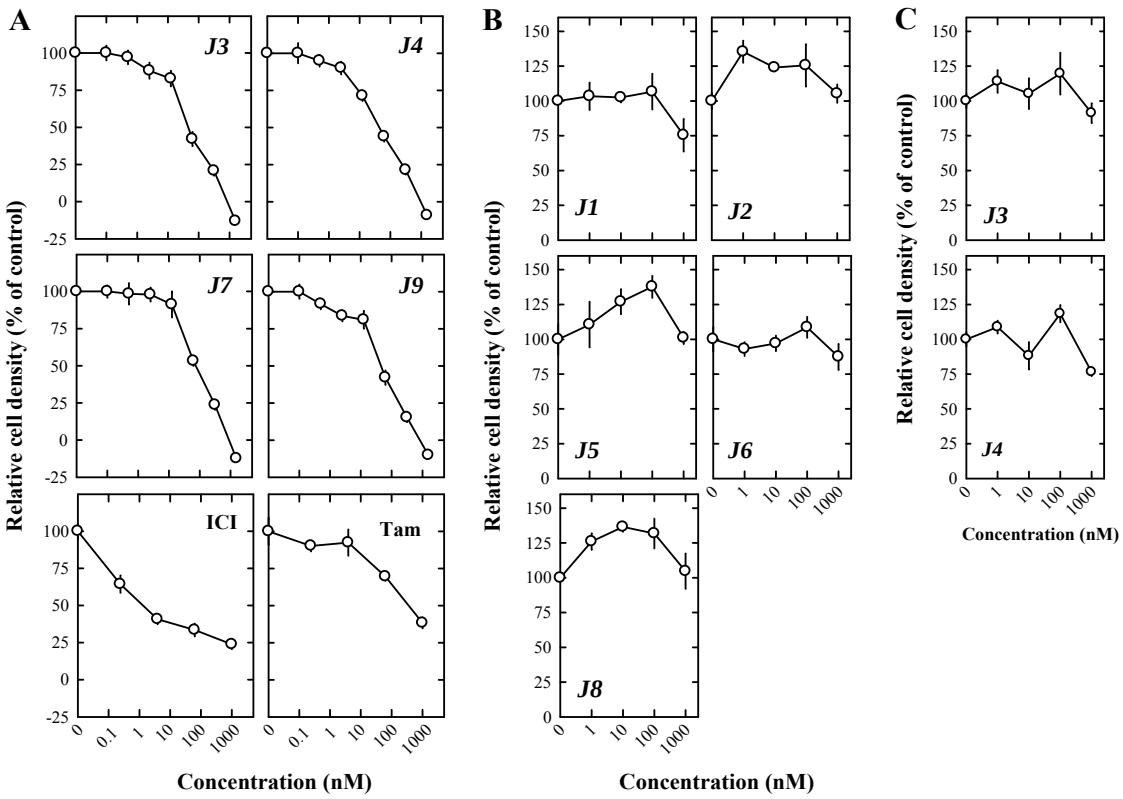
A
B
C
J3
J4
J7
J9
ICI
Tam
J1
J2
J5
J6
J8
J3
J4
Relative cell density (% of control)
Concentration (nM)
0
0.1
1
10
100
1000

Figure 19 Effect of ***J1-J9*** on the proliferation of breast cancer cell lines. The ER-positive MCF-7 and the ER-negative MDA-MB-231 human breast cancer cell lines were cultured and seeded in 96-well plates. Different final concentrations of the ER ligands (at 0, 0.1, 0.32, 1.6, 8, 40, 200, and 1000 nM) were added to the cell culture medium for 6 days with one medium change on the third day. Cell density was determined by using the crystal violet staining method as described previously (Liu and Zhu, 2004). Each point was the mean ± S.E.M (N = 6). Each experiment was repeated two or three times. **A**. Four synthesized E_2 analogs showed an inhibitory effect on the growth of MCF-7 cells. **B**. Five of the other synthesized E_2 analogs did not have an appreciable effect on the growth of MCF-7 cells. **C**. Two representative ER antagonists did not affect the growth of the ER-negative MDA-MB-231 cells.

Computational molecular modeling study

The three-dimensional structures of the ERα LBD in association with both an agonist and an antagonist have been resolved using the *X*-ray crystallography (Brzozowski et al., 1997). The most notable difference between these two conformations is that in the antagonist-binding conformation, helix-12 (H12), which is crucial for ER dimerization and activation, is forced to leave its initial position. With this conformation, the ERα proteins cannot dimerize to form homodimers, and as a result, the transcriptional activity of ERα is not activated. Using the ERα LBD in complex with RAL (an ER antagonist) as a template, we analyzed the binding interactions of the novel ER antagonists developed in this study with human ERα LBD using computational docking tools.

As shown in **Figure 20A** and **20B**, both ICI-182,780 and ***J9*** can bind rather tightly inside the binding pocket of human ERα, and their steroidal rings, especially their C-3 and C-17β hydroxyl groups, overlapped with each other extensively. Their hydroxyl groups form hydrogen bonds with the amino acid residues E353, R394, and H524 of ERα in a similar way as those of E_2. In addition to the formation of hydrogen bonds between the C-3 or C-17β hydroxyl groups of ***J9*** and ERα, its side chain may also form an additional hydrogen bond with N532 of ERα. Using the same method, we also docked ***J3***, ***J4***, and ***J7*** into ERα LBD.

In the docking models developed, these pure antagonists (ICI-182,780 and newly synthesized ***J3***, ***J4***, ***J7***, and ***J9***) adopted a unique binding mode different from E_2 by flipping their core steroidal structure 180^o along the C-3 and C-17β hydroxyl axis. In this way, the long C-7α side chain was positioned in the C-11β channel and then exited the ligand binding pocket in a similar manner as RAL. However, the characteristic hydrogen bonds of C-3 and C-17β hydroxyl groups with the receptor binding pocket basically remain unchanged. This binding mode was consistent with the reported crystal structure of human ERβ in complex with ICI-164,384 (an analog of ICI-184,780) (Pike et al., 2001).

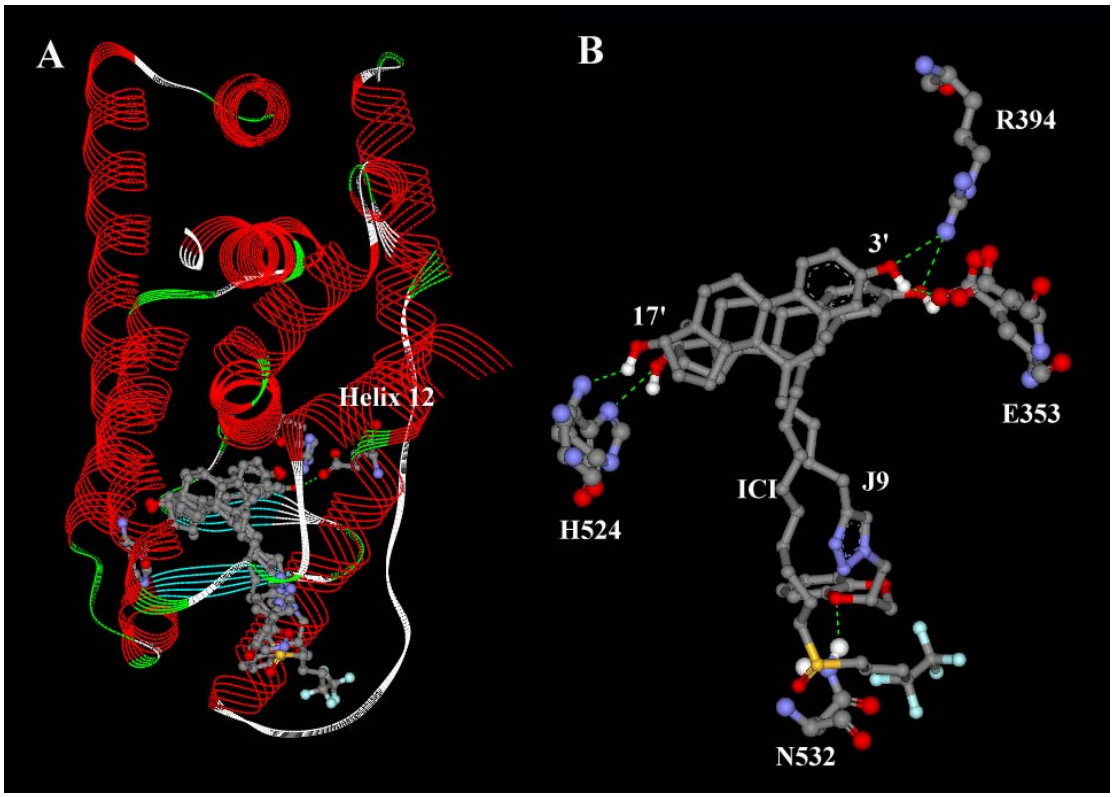

Figure 20 Molecular docking of the ER antagonists with human ERα LBD. **A**. Structure of the ERα ligand binding domain in complex with ICI-182,780 and ***J9***. **B**. Formation of hydrogen bonds between several amino acid residues in the ERα ligand binding domain and the antagonistic ligand, ICI-182,780 or ***J9***. The protein structure is shown in colored ribbons according to the secondary structures (red for α-helix, blue for β-sheets, green for turns, and white for coils). Amino acids and ligands are rendered in ball and stick format. Oxygen, nitrogen, carbon, and fluorine atoms are colored red, blue, gray, and cyan, respectively. Hydrogens are omitted from all structures.

CONCLUSIONS

In this study, we designed and synthesized several new ER antagonists with a shorter but bulky side chain attached to the C-7α position of E_2 compared to ICI-172, 780. Whereas all nine newly-synthesized derivatives were found to have considerable binding affinity for human ERα and ERβ, four of them have ER antagonistic activity, based on the ER transactivation activity assay and the proliferation assay in ER-positive human breast cancer cells. Computational docking studies were conducted to model the interactions of these antagonists with the LBD of human ERα. These newly-synthesized ER antagonists can tightly bind the ERα binding pocket in a similar way as other known ERα antagonists such as ICI-182,780, which helps explain the mechanism of their antiestrogenic actions. The results of this study provide an example that attachment of a short but bulky structure to the C-7α position of E_2 can yield ER antagonists with comparable receptor binding affinity as ICI-182,780, a prototypic pure ER antagonist. Taken together, these four new ER antagonists are good candidates for further structural modifications as well as for further testing of their usefulness in the prevention and treatment of ER-positive breast cancer.

CHAPTER SEVEN

STRUCTURAL CHARACTERIZATION OF THE ESTRADIOL-BINDING SITE OF HUMAN PDIP: INDISPENSABLE ROLE OF THE HYDROGEN BOND BETWEEN PDIP-HIS278 AND THE 3-HYDROXYL GROUP OF ESTRADIOL

INTRODUCTION

Estradiol (E_2), an important endogenous female sex hormone, exerts a wide array of biological functions in various target organs or tissues in a women's body, such as reproductive organs. Many of the well-known physiological functions of E_2 are mediated by the genomic actions of the estrogen receptors (ER) α and β (Ciocca and Roig, 1995), which are transcription factors that can initiate the expression of various target genes.

Besides ERs, a few other proteins have also been found to have the ability to bind endogenous estrogens, serving as important modulators of the biological actions of these female hormones. For instance, the sex hormone binding globulin (SHBG), a well-known estrogen-binding protein present in large quantities in circulation, can profoundly modulate the bioavailability of free circulating estrogens, subsequently altering the tissue and intracellular levels of estrogens and their hormonal activities in various target sites (Fortunati and Catalano, 2006; Zhang et al., 2005). Protein disulfide isomerase (PDI), a well-known protein folding catalyst (Wilkinson and Gilbert, 2004), can also bind estrogens (Primm and Gilbert, 2001; Tsibris et al., 1989) and modulate estrogen level and hormonal actions in human breast cancer cells (Fu et al., 2008). Recently, we reported, for the first time, that the human pancreas-specific PDI homolog (PDIp), which is highly expressed in pancreatic acinar cells (Desilva et al., 1996; Desilva et al., 1997) and has both disulfide isomerase (Desilva et al., 1996; Fu and Zhu, 2010) and chaperone activities (Fu and Zhu, 2010; Klappa et al., 1998), is another intracellular E_2-binding protein that

can modulate estrogen actions in mammalian cells (Fu and Zhu, 2009). In light of these earlier observations, and given the fact that these two intracellular proteins are present at unusually high levels in certain human tissues or cells, it was speculated that PDI and PDIp may function as important intracellular E_2-storage proteins in these cells (Fu et al., 2008; Fu and Zhu, 2009; Primm and Gilbert, 2001).

At present, the E_2-binding site structure of human PDIp is not known, although a few earlier studies have suggested that the peptide-binding sites may overlap with the E_2-binding sites (Klappa et al., 2001; Klappa et al., 1998; Primm and Gilbert, 2001). Elucidation of the estrogen-binding site structures of these intracellular proteins will aid in the identification of potential xenobiotics that may can alter estrogen's action by modulating the estrogen-binding activity. The main purpose of our present study, therefore, was to delineate the structural basis of human PDIp's E_2-binding activity.

Based on what we learned from **AIM 1** on the three-dimensional interactions of estrogens with ERs, I applied computational molecular modeling methods to predict the binding site structure of PDIp for the endogenous estrogen E_2 as well as its binding interaction with E_2. The predicted models were confirmed by site-directed mutagenesis of amino acids and selective ligand modifications. We precisely located the PDIp's E_2-binding site to a hydrophobic pocket between the *b* and *b'* domains, and we have also identified a hydrogen bond that is essential for human PDIp's E_2-binding activity (The biochemical part of the study was done by Dr. Xinmiao Fu in Dr. Zhu's lab).

RESULTS AND DISCUSSION

As depicted in **Figure 21A**, human PDIp is composed of four thioredoxin-like domains, *a*, *b*, *b'*, and *a'*, plus a small linker region *x* between *b'* and *a*' and a *C*-terminal acidic extension *c*. To experimentally locate the E_2-binding site in this protein, we designed three truncated human PDIp fragments (namely, *a-b*, *b-b'*, and *b'-x-a'c*, as depicted in **Figure 21A**), with a His-tag attached to their *N*-termini for the convenience of purification. Because these three fragments cover the full length of the PDIp protein with each fragment containing two neighboring main domains (*i.e.*, *a-b*, *b-b'*, and *b'-a'*), theoretically they would allow us to determine whether the E_2-binding site is only associated with any of the individual domains or jointly formed by any of the two neighboring domains. These three PDIp fragments as designed above were selectively over-expressed in *E. coli* cells, purified (left part in **Figure 21B**), and then subjected to *in vitro* analysis of their [^{3}H]E_2-binding ability. The results (**Figure 21C**) showed that the *b-b'* fragment has a distinct, high specific binding affinity for [^{3}H]E_2, although a weak binding activity was detected for the *b'-x-a'-c* fragment. No binding activity was detected for the *a-b* fragment when it was assayed at an equimolar protein concentration under the same conditions. These observations were repeated multiple times by using proteins prepared from several independent experiments, and the *b-b'* fragment was consistently found to have a very high E_2-binding activity. These results clearly suggest that the E_2-binding site is not associated with each individual domain, but rather it is associated with the *b-b'* domain complex.

To further verify the above observations, we selectively expressed the single *b* and *b'* domains for testing of their individual E_2-binding activities. In our initial experiments, we also adopted the strategy of attaching a His-tag to the *b* and *b'* single domain fragments. Unfortunately, the yield of the *b* and *b'* single domain proteins (with a His-tag) was very low when they were individually expressed in *E. coli* cells, likely due to their much smaller sizes and reduced stabilities. After we modified the strategy by attaching a GST tag to the *N*-termini of the *b* and *b'* fragments, the problem of low protein yield was solved. The *b* and *b'* single domain fragments (with a GST-tag) were purified (**Figure 21B**), and then subjected to analysis of their ability to bind [^{3}H]E_2. As expected, the protein fragment that contained either *b* or *b'* single domain did not have an appreciable [^{3}H]E_2-binding activity (**Figure 21C**). The experiment was repeated three times, and each time the same observations were made. For comparison, we have also prepared the single *a'* domain (in the form of *x*-*b'*-*c*), and this fragment also did not have an appreciable [^{3}H]E_2-binding activity (**Figure 21C**).

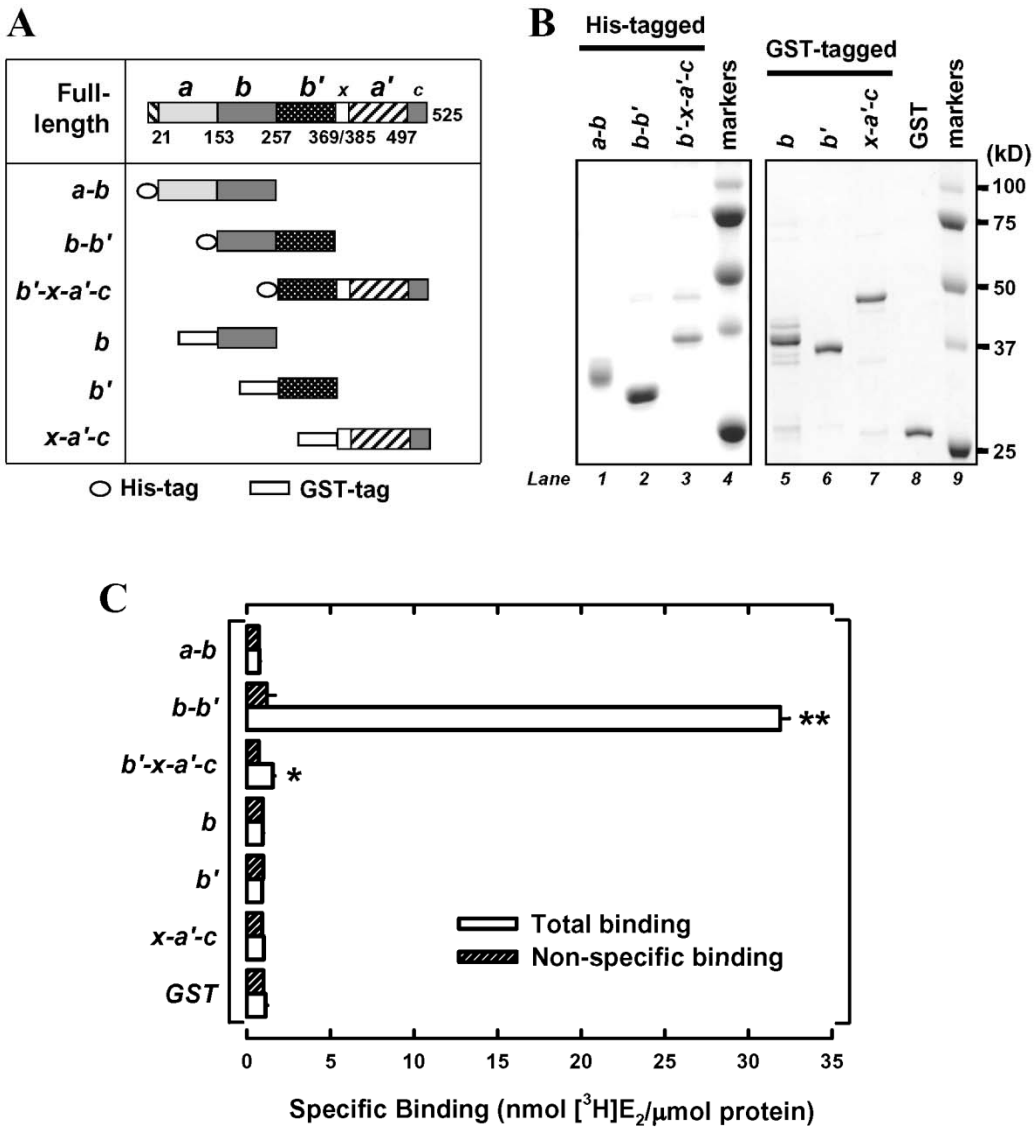
A
Full-length
a
b
b'
x
a'
c
525
21
153
257
369/385
497
a-b
b-b'
b'-x-a'-c
b
b'
x-a'-c
His-tag
GST-tag
B
His-tagged
GST-tagged
a-b
b-b'
b'-x-a'-c
markers
b
b'
x-a'-c
GST
markers
(kD)
100
75
50
37
25
Lane
1
2
3
4
5
6
7
8
9
C
a-b
b-b'
b'-x-a'-c
b
b'
x-a'-c
GST
**
*
Total binding
Non-specific binding
0
5
10
15
20
25
30
35
Specific Binding (nmol [3H]E2/μmol protein)

Figure 21 Human PDIp *b-b'* fragment contains the E_2-binding site. **A.** Domain organization of the human PDIp protein (based on Q13087 in the UniProtKB database). Domain boundaries of human PDIp were determined by sequence alignment of PDIp with PDI, whose domain boundaries are described earlier (Tian et al., 2006). Fragments *a-b, b-b'*, and *b'-x- a'-c* were constructed as histidine-tagged fusion proteins. Fragment *b, b'*, and *x-a'-c* were constructed as GST-tagged fusion proteins. **B**. SDS-PAGE analysis of three histidine-tagged PDIp fragments (left part) and three GST-tagged fragments (right part), which were selectively expressed in *E. coli* cells and then purified using chromatography. **C**. The binding of [^{3}H]E_2 by each of the purified PDIp fragments (at a final concentration of 0.5 μM) after incubation with 4.5 nM [^{3}H]E_2 in 10 mM sodium phosphate buffer (pH 7.4) in the absence or presence of 10 μM cold E_2. Each value is the mean ± S.D. of triplicate determinations. * $P < 0.05$, ** $P < 0.01$, compared to the corresponding non-specific binding. Each experiment was repeated two or three times.

Using the purified *b-b'* fragment, we next determined its E_2-binding affinity (*i.e.*, the K_d value) when different concentrations (1−650 nM) of radiolabeled E_2 were tested as the binding ligand. Analysis of the binding curve pattern as well as the Scatchard plot suggests that the PDIp *b-b'* fragment displays single binding site kinetics, with an apparent K_d value of 153 – 181 nM (**Figure 22A**). To verify that the human PDIp only has a single E_2 binding site, we also determined the [^{3}H]E_2-binding affinity of the full-length PDIp that was selectively over-expressed in cos-7 mammalian cells. The preparation and purification of this protein is summarized in **Figure 23**. Similarly, analysis of the binding curve pattern and Scatchard plot shows that the recombinant full-length human PDIp protein also exhibits single site binding kinetics, with apparent K_d value of approximately 170 nM (**Figure 22B**), which is very similar to the apparent K_d value of the purified recombinant *b-b'* fragment. Taken together, these observations unequivocally suggest that the human PDIp protein only has a single binding site for E_2, and the binding site is located in its *b-b'* fragment.

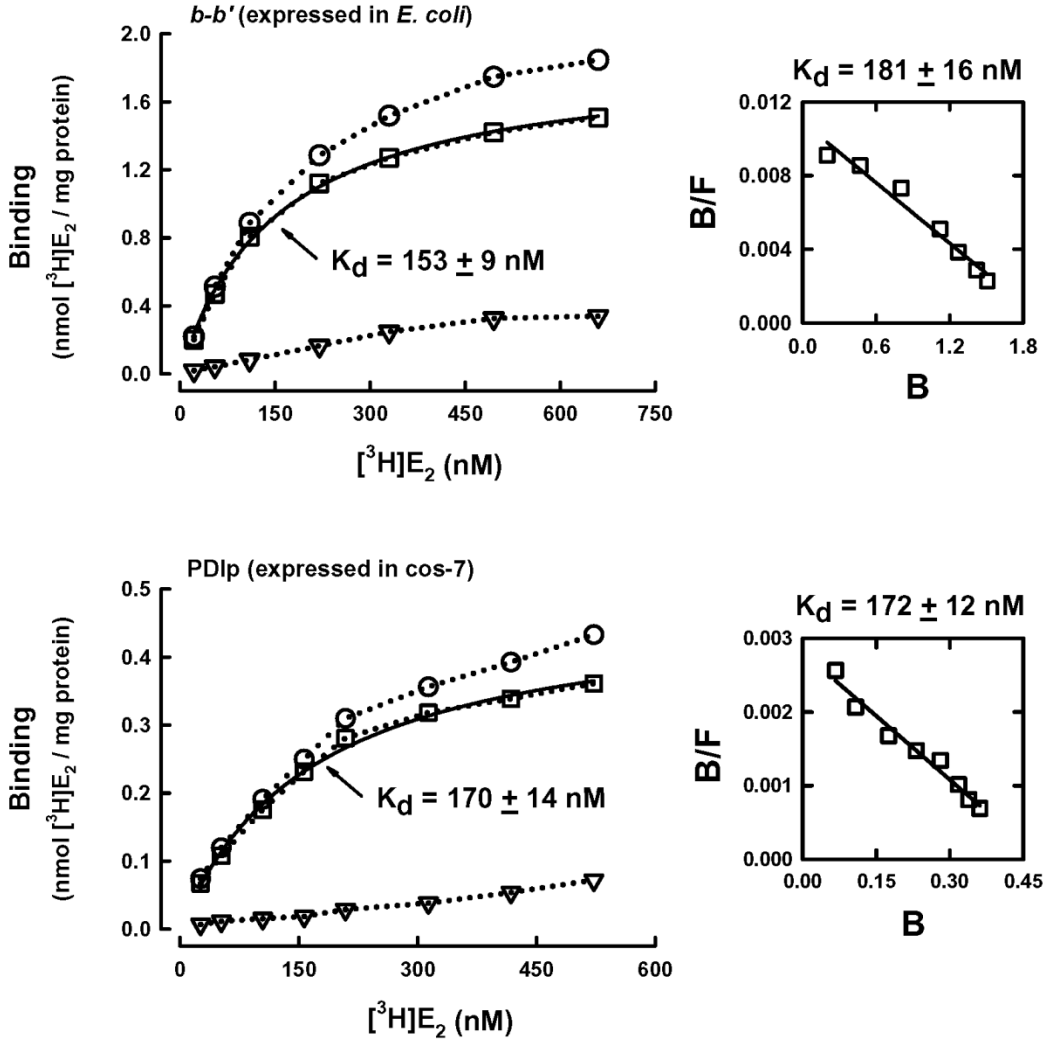
b-b' (expressed in E. coli)
Binding
(nmol [3H]E2 / mg protein)
2.0
1.6
1.2
0.8
0.4
0.0
0
150
300
450
600
750
[3H]E2 (nM)
Kd = 153 ± 9 nM
Kd = 181 ± 16 nM
B/F
0.012
0.008
0.004
0.000
0.0
0.6
1.2
1.8
B
PDlp (expressed in cos-7)
Binding
(nmol [3H]E2 / mg protein)
0.5
0.4
0.3
0.2
0.1
0.0
0
150
300
450
600
[3H]E2 (nM)
Kd = 170 ± 14 nM
Kd = 172 ± 12 nM
B/F
0.003
0.002
0.001
0.000
0.00
0.15
0.30
0.45
B

Figure 22 Determination of the dissociation constant (K_d) of the human *b-b'* fragment and the full-length human PDIp for E_2. Total binding (TB) of [^{3}H]E_2 by the *b-b'* fragment or the full-length PDIp protein (at 20 μg/ml final concentration) was determined in the presence of increasing concentrations of [^{3}H]E_2 (22 to 660 nM) in 10 mM sodium phosphate buffer (pH 7.4). Non-specific binding (NSB) was determined in the presence of excess non-radiolabeled E_2 (10 μM). Total binding (TB) subtracted by non-specific binding (NSB) gives rise to specific binding (SB). The binding curve (left part) was obtained using curve regression analysis (hyperbola model) of the SigmaPlot software. The corresponding Scatchard plot is shown in the right part of each panel. Panel **A** shows the data for the purified recombinant PDIp *b-b'* fragment expressed in *E.coli* cells. Panel **B** shows the data for the purified human PDIp protein selectively expressed in cos-7 cells. Each value is the mean of duplicate measurements.

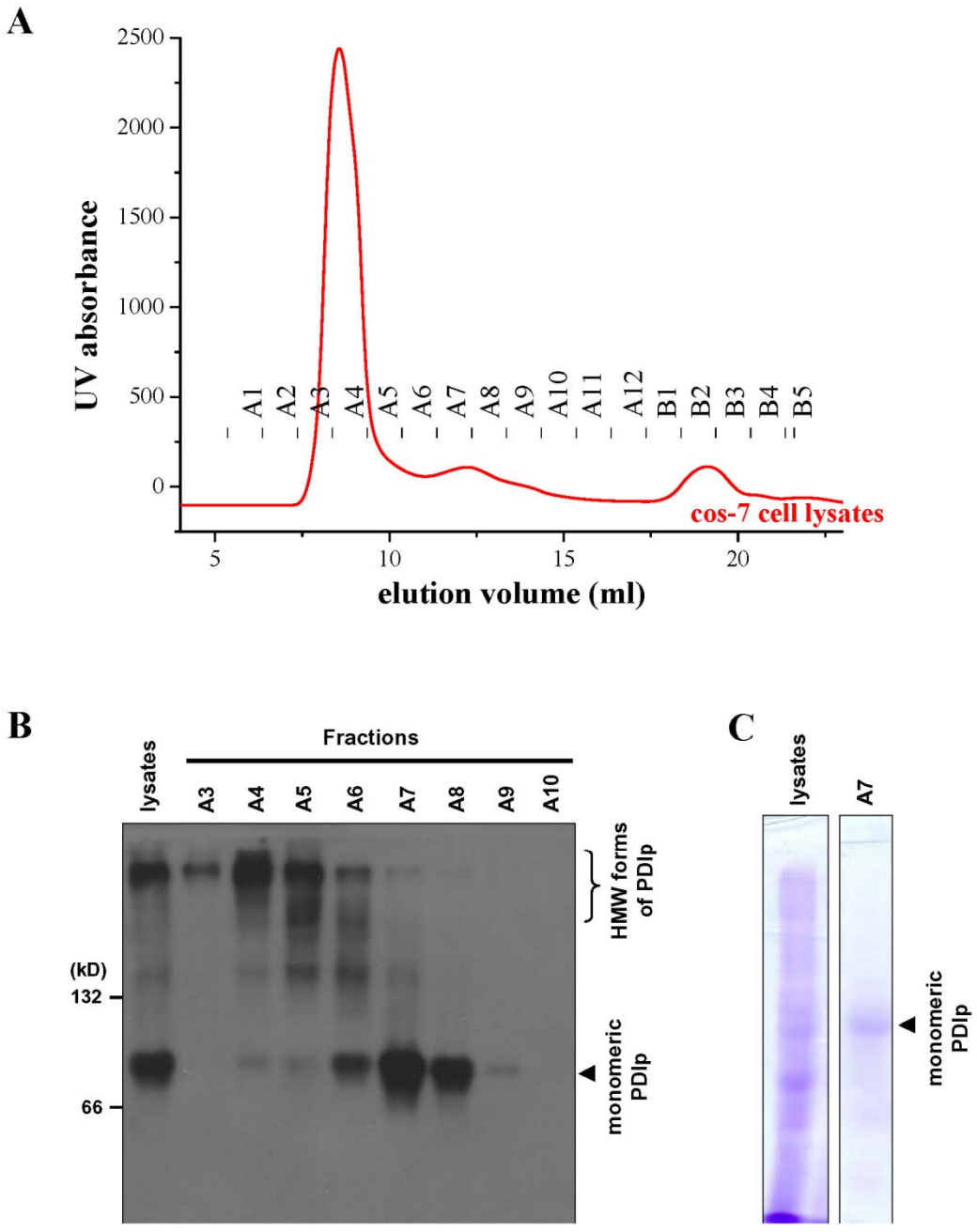
A
2500
2000
1500
1000
500
0
UV absorbance
A1
A2
A3
A4
A5
A6
A7
A8
A9
A10
A11
A12
B1
B2
B3
B4
B5
cos-7 cell lysates
5
10
15
20
elution volume (ml)
B
Fractions
lysates
A3
A4
A5
A6
A7
A8
A9
A10
HMW forms of PDIp
(kD)
132
66
monomeric PDIp
C
lysates
A7
monomeric PDIp

Figure 23 Isolation of PDIp from cos-7 cell lysates by size exclusion chromatography (SEC). **A**. Isolation of PDIp from cos-7 cells by SEC. The cos-7 cell lysates containing over-expressed PDIp were loaded onto a Superdex 200 column and eluted with 10 mM sodium phosphate buffer (pH 7.4). Fractions were collected at 1 ml/tube in an ice bath. **B**. Western blotting analysis of PDIp in the SEC fractions that were isolated by native gel electrophoresis (7.5%). **C**. Native gel (7.5%) separation of total cell lysates and SEC fraction A7 and visualized by Coomassie blue staining. PDIp was dominantly present in fraction A7.

Next, we sought to predict the three-dimensional (3-D) E_2-binding pocket structure of PDIp *b-b'* fragment by using computational modeling analysis. To achieve this goal, we first built the 3-D structure of the *b-b'* fragment by using the homology modeling approach according to the known structure of the *b-b'* fragment of the human PDI protein (Denisov et al., 2009), which shares 38% sequence homology with the human PDIp (as shown **Figure 24A**). Based on the homology structural model of human PDIp *b-b'* fragment, we noticed that its backbone structure is very similar to that of the human PDI *b-b'* fragment (**Figure 24B**), although there are some subtle differences in the side chains and loop structures.

To predict the E_2-binding pocket in the *b-b'* fragment, we used the *Insight II* modeling program to calculate the size of the cavities present in the protein structure. Three cavities were found in the *b-b'* fragment (**Figure 24C**): cavity I is located between the *b* and *b'* domains, *i.e.*, it is formed jointly by these two domains (cavity size = 376 $Å^3$). In comparison, cavity II is solely formed by the *b* domain (size = 207 $Å^3$), and cavity III is solely formed by the *b'* domain (size = 129 $Å^3$). Based on the experimental data, which showed that the single *b* or *b'* domain does not have an intact E_2-binding site whereas the *b-b'* domain complex has the binding site, these experimental data were considered as the scientific basis for excluding cavities II and III from further consideration as viable E_2-binding sites. By contrast, cavity I matches perfectly with the experimental findings, *i.e.*, the binding pocket is formed by both *b* and *b'* domains but not by an individual domain present alone. Here it should also be noted that cavity I also has

an optimal size that would enable it to function as a low affinity E_2-binding site. Earlier studies (Brzozowski et al., 1997; Manas et al., 2004; Manas et al., 2004) showed that the volumes of the E_2-binding pockets of human ERα and ERβ are 266 and 275 $Å^3$, respectively. The fact that the size of cavity I (376 $Å^3$) is slightly larger than the E_2-binding pockets of human ERs suggests that E_2 will likely bind more loosely inside PDIp's binding pocket due to less hydrophobic interactions than inside the binding pockets of ERs, which agrees perfectly with the known differences in their E_2 binding affinities. On the contrary, the much smaller sizes of cavities I and II than those of the human ERs further suggest that they are unlikely to be viable E_2-binding sites.

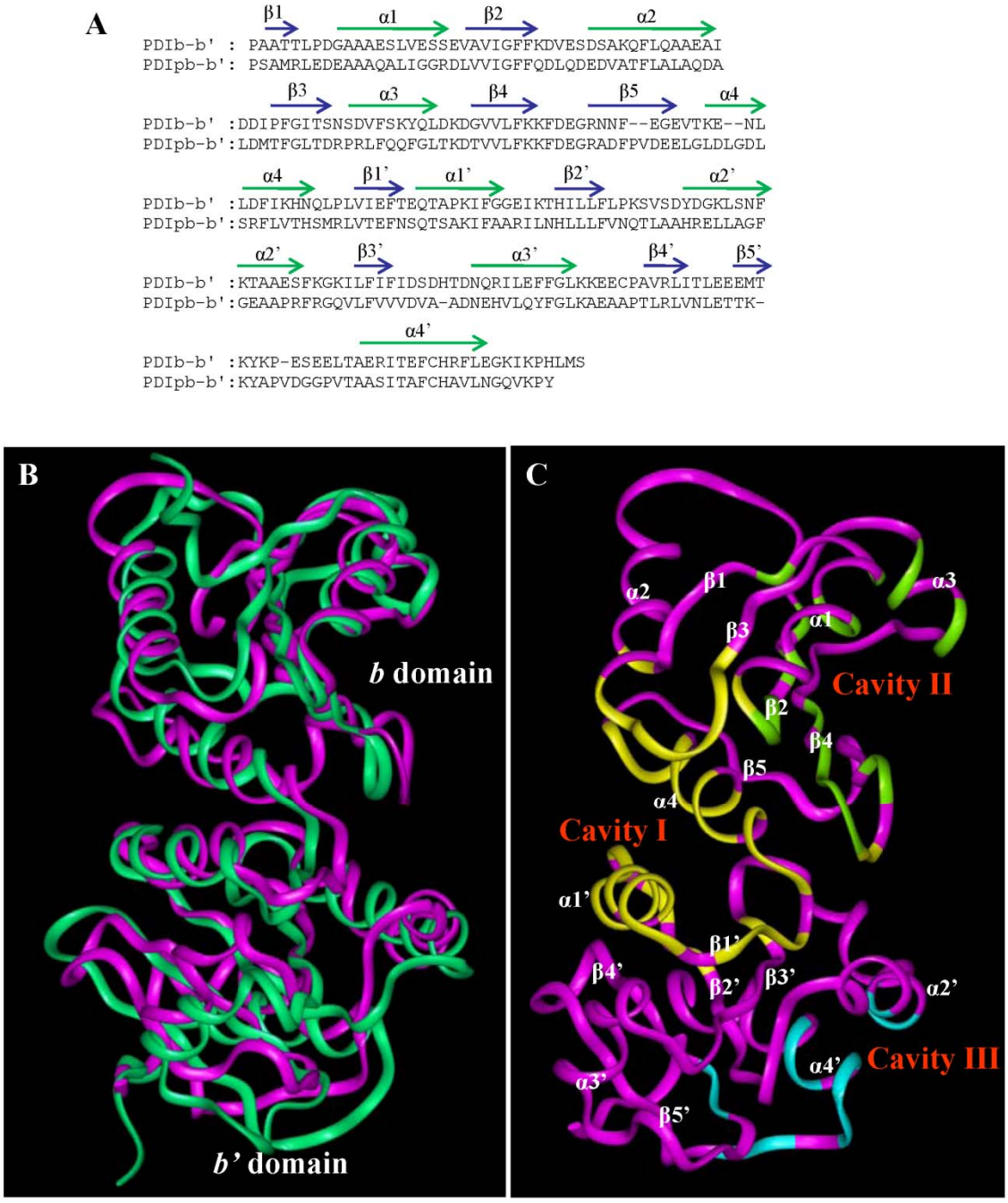
A
β1 α1 β2 α2
PDIb-b' : PAATTLPDGAAAESLVESSEVAVIGFFKDVESDSAKQFLQAAEAI
PDIpb-b': PSAMRLEDEAAAQALIGGRDLVVIGFFQDLQDEDVATFLALAQDA
β3 α3 β4 β5 α4
PDIb-b' :DDIPFGITSNSDVFSKYQLDKDGVVLFKKFDEGRNNF--EGEVTKE--NL
PDIpb-b':LDMTFGLTDRPRLFQQFGLTKDTVVLFKKFDEGRADFPVDEELGLDLGDL
α4 β1' α1' β2' α2'
PDIb-b' :LDFIKHNQLPLVIEFTEQTAPKIFGGEIKTHILLFLPKSVSDYDGKLSNF
PDIpb-b':SRFLVTHSMRLVTEFNSQTSAKIFAARILNHLLLFVNQTLAAHRELLAGF
α2' β3' α3' β4' β5'
PDIb-b' :KTAAESFKGKILFIFIDSDHTDNQRILEFFGLKKEECPAVRLITLEEEMT
PDIpb-b':GEAAPRFRGQVLFVVVDVA-ADNEHVLQYFGLKAEAAPTLRLVNLETTK-
α4'
PDIb-b' :KYKP-ESEELTAERITEFCHRFLEGKIKPHLMS
PDIpb-b':KYAPVDGGPVTAASITAFCHAVLNGQVKPY
B
b domain
b' domain
C
α2
β1
α3
β3
α1
Cavity II
β2
β4
β5
α4
Cavity I
α1'
β1'
β4'
β2'
β3'
α2'
α4'
Cavity III
α3'
β5'

Figure 24 Determination of the E_2-binding sites in PDIp using computational modeling. **A.** Protein sequence alignment of human PDI *b-b'* fragment and human PDIp *b-b'* fragment. Positions of α-helices and β-sheets are labeled by green arrows and blue arrows, respectively. α-Helices and β-sheets in the *b* domain are numbered as α1 - α4 and β1 - β5. α-Helices and β-sheets in the *b'* domain are numbered as α1'- α4' and β1'- β5'. **B.** Structural superimposition of PDI *b-b'* fragment (PDB: 2k18; green color) and PDIp *b-b'* fragment (magenta color). The structure of the PDIp *b-b'* fragment is built using the homology modeling (*Insight II*) based on the template structure of the PDI *b-b'* fragment. Protein structures are shown in ribbons. **C**. The three potential E_2-binding cavities identified in the PDIp *b-b'* fragment. Cavity I, cavity II, and cavity III are colored in yellow, green, and blue, respectively. α-Helices and β-sheets are labeled as in panel **A**.

Next, we used the *Affinity* module of *InsightII* to dock E_2 into cavity I. Two candidate E_2-binding modes are suggested (**Figure 25D**). In both binding modes, E_2 has a very similar overall orientation and positioning inside the binding pocket, and hydrogen bonds are formed between E_2 and PDIp *b-b'* fragment. In mode I (**Figure 25A, 25B, 25C, 25D**), one hydrogen bond is formed between the 3-hydroxyl group of E_2 and the nitrogen atom of PDIp-His278. In mode II (**Figure 25D**), two hydrogen bonds are formed: one between the 3-hydroxyl group of E_2 and PDIp-His278 and the other one between the 17-hydroxyl group of E_2 and PDIp-Gln265.

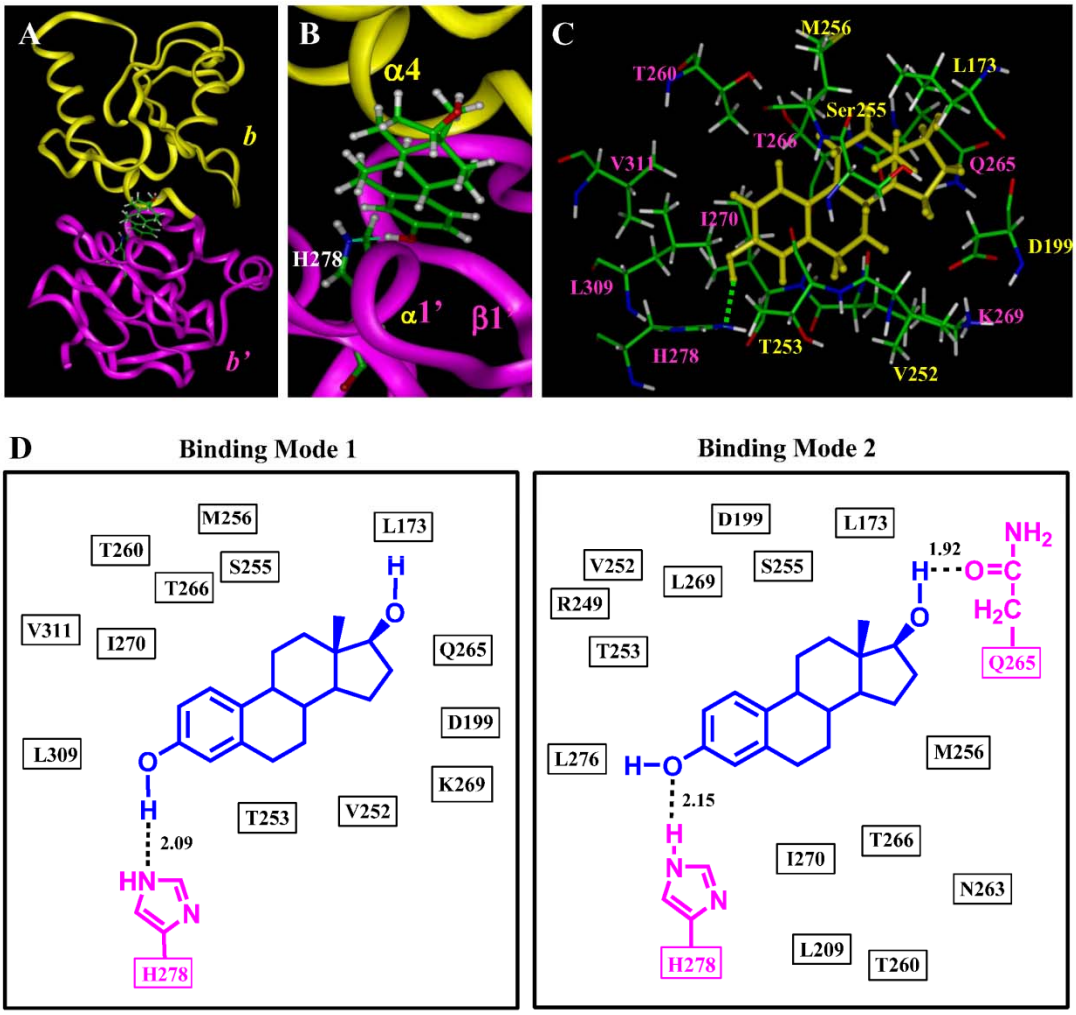
A
b
b'
B
α4
H278
α1'
β1
C
M256
T260
L173
Ser255
T266
V311
Q265
I270
D199
L309
K269
H278
T253
V252
D
Binding Mode 1
M256
L173
T260
S255
T266
V311
I270
Q265
D199
L309
K269
T253
V252
2.09
H278
Binding Mode 2
D199
L173
V252
S255
L269
R249
T253
1.92
Q265
L276
M256
2.15
I270
T266
N263
L209
T260
H278

Figure 25 Docking analysis of the binding mode of E_2 inside human PDIp *b-b'* fragment. **A.** Overview of the docking result (mode I) of E_2 binding inside the PDIp *b-b'* fragment. E_2 and H278 are shown in the ball-and-stick format and colored according to atoms. The protein structure is shown in ribbon. The yellow colored region denotes the *b* domain and magenta colored region denotes the *b'* domain. **B**. A close-up view of the docking result of the E_2-PDIp binding model. **C**. Interaction of E_2 with amino acid residues in the binding pocket (mode I). Labeling of amino acid residues is shown in yellow for the *b* domain and in magenta for the *b'* domain. E_2 is colored in yellow. Amino acids are shown in the ball-and-stick format and colored according to atoms, *i.e.*, green for carbon, red for oxygen, white for hydrogen, and blue for nitrogen. **D**. Plots of the docking results of E_2 binding with PDIp *b-b'* fragment in mode I and II. The distance is in angstroms. E_2 is colored in blue and H278 and Q265 are in magenta.

To experimentally test the binding modes as suggested by our computational docking analysis, we first sought to determine whether the two identified amino acid residues, His278 and Gln265, are indeed involved in the binding interactions between PDIp and E_2 through forming hydrogen bonds. To do so, we introduced point mutations to probe whether changes in these two amino acid residues would alter PDIp's E_2-binding activity.

We first chose to mutate His278 to leucine. The side-chain length of leucine is similar to that of histidine but it does not contain electro-negative atoms that are necessary for the formation of hydrogen bonds. As shown in **Figure 26A**, the purified H278L *b-b'* fragment completely lost [^{3}H]E_2-binding activity. Saturation binding assay further confirmed that this mutant fragment did not have an appreciable [^{3}H]E_2-binding activity even when very high concentrations of [^{3}H]E_2 were present (**Figure 26B**). Similarly, we also created the H278L mutation in the full-length PDIp, which was over-expressed in mammalian cells and isolated by SEC. Assay of the [^{3}H]E_2 binding activity of each of the SEC fractions showed that the PDIp H278L mutant protein does not have an appreciable [^{3}H]E_2-binding activity (**Figure 26C**). Taken together, these data show that PDIp's His278 is indispensable for its binding interaction with E_2.

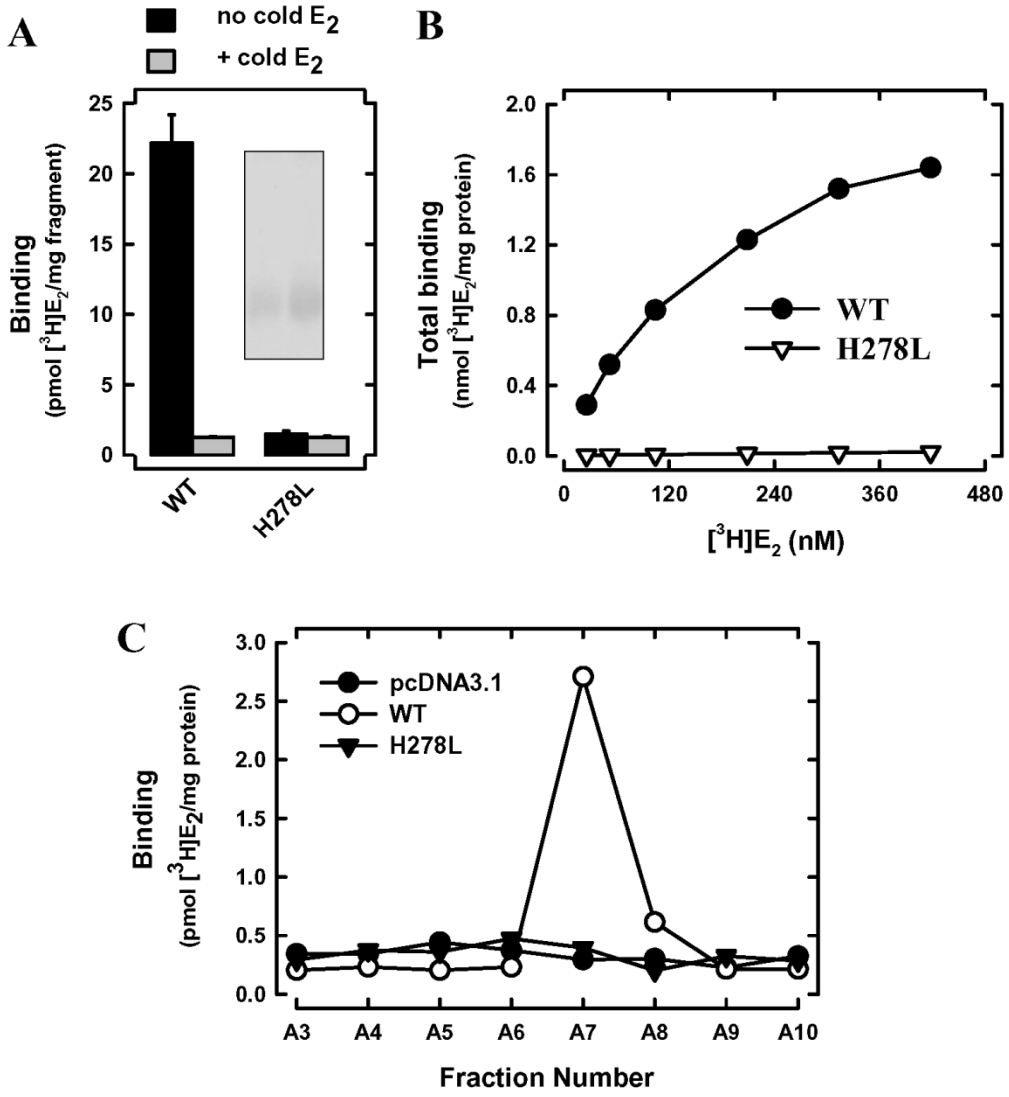
A
no cold E_2
+ cold E_2
Binding
(pmol [^{3}H]E_2/mg fragment)
25
20
15
10
5
0
WT
H278L
B
Total binding
(nmol [^{3}H]E_2/mg protein)
2.0
1.6
1.2
0.8
0.4
0.0
WT
H278L
0
120
240
360
480
[^{3}H]E_2 (nM)
C
Binding
(pmol [^{3}H]E_2/mg protein)
3.0
2.5
2.0
1.5
1.0
0.5
0.0
pcDNA3.1
WT
H278L
A3
A4
A5
A6
A7
A8
A9
A10
Fraction Number

Figure 26 The H278L mutant protein lacks E_2-binding activity. **A.** Total [^{3}H]E_2 binding by purified PDIp *b-b'* fragments (wild-type and H278L mutant proteins, purified from *E. coli* cells) after incubation with 4.5 nM [^{3}H]E_2 in the absence or presence of excess cold E_2 (10 μM) in 10 mM sodium phosphate buffer. Inset shows the SDS-PAGE analysis of the purified proteins. **B**. Total [^{3}H]E_2 binding by PDIp *b-b'* fragments (at 20 μg/ml final concentration, wild-type protein and H278L mutant protein) was determined in the presence of increasing concentrations of [^{3}H]E_2 (26 to 420 nM) in 10 mM sodium phosphate buffer (pH 7.4). **C.** The total [^{3}H]E_2 binding by SEC fractions of cos-7 cell lysates containing the expressed full-length wild-type PDIp or the H278L mutant protein. The final concentration of [^{3}H]E_2 in these incubations was 4.5 nM. Each value is the mean of duplicate determinations.

Using the same approach, we also mutated Gln265 to leucine. As suggested by the binding mode II (**Figure 25D**), Gln265 may form a hydrogen bond with the 17-hydroxyl group of E_2. [^{3}H]E_2 binding assays showed that the purified Q265L *b-b'* fragment (over-expressed in *E. coli* cells, **Figure 27A**) and the full-length PDIp Q265L mutant protein (over-expressed in cos-7 cells, **Figure 27B**) each displayed similar [^{3}H]E_2-binding activity as the corresponding wild-type proteins. The apparent K_d value for Q265L *b-b'* fragment was found to be 185 ± 8 nM (**Figure 27C**), which is nearly the same as that of the wild-type *b-b'* fragment. In addition, we have also prepared the double mutant protein Q265L/H278L for testing its [^{3}H]E_2-binding activity. As expected, this double mutant protein does not have any [^{3}H]E_2-binding activity. Collectively, these observations suggest that PDIp's Gln265 may either form a non-essential, weak hydrogen bond with the 17-hydroxyl group of E_2 (as suggested by the binding mode II, **Figure 25D**), or it may not form a viable hydrogen bond at all (as suggested by the binding mode I, **Figure 25D**).

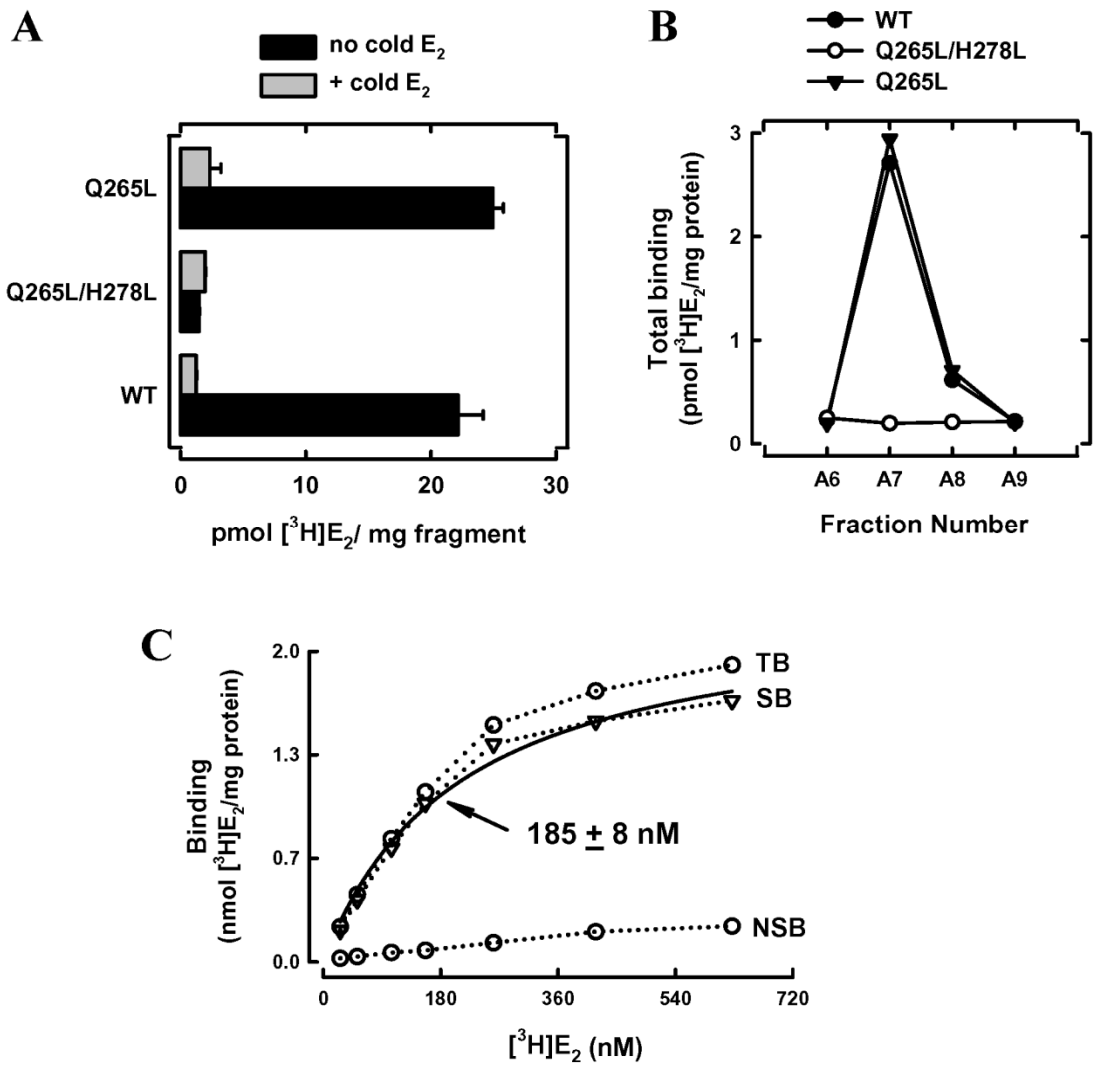
A
no cold E_2
+ cold E_2
Q265L
Q265L/H278L
WT
0
10
20
30
pmol [^{3}H]E_2/ mg fragment
B
WT
Q265L/H278L
Q265L
Total binding
(pmol [^{3}H]E_2/mg protein)
3
2
1
0
A6
A7
A8
A9
Fraction Number
C
Binding
(nmol [^{3}H]E_2/mg protein)
2.0
1.3
0.7
0.0
TB
SB
185 ± 8 nM
NSB
0
180
360
540
720
[^{3}H]E_2 (nM)

Figure 27 PDIP Q265L mutant protein retains similar E_2-binding activity. **A.** Total [^{3}H]E_2 binding by purified PDIp *b-b′* fragments (wild-type, Q265L, and Q265L/H278L mutant proteins, purified from *E. coli* cells) after incubation with 4.5 nM [^{3}H]E_2 in the absence or presence of excess cold E_2 (10 μM) in 10 mM sodium phosphate buffer. **B.** Total [^{3}H]E_2 binding by SEC fractions of cos-7 cell lysates containing the expressed full-length PDIp proteins (wild-type, Q265L, or Q265L/H278L mutant), after incubation with 4.5 nM [^{3}H]E_2. **C**. Total [^{3}H]E_2 binding (TB) by PDIp *b-b′* Q265L fragment (at 20 μg/ml final concentration) was determined in the presence of increasing concentrations of [^{3}H]E_2 (22 to 660 nM) in 10 mM sodium phosphate buffer (pH 7.4). Non-specific binding (NSB) was determined in the presence of 10 μM excess of cold E_2. Total binding subtracted by the non-specific binding gives rise to specific binding (SB). The binding curve is obtained by curve regression analysis using a hyperbola model in the SigmaPlot software. Each data point is the mean of duplicate determinations.

To provide further experimental support for the conclusions of the mutagenesis studies, we employed an alternative approach by using a number of E_2 derivatives that share the same core structure as E_2 but with their C-3 or C-17 hydroxyl group selectively modified such that they cannot form the same type of hydrogen bonds with PDIp as does E_2. In these experiments, both purified *b-b'* fragment (expressed in *E. coli* cells) and purified full-length recombinant human PDIp (expressed in cos-7 cells) were used to assay their relative binding activity by measuring their ability to compete off the binding of [^{3}H]E_2. We found that E_1, E_3, and C2, all of which contain an intact 3-hydroxyl group but differ in their 17-hydroxyl group (structures shown in **Figure 28A**), could efficiently compete with [^{3}H]E_2 for binding to the *b-b'* fragment or the full-length PDIp (**Figure 28B**). There is no significant difference between the IC_{50} values of E_2, E_1, and C2 (**Figure 28C**). In contrast, C3, which lacks the 3-hydroxyl group (**Figure 28A**), displayed no appreciable binding activity (**Figure 28B**). These observations provide further support for the suggestion that the 3-hydroxyl group of E_2 is essential for the binding interaction with PDIp by forming hydrogen bond(s), whereas the 17-hydroxyl group of E_2 is not important. These results are in complete agreement with the observations made with the point mutation studies described above.

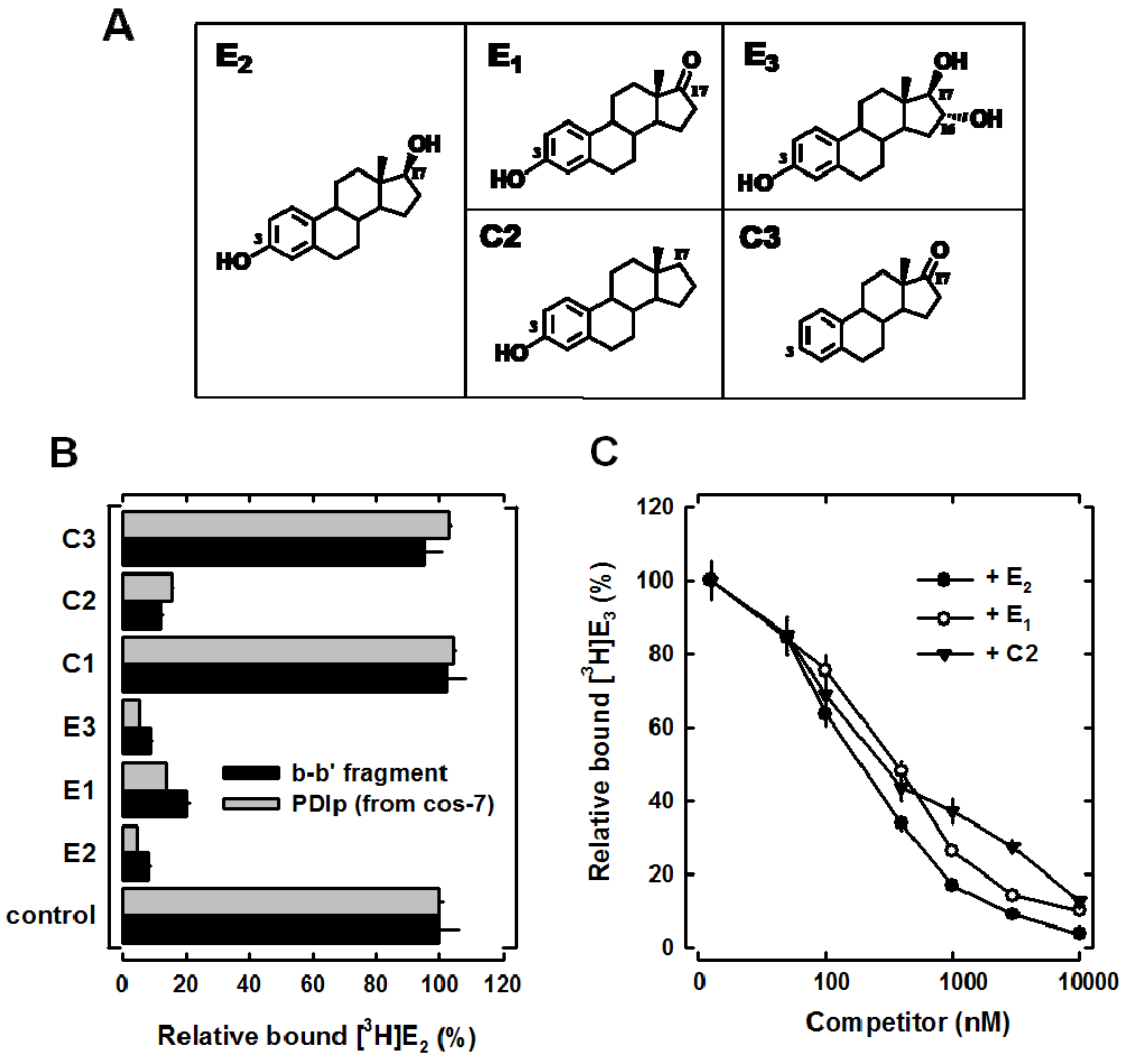
A
E2
E1
E3
C2
C3
B
C3
C2
C1
E3
E1
E2
control
b-b' fragment
PDIp (from cos-7)
0
20
40
60
80
100
120
Relative bound [3H]E2 (%)
C
Relative bound [3H]E3 (%)
+ E2
+ E1
+ C2
0
100
1000
10000
Competitor (nM)

Figure 28 Relative binding activity of PDIp for several E_2 derivatives. **A.** Chemical structures of E_2 and several of its analogs used in this study. **B**. Relative binding of [^{3}H]E_2 by recombinant PDIp *b-b'* fragment (at 20 μg/ml final concentration, purified from *E.coli* cells) (see **Figure 21B**) or by purified recombinant full-length PDIp protein expressed in cos-7 cells (at 20 μg/ml final concentration, see **Figure 23**). Protein was incubated with 4.5 nM [^{3}H]E_2 in the absence or presence of 10 μM E_2 or its analogs in sodium phosphate buffer (10 mM, pH 7.4). **C.** Relative [^{3}H]E_2 binding by the PDIp *b-b'* fragment purified from *E. coli* cells after incubation with 4.5 nM [^{3}H]E_2 in 10 mM sodium phosphate buffer (pH 7.4) in the absence (control, set as 100%) or presence of increasing concentrations of E_2, E_1, and C2. Each value is the mean ± S.D. of triplicate determinations.

Notably, whereas the two binding modes suggested by the docking studies are very similar in their overall structure and binding interaction, there are also some notable subtle differences. In mode I, the 3-hydroxyl group of E_2 is a hydrogen bond donor and the nitrogen atom of PDIp-His278 is a hydrogen bond acceptor. In mode 2, the 3-hydroxyl group of E_2 serves as a hydrogen bond acceptor and PDIp-His278 as a hydrogen bond donor in the formation of a hydrogen bond. Based on our earlier experience, it is almost certain that only one of the modes is the preferred binding mode. Based on the known difference in the strength of the OH—N hydrogen bond (6.9 kcal/mol) *vs.* the O—HN hydrogen bond (1.9 kcal/mol) (Emsley, 1980), it is predicted that binding mode I, which contains the stronger OH—N hydrogen bond, would be the preferred binding mode over mode II, which contains the weaker O—HN hydrogen bond. To provide experimental evidence for this prediction, we chose to determine the binding activity of 3-methoxyestradiol (structure shown in **Figure 29A**) for PDIp. Theoretically, the oxygen atom in the 3-methoxy group of 3-methoxyestradiol will only be able to serve as a hydrogen bond acceptor but not a hydrogen bond donor in forming a hydrogen bond (*i.e.*, it can only bind to PDIp in mode I but not in mode II). Computational docking analysis showed that 3-methoxyestradiol can still bind inside the pocket in a similar way as does E_2, and there is enough space around His278 to fully accommodate the methoxy group (**Figure 29B**). As expected, the model showed that 3-methoxyestradiol (serving as a hydrogen bond acceptor) still can form a hydrogen bond with His278 (serving as a hydrogen bond donor). However, in the binding assay, we found that 3-methoxyestradiol has no appreciable binding activity for the *b-b'* fragment or the full-length human PDIp

(**Figure 29C**). This experimental observation suggests that the hydrogen bond formed between 3-methoxyestradiol and His278 likely is either extremely weak, or, more likely, is not formed at all. Taken together, it is concluded that E_2 binds PDIp by forming a hydrogen bond between the 3-hydroxyl group of E_2 and PDIp-His278 according to binding mode I, but not binding mode II (**Figure 25D**).

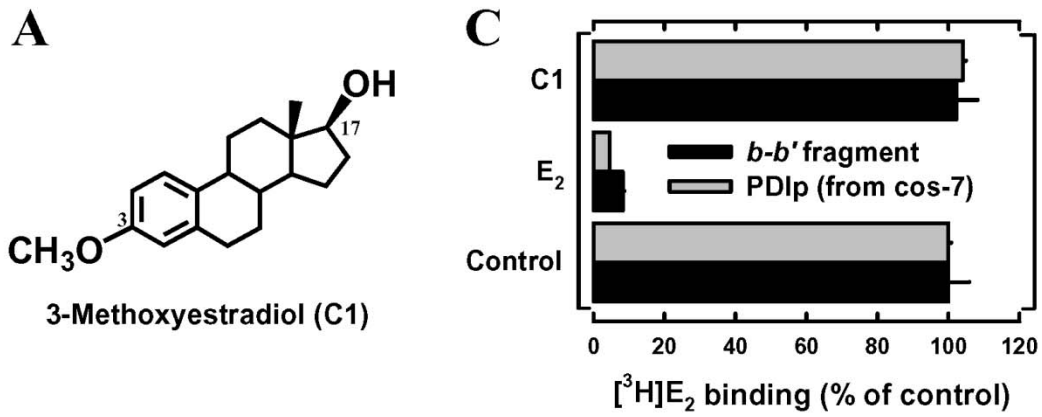
A
OH
17
3
CH_3O
3-Methoxyestradiol (C1)
C
C1
E_2
Control
b-b' fragment
PDIp (from cos-7)
0
20
40
60
80
100
120
[^{3}H]E_2 binding (% of control)

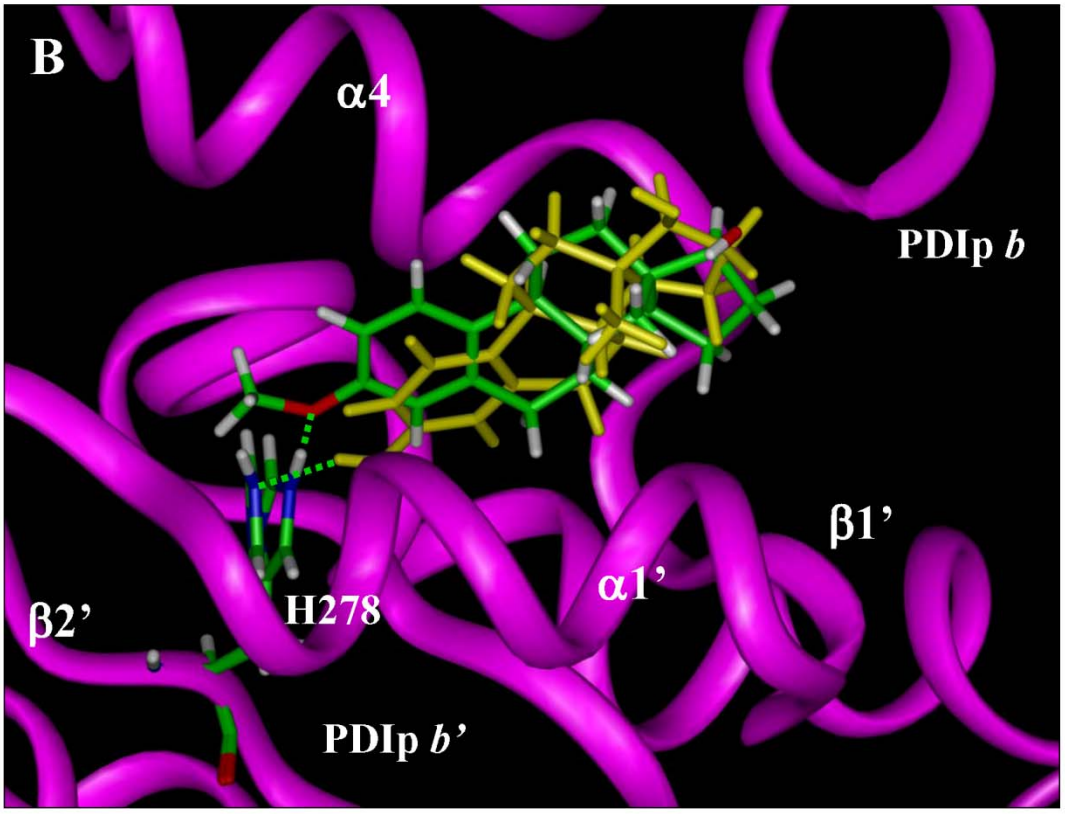
B
α4
PDIp b
β1'
α1'
β2'
H278
PDIp b'

Figure 29 Docking analysis of the interaction of PDIp with E_2 analog C1. **A**. Chemical structure of 3-methoxyestradiol (C1). **B**. Docking analysis of the binding modes of E_2 and C1 in the binding pocket of the PDIp *b-b'* fragment. Protein structure is shown in ribbon and colored in magenta. E_2, C1, and His278 are shown in the ball-and-stick format. C1 and His 278 are colored according to atoms and E_2 is colored yellow. Green dashes denote hydrogen bonds. α-Helices and β-sheets are labeled as in **Figure 24**. **C**. Relative [^{3}H]E_2 binding by recombinant PDIp *b-b'* fragment or by purified recombinant full-length PDIp protein in the absence or presence of 10 μM E_2 or its C1 analog. Each value is the mean ± S.D. of triplicate determinations.

Notably, it is well known that the 3-hydroxyl group of E_2 also plays an essential role in the binding interaction of E_2 with human ERα and ERβ by forming hydrogen bonds (Brzozowski et al., 1997; Gabbard and Segaloff, 1983; Zhu et al., 2006). The structural model developed in the present study offers a good explanation for the experimental observation that the human PDIp has a much lower E_2-binding affinity than human ERs, for the following reasons: (***i***) PDIp forms only one hydrogen bond with the 3-hydroxyl group of E_2, whereas human ERs form two hydrogen bonds with this hydroxyl group. (***ii***) Whereas the 17β-hydroxyl group of E_2 also plays an important role in its interaction with human ERα or ERβ (Zhu et al., 2006), its role in the interaction with human PDIp appears to be of minimal importance or simply nonexistent. (***iii***) The E_2-binding site of PDIp is significantly larger than those of human ERα and ERβ, *i.e.*, it is less compact, which would suggest a relatively looser binding interaction due to less hydrophobic interactions between E_2 and PDIp. (***iv***) For both ERα and ERβ, almost all amino acid residues in their binding pockets, except those that form hydrogen bonds with E_2, are hydrophobic residues, which provide stronger interactions with the four aliphatic rings of E_2 compared to PDIp. However, in the case of PDIp, some polar residues (Thr253, Thr260, Thr266, Ser225, and Gln265 shown in **Figure 25C, 25D**) are also present in the binding pocket, which may reduce the hydrophobic interactions with E_2. These notable differences distinguish human ERs from PDIp in their binding interactions with E_2.

The results of this study also provide a good explanation for our early observation

that while PDIp has no appreciable binding affinity for tamoxifen, PDIp still retains considerable binding affinity for ICI-172,780 (Fu and Zhu, 2009) (also see **Figure 30B**). It is known that tamoxifen does not have a phenolic OH group in its structure (see **Figure 30A**), and thus it cannot form the necessary hydrogen bond with His278 of PDIp. In comparison, ICI-172,780 has the same core steroid structure as E_2 (see **Figure 30D**). Our docking analysis showed that ICI-172,780 can still bind inside PDIp's binding pocket in a similar way as E_2 (**Figure 30C, 30D**), although its long side chain at the C-7 position slightly interferes with the binding, which is consistent with its lower binding affinity (**Figure 30B**). Lastly, it is of note that observations made in the present study may shed light on understanding the binding interaction of PDIp with its substrate peptides, which was shown to be inhibited by E_2 and its analogs (Klappa et al., 2001; Klappa et al., 1998). Interestingly, an earlier study reported that the specificity of the peptide substrates during interaction with PDIp is associated with the tyrosine and/or tryptophan residues in the peptide substrates (Ruddock et al., 2000). Because these two residues contain free phenolic hydroxyl and amino groups, respectively, it is tempting to suggest that the presence of these amino acid residues may serve as hydrogen bond donors in forming hydrogen bonds with PDIp-His278 during PDIp-peptide interactions, in a similar way as observed for the 3-hydroxyl phenolic group in E_2. This possibility merits further investigation.

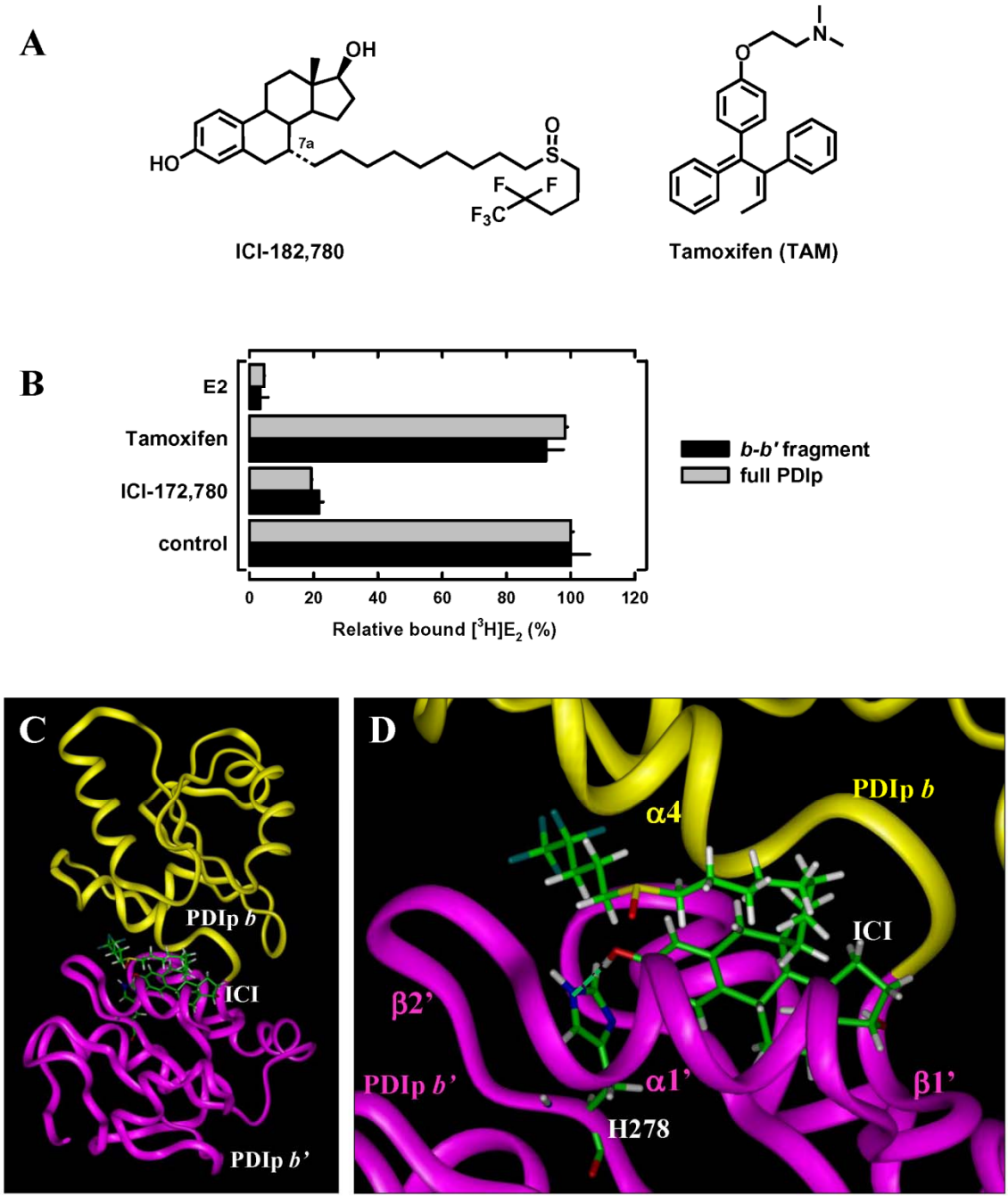
A
OH
HO
7a
O
S
F
F
F3C
ICI-182,780
O
N
Tamoxifen (TAM)
B
E2
Tamoxifen
ICI-172,780
control
0
20
40
60
80
100
120
Relative bound [3H]E2 (%)
b-b' fragment
full PDIp
C
PDIp b
ICI
PDIp b'
D
PDIp b
α4
ICI
β2'
PDIp b'
α1'
β1'
H278

Figure 30 Docking analysis of the interaction of PDIp with ICI-172,780. **A.** Chemical structures of ICI-172,780 and tamoxifen. **B**. Relative [^{3}H]E_2 binding in the absence or presence of excess E_2, tamoxifen, or ICI compound (10 μM) by the recombinant PDIp *b*-*b'* fragment (at 20 μg/ml final concentration, purified from *E.coli* cells) or by the recombinant full-length PDIp protein (at 20 μg/ml final concentration, purified from cos-7 cells). These proteins were incubated with 4.5 nM [^{3}H]E_2 in sodium phosphate buffer (10 mM, pH 7.4). Each data point is the mean ± S.D. of triplicate determinations. **C.** The docking results showing the binding interaction of ICI-172,780 with the PDIp *b*-*b'* fragment. **D**. A close-up view of the docking result of ICI-172,780 binding in PDIp *b*-*b'* fragment, showing that a hydrogen bond (green dashed line) was formed between the 3-hydroxyl group of ICI-172,780 (hydrogen bond donor) and PDIp-His278 (hydrogen bond acceptor). The protein structure is shown in ribbon. Yellow-colored regions denote the *b* domain and magenta-colored regions denote the *b'* domain. ICI-172,780 and His278 are shown in ball-and-stick format and colored according to atoms. α-Helics and β-sheets are labeled as in **Figure 24**.

CONCLUSIONS

Human PDIp has a single E_2-binding site with an apparent K_d of approximately 170 nM. Computational modeling and docking analyses revealed that the E_2-binding site in the *b*-*b′* fragment is located in a hydrophobic pocket composed mainly of the *b′* domain and partially of the *b* domain. The hydrogen bond formed between the 3-hydroxyl group of E_2 (hydrogen bond donor) and PDIp's His278 (hydrogen bond acceptor) is essential for its binding. By contrast, the 17β-hydroxyl group of E_2 is of negligible importance for E_2 binding. This binding model was confirmed by a series of experiments, such as selective mutation of the binding site amino acid residues and selective modification of the ligand structures. Altogether, these results precisely defined, for the first time, the E_2-binding site structure of human PDIp.

CHAPTER EIGHT

GENERAL SUMMARY AND CONCLUSIONS

SUMMARY OF FINDINGS

SPECIFIC AIM 1: To study the structural characteristics of the interactions of representative estrogen analogs with human ERα and ERβ. This aim contains three closely-related sub-aims.

AIM 1A: To determine the three-dimensional structural characteristics of the interactions of endogenous estrogen metabolites with human ERα and ERβ.

In our earlier study (Zhu et al., 2006), we characterized the relative binding affinities (*RBA*) of some 50 endogenous estrogen metabolites to human ERα and ERβ. Many of these estrogen metabolites had structures similar to E_2 (with only one or two functional groups added), but their *RBAs* for ERs were very different. Studying the interactions of these structurally-similar compounds with ERs sheds light on the detailed structural features of their binding interactions with the receptor proteins.

I first determined the suitability of the molecular docking method to correctly predict the binding modes and interactions of an agonistic ligand in the ligand binding domain (LBD) of the human ERs using diethylstilbestrol and E_2 as examples. I showed that the docked structures of E_2 and diethylstilbestrol in the ERα LBD are almost exactly the same as the known crystal structures of ERα in complex with these two agonistic ligands. Using the validated docking approach, I then docked 27 structurally-similar

estrogen derivatives into the LBDs of human ERα and ERβ to characterize their binding interactions with the ERs. Whereas the binding modes of these estrogen derivatives are very similar to that of E_2, there are distinct subtle differences, and these small differences contribute importantly to their differential binding affinity to the ERs. In the case of *A*-ring estrogen derivatives, there is a strong inverse relationship between the length of the hydrogen bonds formed with ERs and the binding affinities. We found that a better correlation between the computed binding energy values and the experimentally-determined log*RBA* values can be achieved for various *A*-ring derivatives by re-adjusting the relative weights of the VDW interaction energy and the Coulomb interaction energy in computing the overall binding energy values.

AIM 1B: To determine the three-dimensional structural characteristics of the interactions of the non-aromatic steroids with human ERα and ERβ.

All currently known endogenously-formed estrogens are steroids with aromatic A-ring. Based on the results from **AIM 1A** (the computational analysis of the binding characteristics of aromatic estrogens for human ERα and ERβ), we hypothesized that some of the non-aromatic androgen metabolites or precursors with hydroxyl groups at the C-3 and/or C-17 positions may also be able to bind ERα and ERβ with high affinity and thereby may serve as non-aromatic endogenous ER ligands.

Based on this hypothesis, I employed computational molecular modeling tools coupled with *in vitro* bioassays, and identified a group of non-aromatic steroids (potential precursors and/or metabolites of endogenous androgens) that can bind human ERα and ERβ with physiologically-relevant high binding affinity. These non-aromatic steroids can activate the ERs and elicit estrogenic actions in ERα-positive human cancer cells. The results of this study suggest an intriguing possibility that some endogenous androgen precursors or metabolites may serve as male-specific ER modulators. These findings also call for further studies to determine which of these non-aromatic ER modulators can be produced in men at physiologically-relevant quantities and also what are their physiological/pathophysiological functions.

AIM 1C: To determine the three-dimensional structural characteristics of the interactions of E_2-based C-7α derivatives with human ERα and ERβ.

ER pure antagonists are useful in the treatment of ER-positive human breast cancer refractory to tamoxifen. It is known that compounds such as ICI-172,780, with a long linear side chain attached to the C-7α position of E_2, could serve as effective ER antagonists. We hypothesized that estrogen analogs with a shorter but bulky side chain attached to the C-7α position of E_2 may also function as effective ER antagonists with a more stable side-chain structure.

We designed and synthesized nine of the analogs and studied their interactions with human ERα by using molecular docking analysis coupled with *in vitro* ER binding assays, ER-driven reporter assays, and cell proliferation assays. Four of them showed a strong inhibitory effect on the ER transactivation activity in the reporter assay. Similarly, these four compounds also exerted a strong inhibition of ER-positive human breast cancer cell growth *in vitro*. Computational docking studies were conducted to model the interactions of these antagonists with the ligand binding domain (LBD) of human ERα. These newly-synthesized ER antagonists could tightly bind to the ERα binding pocket similar to other known ERα antagonists such as ICI-182,780, which helped to explain the mechanism of their antiestrogenic actions. The results of this study demonstrated that attachment of a short but bulky structure to the C-7α position of E_2 yielded ER antagonists with receptor binding affinity comparable to ICI-182,780, a prototypical pure ER antagonist. These compounds are believed to be promising candidates for further testing as anti-breast cancer agents.

SPECIFIC AIM 2: To study the interactions of E_2 with a novel estrogen-binding protein PDIp.

Recently, we identified a new intracellular E_2-binding protein, namely, the pancreas-specific protein disulfide isomerase (PDIp), and we found that it can modulate estrogen actions in mammalian cells. In light of these observations, and also based on the fact that this intracellular protein is present at unusually high levels in certain tissues or

cells, it was speculated that PDIp may function as an important intracellular E_2-storage protein in these cells. Biochemical analyses of various truncated PDIp proteins showed that the *b*-*b′* fragment contained an intact E_2-binding site that has the same binding affinity as the full-length PDIp protein. However, the structures of its estrogen-binding site are not known. Based on what we learned from **AIM 1** on the three-dimensional interactions of estrogens with ERs, I applied computational molecular modeling methods to predict the binding site structure of PDIp for the endogenous estrogen E_2 as well as its binding interaction with E_2.

Computational modeling and docking analyses revealed that the E_2-binding site in the *b*-*b′* fragment is located in a hydrophobic pocket composed mainly of the *b′* domain and partially of the *b* domain. The hydrogen bond, formed between the 3-hydroxyl group of E_2 (hydrogen bond donor) and PDIp's His278 (hydrogen bond acceptor) is essential for its binding. By contrast, the 17β-hydroxyl group of E_2 is of negligible importance for E_2 binding. This binding model was confirmed by a series of experiments, such as selective mutation of the binding site amino acid residues and selective modification of the ligand structures. Altogether, these results precisely defined, for the first time, the E_2-binding site structure of human PDIp.

OVERALL CONCLUSIONS

In my dissertation research work, I explored the usefulness of the computational molecular modeling methods as a tool to study the interactions of a number of representative estrogen analogs (i.e., estrogen metabolites, non-aromatic steroids, and synthetic antiestrogens) with human ERα and ERβ as well as the recently-identified intracellular estrogen-binding protein PDIp. I found that the molecular docking analysis is reliable in predicting the binding modes of estrogens with their receptors/binding proteins. Subtle differences in the ligand structures that alter the strength/formation of hydrogen bonds between the ligands and the receptors or binding proteins contribute importantly to their differential binding affinity.

The significance of the study is that it provides insights into the three-dimensional structural characteristics of the binding interactions of estrogen analogs with the receptors and cellular binding proteins. These studies provide a platform for future efforts in developing an automated docking-based computational approach that can screen environmental compounds for their potential human binding affinities for human ERs as well as other binding proteins.

LITERATURES CITED

Abaci A, Demir K, Bober E and Buyukgebiz A (2009) Endocrine disrupters - with special emphasis on sexual development. *Pediatr Endocrinol Rev* **6**: 464-475

Adams JY, Leav I, Lau KM, Ho SM and Pflueger SM (2002) Expression of estrogen receptor beta in the fetal, neonatal, and prepubertal human prostate. *Prostate* **52**: 69-81

Ball P and Knuppen R (1980) Catecholoestrogens (2-and 4-hydroxyoestrogens): Chemistry, biogenesis, metabolism, occurrence and physiological significance. *Acta Endocrinol Suppl (Copenh)* **232**: 1-127

Bern HA, Mills KT, Hatch DL, Ostrander PL and Iguchi T (1992) Altered mammary responsiveness to estradiol and progesterone in mice exposed neonatally to diethylstilbestrol. *Cancer Lett* **63**: 117-124

Bernstein L (2002) Epidemiology of endocrine-related risk factors for breast cancer. *J Mammary Gland Biol Neoplasia* **7**: 3-15

Bosland MC (2006) Sex steroids and prostate carcinogenesis: Integrated, multifactorial working hypothesis. *Ann N Y Acad Sci* **1089**: 168-176

Brody JG, Moysich KB, Humblet O, Attfield KR, Beehler GP and Rudel RA (2007) Environmental pollutants and breast cancer: Epidemiologic studies. *Cancer* **109**: 2667-2711

Brooks SC and Horn L (1971) Hepatic sulfation of estrogen metabolites. *Biochim Biophys Acta* **231**: 233-241

Brzozowski AM, Pike AC, Dauter Z, Hubbard RE, Bonn T, Engstrom O, Ohman L,

Greene GL, Gustafsson JA and Carlquist M (1997) Molecular basis of agonism and antagonism in the oestrogen receptor. *Nature* **389**: 753-758

Christiansen C, Christensen MS and Transbol I (1981) Bone mass in postmenopausal women after withdrawal of oestrogen/gestagen replacement therapy. *Lancet* **1**: 459-461

Ciocca DR and Roig LM (1995) Estrogen receptors in human nontarget tissues: Biological and clinical implications. *Endocr Rev* **16**: 35-62

Colborn T, vom Saal FS and Soto AM (1993) Developmental effects of endocrine-disrupting chemicals in wildlife and humans. *Environ Health Perspect* **101**: 378-384

Cramer RD, 3rd, Patterson DE and Bunce JD (1989) Recent advances in comparative molecular field analysis (comfa). *Prog Clin Biol Res* **291**: 161-165

de Ronde W, Pols HA, van Leeuwen JP and de Jong FH (2003) The importance of oestrogens in males. *Clin Endocrinol (Oxf)* **58**: 529-542

Delmas PD, Bjarnason NH, Mitlak BH, Ravoux AC, Shah AS, Huster WJ, Draper M and Christiansen C (1997) Effects of raloxifene on bone mineral density, serum cholesterol concentrations, and uterine endometrium in postmenopausal women. *N Engl J Med* **337**: 1641-1647

Denisov AY, Maattanen P, Dabrowski C, Kozlov G, Thomas DY and Gehring K (2009) Solution structure of the bb' domains of human protein disulfide isomerase. *FEBS J* **276**: 1440-1449

Desilva MG, Lu J, Donadel G, Modi WS, Xie H, Notkins AL and Lan MS (1996)

Characterization and chromosomal localization of a new protein disulfide isomerase, pdip, highly expressed in human pancreas. *DNA Cell Biol* **15**: 9-16

Desilva MG, Notkins AL and Lan MS (1997) Molecular characterization of a pancreas-specific protein disulfide isomerase, pdip. *DNA Cell Biol* **16**: 269-274

Diamanti-Kandarakis E, Bourguignon JP, Giudice LC, Hauser R, Prins GS, Soto AM, Zoeller RT and Gore AC (2009) Endocrine-disrupting chemicals: An endocrine society scientific statement. *Endocr Rev* **30**: 293-342

Dupont WD and Page DL (1991) Menopausal estrogen replacement therapy and breast cancer. *Arch Intern Med* **151**: 67-72

Ellem SJ and Risbridger GP (2007) Treating prostate cancer: A rationale for targeting local oestrogens. *Nat Rev Cancer* **7**: 621-627

Ellgaard L and Ruddock LW (2005) The human protein disulphide isomerase family: Substrate interactions and functional properties. *EMBO Rep* **6**: 28-32

Emsley J (1980) Very strong hydrogen bonds. *Chemical Society Reviews* **9**: 91-124

Enmark E, Pelto-Huikko M, Grandien K, Lagercrantz S, Lagercrantz J, Fried G, Nordenskjold M and Gustafsson JA (1997) Human estrogen receptor beta-gene structure, chromosomal localization, and expression pattern. *J Clin Endocrinol Metab* **82**: 4258-4265

Eriksen EF, Colvard DS, Berg NJ, Graham ML, Mann KG, Spelsberg TC and Riggs BL (1988) Evidence of estrogen receptors in normal human osteoblast-like cells. *Science* **241**: 84-86

Falck F, Jr., Ricci A, Jr., Wolff MS, Godbold J and Deckers P (1992) Pesticides and

polychlorinated biphenyl residues in human breast lipids and their relation to breast cancer. *Arch Environ Health* **47**: 143-146

Filardo E, Quinn J, Pang Y, Graeber C, Shaw S, Dong J and Thomas P (2007) Activation of the novel estrogen receptor g protein-coupled receptor 30 (gpr30) at the plasma membrane. *Endocrinology* **148**: 3236-3245

Fisher BCostantino JPWickerham DLCecchini RSCronin WMRobidoux ABevers TBKavanah MTAtkins JNMargolese RG, et al. (2005) Tamoxifen for the prevention of breast cancer: Current status of the national surgical adjuvant breast and bowel project p-1 study. *J Natl Cancer Inst* **97**: 1652-1662

Fortunati N, Becchis M, Catalano MG, Comba A, Ferrera P, Raineri M, Berta L and Frairia R (1999) Sex hormone-binding globulin, its membrane receptor, and breast cancer: A new approach to the modulation of estradiol action in neoplastic cells. *J Steroid Biochem Mol Biol* **69**: 473-479

Fortunati N and Catalano MG (2006) Sex hormone-binding globulin (shbg) and estradiol cross-talk in breast cancer cells. *Horm Metab Res* **38**: 236-240

Fortunati N, Fissore F, Fazzari A, Becchis M, Comba A, Catalano MG, Berta L and Frairia R (1996) Sex steroid binding protein exerts a negative control on estradiol action in mcf-7 cells (human breast cancer) through cyclic adenosine 3',5'-monophosphate and protein kinase a. *Endocrinology* **137**: 686-692

Fortunati N, Fissore F, Fazzari A, Piovano F, Catalano MG, Becchis M, Berta L and Frairia R (1999) Estradiol induction of camp in breast cancer cells is mediated by foetal calf serum (fcs) and sex hormone-binding globulin (shbg). *J Steroid*

Biochem Mol Biol **70**: 73-80

Fortunati N, Raineri M, Cignetti A, Hammond GL and Frairia R (1998) Control of the membrane sex hormone-binding globulin-receptor (shbg-r) in mcf-7 cells: Effect of locally produced shbg. *Steroids* **63**: 282-284

Freedman RB, Klappa P and Ruddock LW (2002) Model peptide substrates and ligands in analysis of action of mammalian protein disulfide-isomerase. *Methods Enzymol* **348**: 342-354

Fu X, Wang P and Zhu BT (2008) Protein disulfide isomerase is a multifunctional regulator of estrogenic status in target cells. *J Steroid Biochem Mol Biol* **112**: 127-137

Fu X and Zhu BT (2009) Human pancreas-specific protein disulfide isomerase homolog (pdip) is an intracellular estrogen-binding protein that modulates estrogen levels and actions in target cells. *J Steroid Biochem Mol Biol* **115**: 20-29

Fu XM and Zhu BT (2009) Human pancreas-specific protein disulfide isomerase homolog (pdip) is an intracellular estrogen-binding protein that modulates estrogen levels and actions in target cells. *J Steroid Biochem Mol Biol* **115**: 20-29

Fu XM and Zhu BT (2010) Human pancreas-specific protein disulfide-isomerase (pdip) can function as a chaperone independently of its enzymatic activity by forming stable complexes with denatured substrate proteins. *Biochem J* **429**: 157-169

Gabbard RB and Segaloff A (1983) Structure-activity relationships of estrogens. Effects of 14-dehydrogenation and axial methyl groups at c-7, c-9 and c-11. *Steroids* **41**: 791-805

Garcia-Segura LM, Naftolin F, Hutchison JB, Azcoitia I and Chowen JA (1999) Role of astroglia in estrogen regulation of synaptic plasticity and brain repair. *J Neurobiol* **40**: 574-584

Grady D, Rubin SM, Petitti DB, Fox CS, Black D, Ettinger B, Ernster VL and Cummings SR (1992) Hormone therapy to prevent disease and prolong life in postmenopausal women. *Ann Intern Med* **117**: 1016-1037

Green PS, Bishop J and Simpkins JW (1997) 17 alpha-estradiol exerts neuroprotective effects on sk-n-sh cells. *J Neurosci* **17**: 511-515

Green S, Walter P, Kumar V, Krust A, Bornert JM, Argos P and Chambon P (1986) Human oestrogen receptor cdna: Sequence, expression and homology to v-erb-a. *Nature* **320**: 134-139

Grosse J, Anielski P, Hemmersbach P, Lund H, Mueller RK, Rautenberg C and Thieme D (2005) Formation of 19-norsteroids by in situ demethylation of endogenous steroids in stored urine samples. *Steroids* **70**: 499-506

Gruber CW, Cemazar M, Heras B, Martin JL and Craik DJ (2006) Protein disulfide isomerase: The structure of oxidative folding. *Trends Biochem Sci* **31**: 455-464

Grune T, Reinheckel T, Li R, North JA and Davies KJ (2002) Proteasome-dependent turnover of protein disulfide isomerase in oxidatively stressed cells. *Arch Biochem Biophys* **397**: 407-413

Hall JM and McDonnell DP (1999) The estrogen receptor beta-isoform (erbeta) of the human estrogen receptor modulates eralpha transcriptional activity and is a key regulator of the cellular response to estrogens and antiestrogens. *Endocrinology*

140: 5566-5578

Henderson BE, Ross RK and Pike MC (1991) Toward the primary prevention of cancer. *Science* **254**: 1131-1138

Hillier SG, Whitelaw PF and Smyth CD (1994) Follicular oestrogen synthesis: The 'two-cell, two-gonadotrophin' model revisited. *Mol Cell Endocrinol* **100**: 51-54

Howell A, Osborne CK, Morris C and Wakeling AE (2000) Ici 182,780 (faslodex): Development of a novel, "Pure" Antiestrogen. *Cancer* **89**: 817-825

Jordan VC (2003) Antiestrogens and selective estrogen receptor modulators as multifunctional medicines. 1. Receptor interactions. *J Med Chem* **46**: 883-908

Karas RH, Patterson BL and Mendelsohn ME (1994) Human vascular smooth muscle cells contain functional estrogen receptor. *Circulation* **89**: 1943-1950

Katzenellenbogen BS, Bhardwaj B, Fang H, Ince BA, Pakdel F, Reese JC, Schodin D and Wrenn CK (1993) Hormone binding and transcription activation by estrogen receptors: Analyses using mammalian and yeast systems. *J Steroid Biochem Mol Biol* **47**: 39-48

Kim HP, Lee JY, Jeong JK, Bae SW, Lee HK and Jo I (1999) Nongenomic stimulation of nitric oxide release by estrogen is mediated by estrogen receptor alpha localized in caveolae. *Biochem Biophys Res Commun* **263**: 257-262

Klappa P, Freedman RB, Langenbuch M, Lan MS, Robinson GK and Ruddock LW (2001) The pancreas-specific protein disulphide-isomerase pdip interacts with a hydroxyaryl group in ligands. *Biochem J* **354**: 553-559

Klappa P, Ruddock LW, Darby NJ and Freedman RB (1998) The b' domain provides the

principal peptide-binding site of protein disulfide isomerase but all domains contribute to binding of misfolded proteins. *EMBO J* **17**: 927-935

Klappa P, Stromer T, Zimmermann R, Ruddock LW and Freedman RB (1998) A pancreas-specific glycosylated protein disulphide-isomerase binds to misfolded proteins and peptides with an interaction inhibited by oestrogens. *Eur J Biochem* **254**: 63-69

Kuiper GG and Gustafsson JA (1997) The novel estrogen receptor-beta subtype: Potential role in the cell- and promoter-specific actions of estrogens and anti-estrogens. *FEBS Lett* **410**: 87-90

Landel CC, Potthoff SJ, Nardulli AM, Kushner PJ and Greene GL (1997) Estrogen receptor accessory proteins augment receptor-DNA interaction and DNA bending. *J Steroid Biochem Mol Biol* **63**: 59-73

Lee AJ, Cai MX, Thomas PE, Conney AH and Zhu BT (2003) Characterization of the oxidative metabolites of 17beta-estradiol and estrone formed by 15 selectively expressed human cytochrome p450 isoforms. *Endocrinology* **144**: 3382-3398

Lewis PJ (1994) Risk factors for breast cancer. Pollutants and pesticides may be important. *BMJ* **309**: 1662

Li Y, Trush MA and Yager JD (1994) DNA damage caused by reactive oxygen species originating from a copper-dependent oxidation of the 2-hydroxy catechol of estradiol. *Carcinogenesis* **15**: 1421-1427

Liehr JG, Fang WF, Sirbasku DA and Ari-Ulubelen A (1986) Carcinogenicity of catechol estrogens in syrian hamsters. *J Steroid Biochem* **24**: 353-356

Lindzey J, Wetsel WC, Couse JF, Stoker T, Cooper R and Korach KS (1998) Effects of castration and chronic steroid treatments on hypothalamic gonadotropin-releasing hormone content and pituitary gonadotropins in male wild-type and estrogen receptor-alpha knockout mice. *Endocrinology* **139**: 4092-4101

Lippman ME and Bolan G (1975) Oestrogen-responsive human breast cancer in long term tissue culture. *Nature* **256**: 592-593

Liu ZJ and Zhu BT (2004) Concentration-dependent mitogenic and antiproliferative actions of 2-methoxyestradiol in estrogen receptor-positive human breast cancer cells. *J Steroid Biochem Mol Biol* **88**: 265-275

Lucier GW and McDaniel OS (1977) Steroid and non-steroid udp glucuronyltransferase: Glucuronidation of synthetic estrogens as steroids. *J Steroid Biochem* **8**: 867-872

Ma L (2009) Endocrine disruptors in female reproductive tract development and carcinogenesis. *Trends Endocrinol Metab* **20**: 357-363

Maattanen P, Kozlov G, Gehring K and Thomas DY (2006) Erp57 and pdi: Multifunctional protein disulfide isomerases with similar domain architectures but differing substrate-partner associations. *Biochem Cell Biol* **84**: 881-889

Makridakis NM, di Salle E and Reichardt JK (2000) Biochemical and pharmacogenetic dissection of human steroid 5 alpha-reductase type ii. *Pharmacogenetics* **10**: 407-413

Manas ESUnwalla RJXu ZBMalamas MSMiller CPHarris HAHsiao CAkopian THum WTMalakian K, et al. (2004) Structure-based design of estrogen receptor-beta selective ligands. *J Am Chem Soc* **126**: 15106-15119

Manas ES, Xu ZB, Unwalla RJ and Somers WS (2004) Understanding the selectivity of genistein for human estrogen receptor-beta using x-ray crystallography and computational methods. *Structure* **12**: 2197-2207

Manolagas SC, Jilka RL, Girasole G, Passeri G and Bellido T (1993) Estrogen, cytokines, and the control of osteoclast formation and bone resorption in vitro and in vivo. *Osteoporos Int* **3 Suppl 1**: 114-116

Martucci CP and Fishman J (1993) P450 enzymes of estrogen metabolism. *Pharmacol Ther* **57**: 237-257

Morales DE, McGowan KA, Grant DS, Maheshwari S, Bhartiya D, Cid MC, Kleinman HK and Schnaper HW (1995) Estrogen promotes angiogenic activity in human umbilical vein endothelial cells in vitro and in a murine model. *Circulation* **91**: 755-763

Naftolin F, Garcia-Segura LM, Keefe D, Leranth C, Maclusky NJ and Brawer JR (1990) Estrogen effects on the synaptology and neural membranes of the rat hypothalamic arcuate nucleus. *Biol Reprod* **42**: 21-28

Nandi S, Guzman RC and Yang J (1995) Hormones and mammary carcinogenesis in mice, rats, and humans: A unifying hypothesis. *Proc Natl Acad Sci U S A* **92**: 3650-3657

Paganini-Hill A and Henderson VW (1996) Estrogen replacement therapy and risk of alzheimer disease. *Arch Intern Med* **156**: 2213-2217

Peltoketo H, Luu-The V, Simard J and Adamski J (1999) 17beta-hydroxysteroid dehydrogenase (hsd)/17-ketosteroid reductase (ksr) family; nomenclature and

main characteristics of the 17hsd/ksr enzymes. *J Mol Endocrinol* **23**: 1-11

Peterson TJ, Karmakar S, Pace MC, Gao T and Smith CL (2007) The silencing mediator of retinoic acid and thyroid hormone receptor (smrt) corepressor is required for full estrogen receptor alpha transcriptional activity. *Mol Cell Biol* **27**: 5933-5948

Pike AC, Brzozowski AM and Hubbard RE (2000) A structural biologist's view of the oestrogen receptor. *J Steroid Biochem Mol Biol* **74**: 261-268

Pike AC, Brzozowski AM, Walton J, Hubbard RE, Thorsell AG, Li YL, Gustafsson JA and Carlquist M (2001) Structural insights into the mode of action of a pure antiestrogen. *Structure* **9**: 145-153

Porter JC (1974) Proceedings: Hormonal regulation of breast development and activity. *J Invest Dermatol* **63**: 85-92

Primm TP and Gilbert HF (2001) Hormone binding by protein disulfide isomerase, a high capacity hormone reservoir of the endoplasmic reticulum. *J Biol Chem* **276**: 281-286

Prins GS, Birch L, Couse JF, Choi I, Katzenellenbogen B and Korach KS (2001) Estrogen imprinting of the developing prostate gland is mediated through stromal estrogen receptor alpha: Studies with alphaerko and betaerko mice. *Cancer Res* **61**: 6089-6097

Rochira V, Balestrieri A, Madeo B, Baraldi E, Faustini-Fustini M, Granata AR and Carani C (2001) Congenital estrogen deficiency: In search of the estrogen role in human male reproduction. *Mol Cell Endocrinol* **178**: 107-115

Rogan WJ and Ragan NB (2003) Evidence of effects of environmental chemicals on the

endocrine system in children. *Pediatrics* **112**: 247-252

Rollerova E and Urbancikova M (2000) Intracellular estrogen receptors, their characterization and function (review). *Endocr Regul* **34**: 203-218

Roncaglioni A and Benfenati E (2008) In silico-aided prediction of biological properties of chemicals: Oestrogen receptor-mediated effects. *Chem Soc Rev* **37**: 441-450

Ruddock LW, Freedman RB and Klappa P (2000) Specificity in substrate binding by protein folding catalysts: Tyrosine and tryptophan residues are the recognition motifs for the binding of peptides to the pancreas-specific protein disulfide isomerase pdip. *Protein Sci* **9**: 758-764

Rudel RA, Attfield KR, Schifano JN and Brody JG (2007) Chemicals causing mammary gland tumors in animals signal new directions for epidemiology, chemicals testing, and risk assessment for breast cancer prevention. *Cancer* **109**: 2635-2666

Schultz-Norton JR, McDonald WH, Yates JR and Nardulli AM (2006) Protein disulfide isomerase serves as a molecular chaperone to maintain estrogen receptor alpha structure and function. *Mol Endocrinol* **20**: 1982-1995

Simard J, Ricketts ML, Gingras S, Soucy P, Feltus FA and Melner MH (2005) Molecular biology of the 3beta-hydroxysteroid dehydrogenase/delta5-delta4 isomerase gene family. *Endocr Rev* **26**: 525-582

Simpson ER and Davis SR (2001) Minireview: Aromatase and the regulation of estrogen biosynthesis--some new perspectives. *Endocrinology* **142**: 4589-4594

Spyridopoulos I, Sullivan AB, Kearney M, Isner JM and Losordo DW (1997) Estrogen-receptor-mediated inhibition of human endothelial cell apoptosis. Estradiol as a

survival factor. *Circulation* **95**: 1505-1514

Strom A, Hartman J, Foster JS, Kietz S, Wimalasena J and Gustafsson JA (2004) Estrogen receptor beta inhibits 17beta-estradiol-stimulated proliferation of the breast cancer cell line t47d. *Proc Natl Acad Sci U S A* **101**: 1566-1571

Tanaka S, Uehara T and Nomura Y (2000) Up-regulation of protein-disulfide isomerase in response to hypoxia/brain ischemia and its protective effect against apoptotic cell death. *J Biol Chem* **275**: 10388-10393

Tanenbaum DM, Wang Y, Williams SP and Sigler PB (1998) Crystallographic comparison of the estrogen and progesterone receptor's ligand binding domains. *Proc Natl Acad Sci U S A* **95**: 5998-6003

Taylor RD, Jewsbury PJ and Essex JW (2002) A review of protein-small molecule docking methods. *J Comput Aided Mol Des* **16**: 151-166

Thomas P, Pang Y, Filardo EJ and Dong J (2005) Identity of an estrogen membrane receptor coupled to a g protein in human breast cancer cells. *Endocrinology* **146**: 624-632

Tian G, Xiang S, Noiva R, Lennarz WJ and Schindelin H (2006) The crystal structure of yeast protein disulfide isomerase suggests cooperativity between its active sites. *Cell* **124**: 61-73

Tsibris JC, Hunt LT, Ballejo G, Barker WC, Toney LJ and Spellacy WN (1989) Selective inhibition of protein disulfide isomerase by estrogens. *J Biol Chem* **264**: 13967-13970

Turner RT, Riggs BL and Spelsberg TC (1994) Skeletal effects of estrogen. *Endocr Rev*

15: 275-300

Uehara T, Nakamura T, Yao D, Shi ZQ, Gu Z, Ma Y, Masliah E, Nomura Y and Lipton SA (2006) S-nitrosylated protein-disulphide isomerase links protein misfolding to neurodegeneration. *Nature* **441**: 513-517

Weihua Z, Lathe R, Warner M and Gustafsson JA (2002) An endocrine pathway in the prostate, erbeta, ar, 5alpha-androstane-3beta,17beta-diol, and cyp7b1, regulates prostate growth. *Proc Natl Acad Sci U S A* **99**: 13589-13594

White RE, Darkow DJ and Lang JL (1995) Estrogen relaxes coronary arteries by opening bkca channels through a cgmp-dependent mechanism. *Circ Res* **77**: 936-942

Wilkinson B and Gilbert HF (2004) Protein disulfide isomerase. *Biochim Biophys Acta* **1699**: 35-44

Witkowska HE, Carlquist M, Engstrom O, Carlsson B, Bonn T, Gustafsson JA and Shackleton CH (1997) Characterization of bacterially expressed rat estrogen receptor beta ligand binding domain by mass spectrometry: Structural comparison with estrogen receptor alpha. *Steroids* **62**: 621-631

Woolley CS, Weiland NG, McEwen BS and Schwartzkroin PA (1997) Estradiol increases the sensitivity of hippocampal ca1 pyramidal cells to nmda receptor-mediated synaptic input: Correlation with dendritic spine density. *J Neurosci* **17**: 1848-1859

Xu HGouras GKGreenfield JPVincent BNaslund JMazzarelli LFried GJovanovic JNSeeger MRelkin NR, et al. (1998) Estrogen reduces neuronal generation of alzheimer beta-amyloid peptides. *Nat Med* **4**: 447-451

Yager JD and Liehr JG (1996) Molecular mechanisms of estrogen carcinogenesis. *Annu*

Rev Pharmacol Toxicol **36**: 203-232

Zhang Y, Graubard BI, Klebanoff MA, Ronckers C, Stanczyk FZ, Longnecker MP and McGlynn KA (2005) Maternal hormone levels among populations at high and low risk of testicular germ cell cancer. *Br J Cancer* **92**: 1787-1793

Zhao C, Matthews J, Tujague M, Wan J, Strom A, Toresson G, Lam EW, Cheng G, Gustafsson JA and Dahlman-Wright K (2007) Estrogen receptor beta2 negatively regulates the transactivation of estrogen receptor alpha in human breast cancer cells. *Cancer Res* **67**: 3955-3962

Zhu BT and Conney AH (1998) Functional role of estrogen metabolism in target cells: Review and perspectives. *Carcinogenesis* **19**: 1-27

Zhu BT, Han GZ, Shim JY, Wen Y and Jiang XR (2006) Quantitative structure-activity relationship of various endogenous estrogen metabolites for human estrogen receptor alpha and beta subtypes: Insights into the structural determinants favoring a differential subtype binding. *Endocrinology* **147**: 4132-4150

Zumoff B (1993) Hormone replacement and cardiovascular risk factors. *N Engl J Med* **329**: 1041; author reply 1042-1043